AN ANALYSIS OF THE FLUTTER AND DAMPING CHARACTERISTICS OF HELICOPTER ROTORS

A THESIS

Presented to

The Faculty of the Division of Graduate

Studies and Research

By

Sathy Padmanaban Viswanathan

In Partial Fulfillment

of the Requirements for the Degree

Doctor of Philosophy

in the School of Aerospace Engineering

Georgia Institute of Technology

January, 1977

AN ANALYSIS OF THE FLUTTER AND

DAMPING CHARACTERISTICS OF HELICOPTER ROTORS

Approved:

G. Alvin Pierce, Chairman

Robin B. Gray

C. Virgil Smith

Date approved by Chairman: 3.7.77

ACKNOWLEDGMENTS

I wish to express my sincere gratitude to Dr. G. A. Pierce for his kind guidance and assistance during this study. The many discussions I had with him greatly helped me understand aeroelasticity.

Grateful appreciation is extended to Dr. C. V. Smith for his valuable suggestions for improvement. I would like to thank other members of my reading committee, Dr. R. B. Gray, Dr. D. J. McGill, and Dr. Ueng for their contributions.

I wish to thank Dr. M. B. Sledd for impressing upon me the philosophical approach to Mathematical Physics. Dr. M. Stallybrass kindly found the time to help me with problems in mathematics.

The discussions I had with Dr. V. R. Murthy greatly contributed to my understanding of structural dynamic problems. Also I wish to thank Dr. K. S. S. Nagaraja and Mr. R. Srinivasan for their helpful suggestions.

My sincere thanks to Mrs. Peggy Weldon for her patience and skill in typing the thesis.

My parents and other members of my family made many sacrifices during my academic career. My uncle the late Dr. S. Balakrishnan, my aunt, and my grandmother greatly helped me during my school days, and without their help, higher education may not have been possible for me.

TABLE OF CONTENTS

TABLE OF CONTENTS (Continued)

LIST OF TABLES

LIST OF ILLUSTRATIONS

LIST OF ILLUSTRATIONS (Continued)

LIST OF ILLUSTRATIONS (Continued)

NOMENCLATURE

$[A]$	generalized aerodynamic force coefficient matrix
A_{rn}	element of matrix [A] defined by Equation (45)
A_{ℓ}	undetermined coefficients of the various pressure modes
a	nondimensional chordwise location of the elastic axis behind the midchord
$\bar{a}$	two dimensional lift curve-slope
a_{∞}	free stream speed of sound
B_{ℓ}	undetermined coefficients of the various pressure modes
b	semi-chord of the airfoil
b_{ref}	reference semi-chord
E	length of the vortex sheet considered in the analysis on either side of the airfoil
EI_1, EI_2	bending rigidities about the major and minor neutral axes
EI	bending rigidity in the out-of-plane direction
e	distance by which mass axis lies ahead of the elastic axis
F	vertical force per unit length of the beam
f	time dependent part of the vertical force intensity
f_o	time independent part of the vertical force intensity
f_1, f_2	abbreviations defined by Equation (12)
G	wake integral function defined by Equation (97)
GJ	torsional rigidity of the beam
GJ_m	effective torsional rigidity defined by Equation (3)
g	additional structural damping of the k method
g_r	structural damping coefficient of the r-th vacuum normal mode

$g_i^{(j)}$	estimate of the damping present in the i-th aeroelastic mode corresponding to the j-th scanning trial
h	nondimensional wake spacing, see Figure 9
h'	wake spacing, h' = hb
i	imaginary number, $\sqrt{-1}$; also an index for the modes
k	reduced frequency, $\omega b/\Omega y$
k_A	polar radius of gyration of cross sectional area effective in carrying tensile stresses, about elastic axis
k_{m1}, k_{m2}	mass radii of gyration about major neutral axis and about an axis perpendicular to chord through the elastic axis, respectively
k_m	polar radius of gyration of cross sectional mass about elastic axis, $k_m^2 = k_{m1}^2 + k_{m2}^2$
L	lift per unit span
$\bar{L}$	amplitude of the simple harmonic lift per unit span
L_1, L_2	lift coefficients defined by Equation (41)
L_3, L_4	lift coefficients defined by Equation (67)
L_h, L_α	nondimensional unsteady aerodynamic lift coefficients defined by Equation (42)
$L_{hp}, L_{\alpha p}$	p-type aerodynamic lift coefficients defined by Equation (69)
M_{ea}	aerodynamic moment about elastic axis per unit span
$\bar{M}_{ea}$	amplitude of the aerodynamic moment about elastic axis per unit span
M_r	generalized mass of the r-th mode
M_r^*	nondimensional generalized mass defined by Equation (49)
$\tilde{M}_{rs}$	element of the generalized mass matrix defined by Equation (26)
M_h, M_α	nondimensional unsteady aerodynamic moment coefficients defined by Equation (42)
$M_{hp}, M_{\alpha p}$	p-type aerodynamic moment coefficients defined by Equation (69)

M_1, M_2 moment coefficients defined by Equation (41)

M_3, M_4 moment coefficients defined by Equation (68)

M_∞ free stream Mach number, $\Omega y/a_\infty$

m frequency ratio, ω/Ω

m_f frequency ratio at flutter, ω_f/Ω_f

$\bar{m}$ mass per unit length of the beam

$\bar{m}_{ref}$ reference value of $\bar{m}$

N number of vacuum normal modes considered in the flutter analysis

n wake index number

n_1 finite number of lower lying wakes considered in the p-type aerodynamic model

p complex number denoting the decay rate and the frequency of the exponentially damped simple harmonic motion, $p = \gamma\omega + i\omega$

$\tilde{p}$ nondimensional value of p, $\tilde{p} = p/\omega$

Q total torque about elastic axis per unit length of the beam, or the number of blades in the rotor

q time dependent part of the torque per unit length

q_o time independent part of the torque per unit length

R radius of the rotor

T tension in the beam, $\int_y^R \bar{m}\, r\, \Omega^2 dr$

t time coordinate

V_∞ vertical climb rate of the rotor

v_a induced velocity on the airfoil

W total out-of-plane deflection of the beam

w time dependent part of the out-of-plane deflection

w_o time independent part of the out-of-plane deflection

$\bar{w}$	amplitude of the out-of-plane deflection
w_r	out-of-plane mode shape of the r-th vacuum normal mode
w_r^*	nondimensional out-of-plane mode shape, w_r/b_{ref}
w_f^*	nondimensional out-of-plane flutter mode shape
x,y,z	coordinate system as shown in Figure 2
x'	airfoil chordwise coordinate shown in Figure 26
A	total torsional deformation of the beam
α	time dependent part of the torsional deformation
α_o	time independent part of the torsional deformation
$\bar{\alpha}$	amplitude of the torsional deformation
α_r	torsional modal deflection of the r-th vacuum normal mode
α_r^*	nondimensional torsional modal deflection, $\alpha_r^* = \alpha_r$
$\alpha_s(0)$	angle of incidence at the root
β	angle of incidence, or the nondimensional semi-chord, b/b_{ref}
Δ	determinant of a matrix
ε	distance of elastic axis behind the quarter chord axis in terms of semichords, $\varepsilon = 1/2 + a$
Γ_a'	airfoil bound circulation
γ	airfoil motion decay factor or the strength of vorticity on the airfoil and in the wakes
$\lambda_i^{(j)}$	the i-th complex eigenvalue corresponding to the j-th scanning trial m_j in the k method
μ	vortex viscous dissipation factor
Ω	angular velocity of the rotor
Ω^*	nondimensional angular velocity, Ω/ω_{ref}
Ω_f	angular velocity of the rotor at flutter
ω	frequency of vibration

ω_r frequency of vibration of the r-th vacuum normal mode

ω_f flutter frequency of vibration

ω_{ref} reference frequency, $\omega_{ref}^2 = EI/\bar{m}R^4$

$\omega_i^{(j)}$ estimate of the damped natural frequency in the i-th aeroelastic mode corresponding to the j-th scanning trial

ρ_∞ density of the free stream fluid medium

Ξ_r generalized force of the r-th mode

$\bar{\Xi}_r$ amplitude of the generalized force of the r-th mode

ξ_r generalized coordinate of the r-th mode

$\bar{\xi}_r$ amplitude of the generalized coordinate of the r-th mode

$\{\bar{\xi}\}$ column of the amplitudes of the generalized coordinates

ξ' airfoil chordwise coordinate

η nondimensional spanwise coordinate, $\eta = y/R$

Superscripts

' differentiation with respect to spanwise coordinate

. differentiation with respect to time coordinate

Prefixes

Re real part of a complex number

Im imaginary part of a complex number

SUMMARY

Two relatively new methods of vibrational analysis of nonuniform rotor blades in combined flapwise bending and torsion are reviewed. The structural dynamic characteristics of an example blade are evaluated using the Transmission matrix method and are later used in flutter analyses.

An automated procedure is developed to obtain the matched flutter point of a rotor in an axial flight condition. The determinant method of flutter prediction turns out to be impracticable. By developing a method called the approximate true V - g method, it is shown that the failure of the k method to accurately predict the damping at subcritical speeds is mostly due to the method of numerical solution.

The principles of the p - k method are explained and it is shown that this method is well suited to analyze the damping and flutter characteristics of rotor blades. An alternative numerical method of solution is provided based on an eigenvalue analysis. An example flutter problem is solved by various methods. An unsteady rotor aerodynamic theory of the p type is derived and the results from this analysis tend to show that the implied assumption of the p - k method is sound.

CHAPTER I

INTRODUCTION

All rotary wing aircraft such as helicopters, autogyros, VTOL and STOL aircraft fitted with prop-rotors, are subject to the potentially catastrophic phenomenon of rotor blade flutter. This aeroelastic instability is characterized by self excited undamped oscillations of the blade lifting surface in torsion and bending (elastic flapping). This problem is generally solved by mass balancing the blade about the quarter chord and designing the elastic axis to lie at the quarter chord position. This solution usually results in added blade weight. Consequently, the rotor hub has to be designed heavier to withstand the increased centrifugal tensile forces.

Contemporary high performance main rotor systems are made of light weight composite construction. The outboard sections of the blade operate in the compressible subsonic Mach number regime, and are made of cambered airfoil sections to improve the hover aerodynamic efficiency. Furthermore, to augment the stability of the rotor in ground resonance, air resonance, rotor-pylon aeromechanical stability, etc., the kinematic aerodynamic coupling like flap-lag coupling, pitch-lag coupling, pitch-flap coupling etc., are built into the system. These considerations render the advanced rotor systems liable to a variety of potentially dangerous aeroelastic instabilities, one of which is rotor blade flutter. In the next decade, the rotor system designer will have a great need for

being able to accurately predict the amount of stability present in the various aeroelastic modes at subcritical speeds. These data are very important for correlating with and guiding the flight flutter testing and non-destructive wind tunnel testing.

In the last two decades, considerable work has been done in the areas of rotor blade structural dynamics, rotor unsteady aerodynamics and rotor aeroelasticity. The state of the art can now be considered satisfactory in the area of structural dynamics. The task of obtaining the unsteady aerodynamic forces on the helicopter rotor blade in forward flight still remains formidable. The unsteady aerodynamic problem of a rotor in hover or ascending vertical flight, or that of a prop-rotor in the propeller mode of operation, seems to have been relatively well solved. This thesis deals with the aeroelastic analysis of the rotor under such an axial flight condition.

The structural dynamic principles are briefly discussed and an example problem is solved in Chapter II. The aerodynamic theories are reviewed and flutter equations of motion are derived in Chapter III.

The conventional method of flutter analysis consists of employing an unsteady aerodynamic theory suitable for simple harmonic motion of the lifting surface. By some approximate considerations, this method provides an estimate of the stability present in the system at subcritical speeds. This method is called the k method or the conventional V - g method. While this method is satisfactory for prediction of the flutter boundary flight condition, the estimation of the stability present in the system is not acceptable at speeds below the critical speed. The k method needs to be considerably modified before it can be employed for

subcritical damping predictions. Results of one such analysis carried out by Pierce and White [1] are shown in Figure 1. The modal damping is oscillatory with respect to rotor speed and is even multivalued. They recommended that the flutter criteria be based on the curve labeled effective damping.

One main objective of this thesis is to explore methods that will estimate the stability at subcritical speeds more accurately than the results of Pierce and White. A relatively new method called the p-k method has been highlighted by Hassig [2] in his study to improve the damping prediction of fixed wings.

An aerodynamic theory is considered to be of the p type if it deals with the motion of the lifting surface that decays in an exponentially damped simple harmonic fashion. In general, all sophisticated p type aerodynamic theories require excessive computer time. Hence the p method of aeroelastic solution, which can be considered exact, is numerically time-consuming.

However, if a k type (undamped simple harmonic motion) aerodynamic theory is applied after suitable modifications to a p type motion, a reasonably accurate and simplified formulation results. This is called the p - k method. In Chapter IV the k method is discussed and in Chapter V the p - k method is analyzed. Chapter VI contains a derivation of a p-type rotor aerodynamic theory in an attempt to investigate the implied assumption of the p - k method.

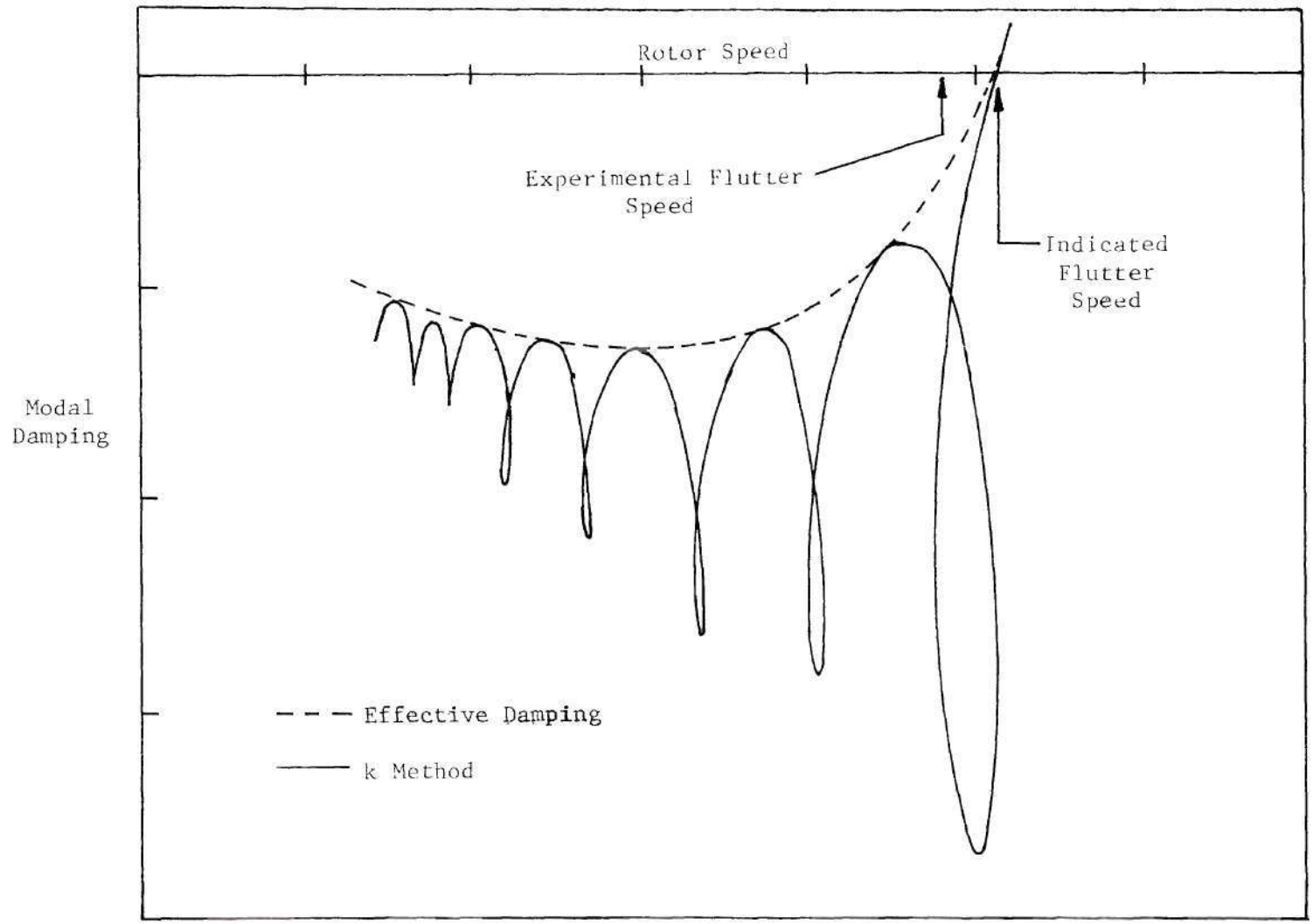

Figure 1. Stability of One Aeroelastic Mode as a Function of Rotor Speed.

CHAPTER II

STRUCTURAL DYNAMICS OF A ROTATING BLADE

The geometry of the rotor blade considered in this thesis is shown in Figure 2. It possesses a smooth planform, and the local center of gravity location gradually changes with the spanwise coordinate y. The blade consists of symmetric airfoil sections with varying angles of incidence relative to the x - y reference plane. The spanwise variation is constituted by the built-in twist (required to optimize the steady aerodynamic performance of the rotor) and the aeroelastic twist (due to the noncoincidence of the center of pressure axis and the elastic axis). This variation in angle of incidence must be added to the angle of incidence at the root (collective pitch) to obtain the local pitch angle. The elastic axis is assumed to be straight.

Throughout this thesis, only torsional and out-of-plane (flapwise-bending) deformations are considered. The edgewise (lead-lag) bending deflections, due to vibration in the horizontal plane of rotation are not considered. For the low inflow case considered here, the edgewise bending oscillations are assumed not to produce any significant unsteady aerodynamic forces.

A self excited vibrational phenomenon known as "ground resonance," which can be catastropic, has been experienced by several helicopters and autogyros [3]. This phenomenon occurs frequently when the helicopter is supported on the ground by relatively soft tires, resulting in

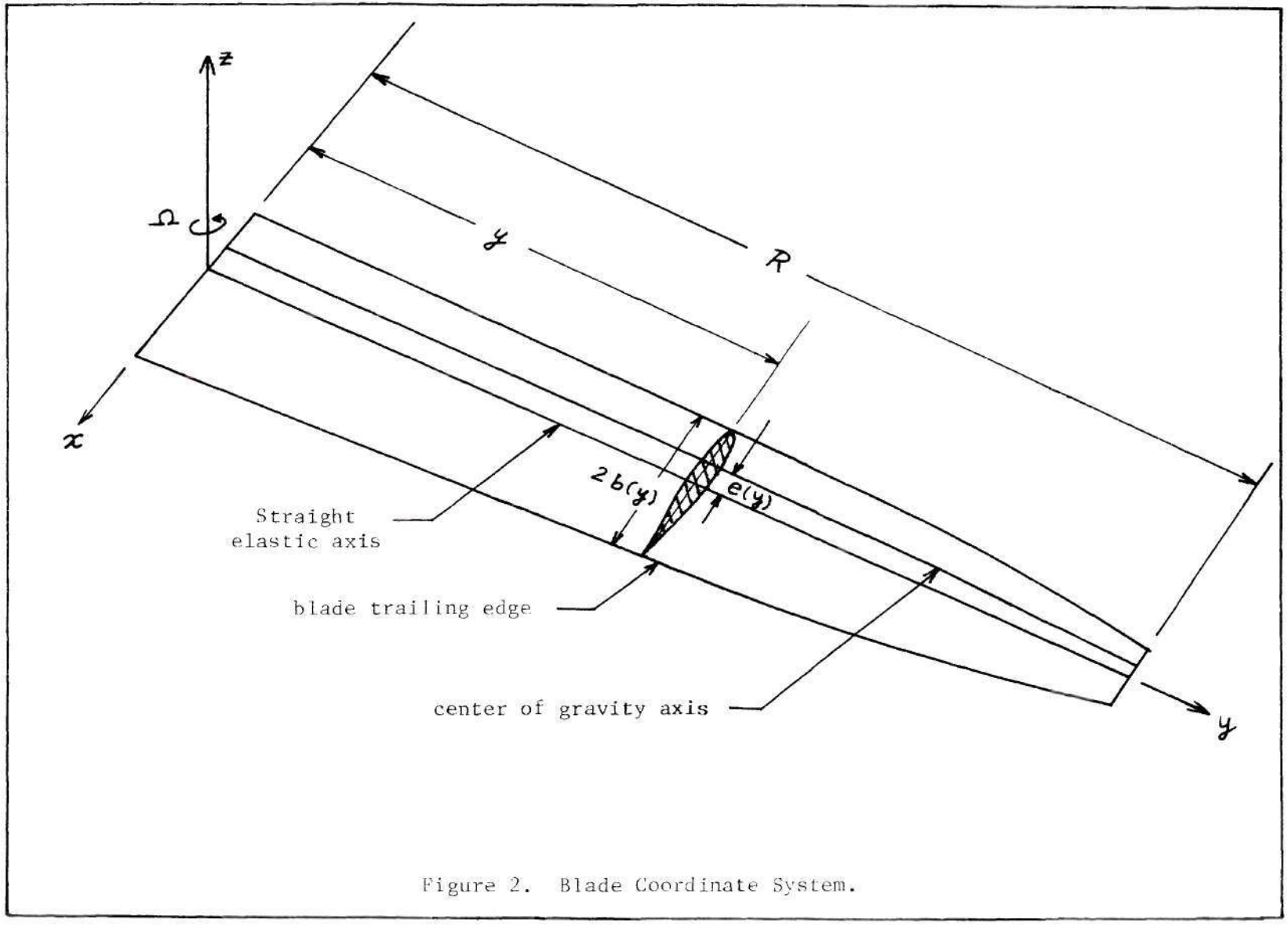

Figure 2. Blade Coordinate System.

a low natural frequency of the machine in the sideward motion. The resonance is characterized by the blade lagging vibrations coupled with the vibration of the aircraft fore and aft, and sidewards. While analyzing self excited vibrations of this kind, blade lag vibrations are of prime importance.

The main objective of this investigation is to develop some numerical programming schemes to automatically determine the true flutter point. Edgewise oscillations are not considered throughout this thesis. Another separate investigation must show the degree of validity of the assumption of ignoring the in-plane oscillations. It is hoped that the new principles brought about in this thesis regarding damping and flutter analysis could be used for solving aeroelastic problems of similar formulation.

Equations of Motion and Boundary Conditions

Houbolt and Brooks [4] have derived a comprehensive set of differential equations of motion for combined flapwise bending, edgewise bending and torsion of a twisted nonuniform rotor blade. The development is based on the principles of beam theory, and secondary effects such as deformation due to shear are not included. Other than assuming that the elastic axis is straight, there are no major restrictions in their derivation. The following additional assumptions are made here:

1) The distance between the elastic axis and the axis about which the blade is rotating is zero at the root.

2) The distance between the area centroid of the tensile member and the elastic axis is zero.

3) The blade is untwisted and the mean angle of incidence at every spanwise station equals the collective pitch.

4) In-plane deformation (edgewise bending deflection) is zero.

The first three assumptions are made simply because the computer program available to carry out the vibration analysis does not have a provision to include these terms. The flutter program to be developed incorporates normal modes as input, so, if normal modes which include these terms are available they can be used in an identical fashion provided the resulting governing equations are formally the same. The last assumption has been discussed already.

With these assumptions, the governing differential equations become:

$$-[(GJ_m)A']' - \Omega^2\bar{m}yeW' + \Omega^2\bar{m}(k_{m2}^2 - k_{m1}^2)A + \bar{m}\,k_m^2\,\ddot{A} - \bar{m}\,e\,\ddot{W} = Q \tag{1}$$

$$-[EIW'']'' + (TW')' - (\Omega^2\bar{m}\,y\,e\,A)' + \bar{m}(-\ddot{W} + e\ddot{A}) = -F \tag{2}$$

where

$$GJ_m = GJ + Tk_A^2 \tag{3}$$

and

$$EI = EI_1 \cos^2\beta + EI_2 \sin^2\beta \tag{4}$$

Separating the time dependent and time independent parts of the external forces and the resulting displacements

$$\begin{aligned} Q(y,t) &= q_o(y) + q(y,t) \\ F(y,t) &= f_o(y) + f(y,t) \\ W(y,t) &= w_o(y) + w(y,t) \\ A(y,t) &= \alpha_o(y) + \alpha(y,t) \end{aligned} \tag{5}$$

Then the following pairs of differential equations are obtained

$$-(GJ_m\alpha_o')' - \Omega^2\bar{m}y_e w_o' + \Omega^2\bar{m}(k_{m2}^2 - k_{m1}^2)\alpha_o = q_o$$

$$-(EIw_o'')'' + (Tw_o')' - (\Omega^2\bar{m}ye\alpha_o)' = -f_o \tag{6}$$

$$-(GJ_m\alpha')' - \Omega^2\bar{m}y_e w' + \Omega^2\bar{m}(k_{m2}^2 - k_{m1}^2)\alpha$$

$$+ \bar{m}k_m^2\ddot{\alpha} - \bar{m}e\ddot{w} = q$$

$$-(EIw'')'' + (Tw')' - (\Omega^2\bar{m}y_e\alpha)' \tag{7}$$

$$+ \bar{m}(-\ddot{w} + e\ddot{\alpha}) = -f \ .$$

In Equation (6) q_o and f_o contain time independent terms proportional to Ω^2 as well as the mean operating constant aerodynamic forces.

To obtain the mean aerodynamic forces knowing the deformation of the blade in addition to the built-in twist, a theory like simple momentum and blade element analysis can be used. A more sophisticated theory like vortex analysis or even good experimental results can be utilized. In general, the relationship of the aerodynamic forces in axial flight with respect to angle of attack at root is nonlinear. Equation (6) represents the static aeroelastic problem where the static equation of equilibrium and the steady aerodynamic relationship must be simultaneously satisfied. Nagaraja [5] has numerically obtained the solution for a typical problem. The static aeroelastic solution establishes the mean inflow; the wake spacing in the axial direction is then known. This factor is important in evaluating the unsteady aerodynamic forces.

Equation (7) represents the dynamic equations of motion of the blade. q and f are the resulting unsteady aerodynamic forces. A linear aerodynamic theory would be employed to relate q and f to α and w. Hence Equation (7) is linear and homogeneous. The following boundary conditions would be employed in the solution.

For hinged root:

$$w(y,t)\big|_{y=0} = 0$$

$$w''(y,t)\big|_{y=0} = 0 \qquad (8a)$$

$$\alpha(y,t)\big|_{y=0} = 0$$

For fixed root

$$w(y,t)\big|_{y=0} = 0$$

$$w'(y,t)\big|_{y=0} = 0 \tag{8b}$$

$$\alpha(y,t)\big|_{y=0} = 0$$

For free tip:

$$w''(y,t)\big|_{y=R} = 0$$

$$[(EI\,w'')' + \Omega^2 \bar{m}\, Re\alpha]\big|_{y=R} = 0 \tag{8c}$$

$$\alpha'(y,t)\big|_{y=R} = 0$$

The above are linear and homogeneous boundary conditions, satisfied by time dependent as well as time independent parts of the deformations A and W.

The Tk_a^2 term contained in the (GJ_m) term and the $(T\,w')'$ term of Equation (7) show the effect of centrifugal forces in increasing the effective torsional and bending stiffness of the beam. There are other terms which arise because of elastic coupling and inertia loading due to vibratory and centrifugal accelerations. The derivation is explained in detail by Houbolt and Brooks [4]. For a nonuniform beam such as the one considered here, GJ, k_a, $\bar{m}$, e, k_{m2}, k_{m1}, k_m, EI_1, EI_2 will be functions of the spanwise coordinate y.

Free Vibration Analysis

In Equation (7), let

$$\alpha = \alpha(y,t) = \tilde{\alpha}(y)\ \exp(i\omega t)$$

$$w = w(y,t) = \tilde{w}(y)\ \exp(i\omega t) \tag{9}$$

$$f = q = 0$$

The following two coupled, homogeneous, ordinary differential equations are obtained:

$$-(GJ_m\tilde{\alpha}')' - f_1\tilde{w}' + f_2\tilde{\alpha} - \bar{m}\omega^2(-e\tilde{w} + k_m^2\tilde{\alpha}) = 0 \tag{10}$$

$$-(EI\tilde{w}'')'' + (T\tilde{w}')' - (f_1\tilde{\alpha})' - \bar{m}\omega^2(-\tilde{w} + e\tilde{\alpha}) = 0 \tag{11}$$

where

$$f_1 = \Omega^2\bar{m}\,y\,e \tag{12a}$$

$$f_2 = \Omega^2\bar{m}(k_{m2}^2 - k_{m1}^2) \tag{12b}$$

The boundary conditions that $\tilde{\alpha}$ and $\tilde{w}$ should satisfy are given by Equation (8) by replacing w and α by $\tilde{w}$ and $\tilde{\alpha}$.

Thus $\tilde{\alpha}$ and $\tilde{w}$ satisfy homogeneous differential equations with homogeneous boundary conditions. If there exists an ω, say ω_r, corresponding to which a nontrivial solution exists, then a natural frequency, ω_r, and a vacuum mode shape, $\alpha_r = \tilde{\alpha}$ and $w_r = \tilde{w}$, are obtained. Some numerical techniques to solve this problem are discussed in detail by Murthy [6]. Two of the methods are briefly summarized here in the interest of completeness.

Transmission Matrix Method

Let $\{Z(y)\}$ be a column vector defining the states at the spanwise station y, given by

$$\{Z(y)\} = \begin{Bmatrix} w(y) \\ w'(y) \\ \alpha(y) \\ Q_y(y) \\ M_x(y) \\ V_z(y) \end{Bmatrix} \tag{13}$$

The governing linear differential equations of vibration can be written as a set of first order equations in matrix form as

$$\frac{d}{dy}\{Z(y)\} = [A(y)]\{Z(y)\} \tag{14}$$

The transmission matrix $[T(y)]$ is defined by

$$\{Z(y)\} = [T(y)]\{Z(0)\} \tag{15}$$

It can be shown that

$$\frac{d}{dy}[T(y)] = [A(y)][T(y)] \tag{16}$$

By shrinking y to 0, it is noted that $[T(0)]$ is an identity matrix. From Equation (15)

$$\{Z(R)\} = [T(R)]\{Z(0)\} \tag{17}$$

Applying the boundary conditions at the root and the tip regarding bending deflection, slope of neutral axis, torsional deflection, shear force, bending moment, and torque, part of Equation (17) can be written as

$$\{0\} = [T_1(R)]\{Z_1(0)\} \tag{18}$$

where $[T_1(R)]$ is a partitioned matrix of $[T(R)]$, and $\{Z_1(0)\}$ is the corresponding part of $\{Z(0)\}$ representing the nonvanishing quantities at the root. Clearly, for a nontrivial solution for $\{Z_1(0)\}$ to exist,

$$|[T_1(R)]| = 0 \tag{19}$$

which becomes the characteristic equation. The elements of $[T_1(R)]$ are obtained through Runge-Kutta numerical integration. S. Rubin [7] is one of the pioneering investigators of this method and Murthy [6] has extended it to cover the vibrational analysis of a very general case of a rotating blade.

Several trial frequencies are chosen in an increasing sequence. The frequency determinant is evaluated at each trial argument and the vanishing of this determinant corresponds to a natural frequency. This frequency choice method has one disadvantage in that if the determinant function is not carefully analyzed, two or more of its zeros may go undetected. Hence caution must be exercised when two natural frequencies are expected to be close together.

Using the above obtained natural frequencies, the boundary conditions of the problem, the transmission matrix obtained through integration,

and the information contained in Equation (18), the mode shapes are readily obtained. One very outstanding feature of this elegant method is that the mode shapes could be obtained at as many spanwise stations as desired without increasing the order of the frequency determinant. Of course, the numerical round off errors might grow if the Runge-Kutta interval of integration is very much reduced.

Integrating Matrix Method

Let $g(x)$ be a continuous and smooth function of one independent variable x in the interval $x_o \leq x \leq x_n$. Let the interval be divided into n equal subintervals and let the values of g be known at these $(n+1)$ interval points as $g(x_j)$, $j = 0,1,2,\ldots,n$. Assume that $g(x)$ can be represented approximately by a polynomial of degree $r(r \leq n)$. This polynomial equation may be expressed in the form of Newton's forward-difference interpolation formula. Using this formula the function can be integrated analytically in terms of the values of the function at the end points of the sub-intervals. The following matrix equation can then be written:

$$\begin{Bmatrix} 0 \\ \int_{x_o}^{x_1} g(x)dx \\ \int_{x_o}^{x_2} g(x)dx \\ \vdots \\ \int_{x_o}^{x_n} g(x)dx \end{Bmatrix} = [\mathcal{J}] \cdot \begin{Bmatrix} g_o \\ g_1 \\ g_2 \\ \vdots \\ g_n \end{Bmatrix} \tag{20}$$

The matrix [$\mathcal{I}$] of Equation (20) is called the integrating matrix. Premultiplying the column matrix consisting of the values of the function at the chosen points by [$\mathcal{I}$], the integrals of the function are obtained.

The solution to the governing differential equations of motion is developed entirely in matrix notation which allows the numerical solution to be developed in a compact and orderly fashion. The matrix differential equations are then integrated repeatedly by using the integrating matrix as an operator. Next, the constants of integration are evaluated by applying the boundary conditions. Finally, the resulting matrix equation is expressed in the familiar concise form of the eigenvalue problem. Hunter [8] used this method to study the vibrational characteristics of propeller blades.

An outstanding feature of this method is that, when carried out numerically accurately, the frequencies of vibration are obtained rapidly. Such an initial estimate could profitably be used as the input to a more sophisticated method like the transmission matrix method and thus the eigenvalues could rapidly be refined.

Example Blades

Although several assumptions have been made and discussed, Equations (10) and (11) still represent a sophisticated description of the problem. The transmission matrix approach is a powerful method to obtain the normal modes accurately. Two example blades have been chosen and their mode shape and frequencies have been computed by the computer program prepared by Murthy [6] which utilizes the transmission matrix. It

is believed that the seven modes obtained and described below for each blade represent an accurate description of their structural dynamic properties. An attempt is made to provide all the details of the blades and the results of the vibration analyses, since it will be a useful reference in the literature. The blades chosen are nearly the same as the model blades tested by Brooks and Baker [9]. It is believed that the example blades will provide a realistic and informative picture of rotor aeroelasticity.

The example blades numbered 1 and 2 are identical except that Blade No. 1 is hinged at the root whereas Blade No. 2 is fixed at the root. These two blades have the following uniform properties along the span:

$\bar{m}$ = 0.00135 slug/inch

EI = 26000 lb-inch^2

GJ = 10000 lb-inch^2

R = 46.0 inch

b = 2.0 inch

e = -0.45 inch.

k_{m1} = 0.1 inch

k_{m2} = 0.976 inch

k_A = 0.948 inch.

The above given data are sufficient to determine the normal modes of the blades.

Figures 3 and 4 show the variation of the natural frequencies of Blades No. 1 and 2 respectively, with rotor speed. The strong effect of centrifugal forces in stiffening the blade is reflected in the

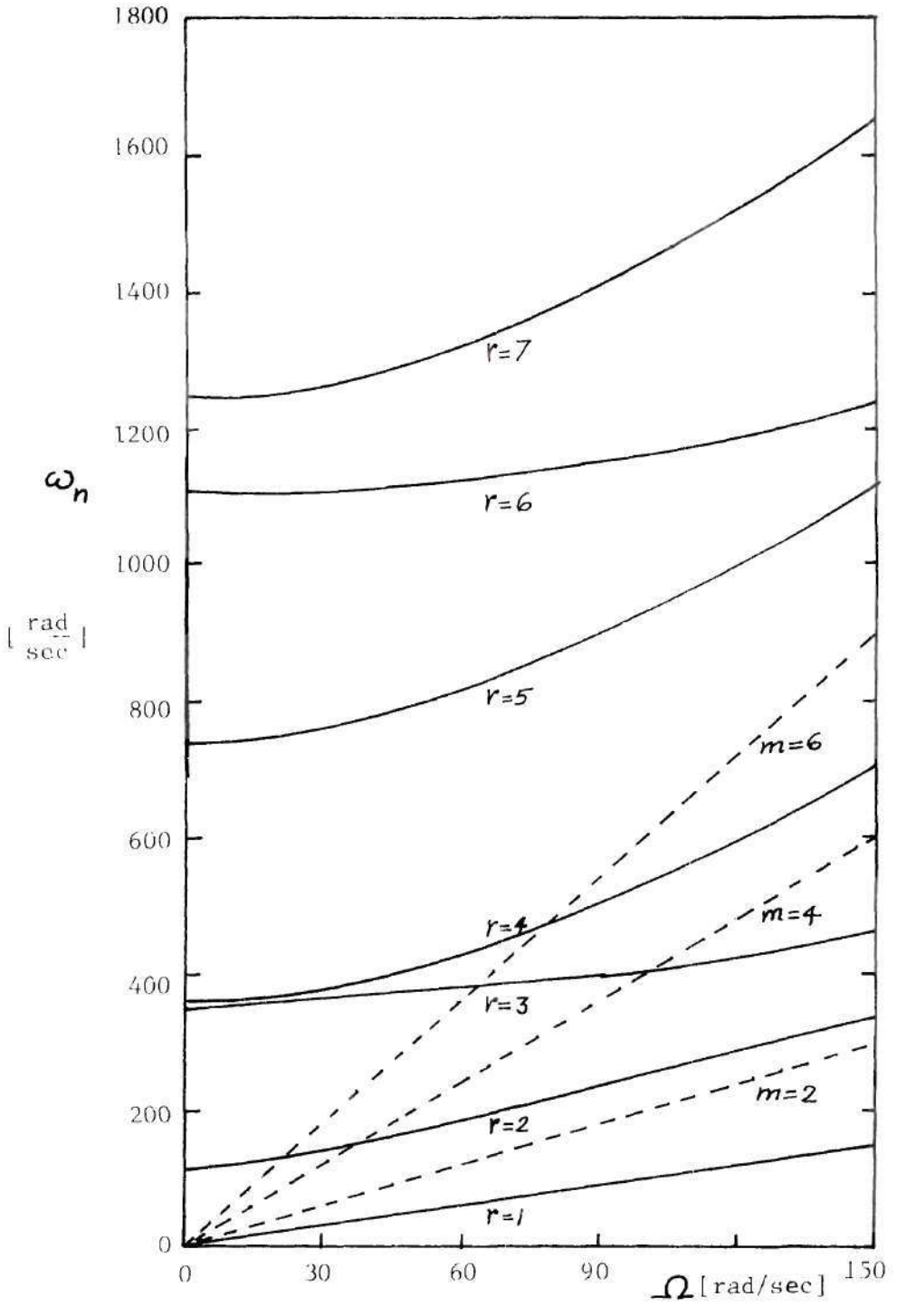

Figure 3. Variation of the Natural Frequencies of Blade No. 1 (Hinged Root) with Rotor Speed.

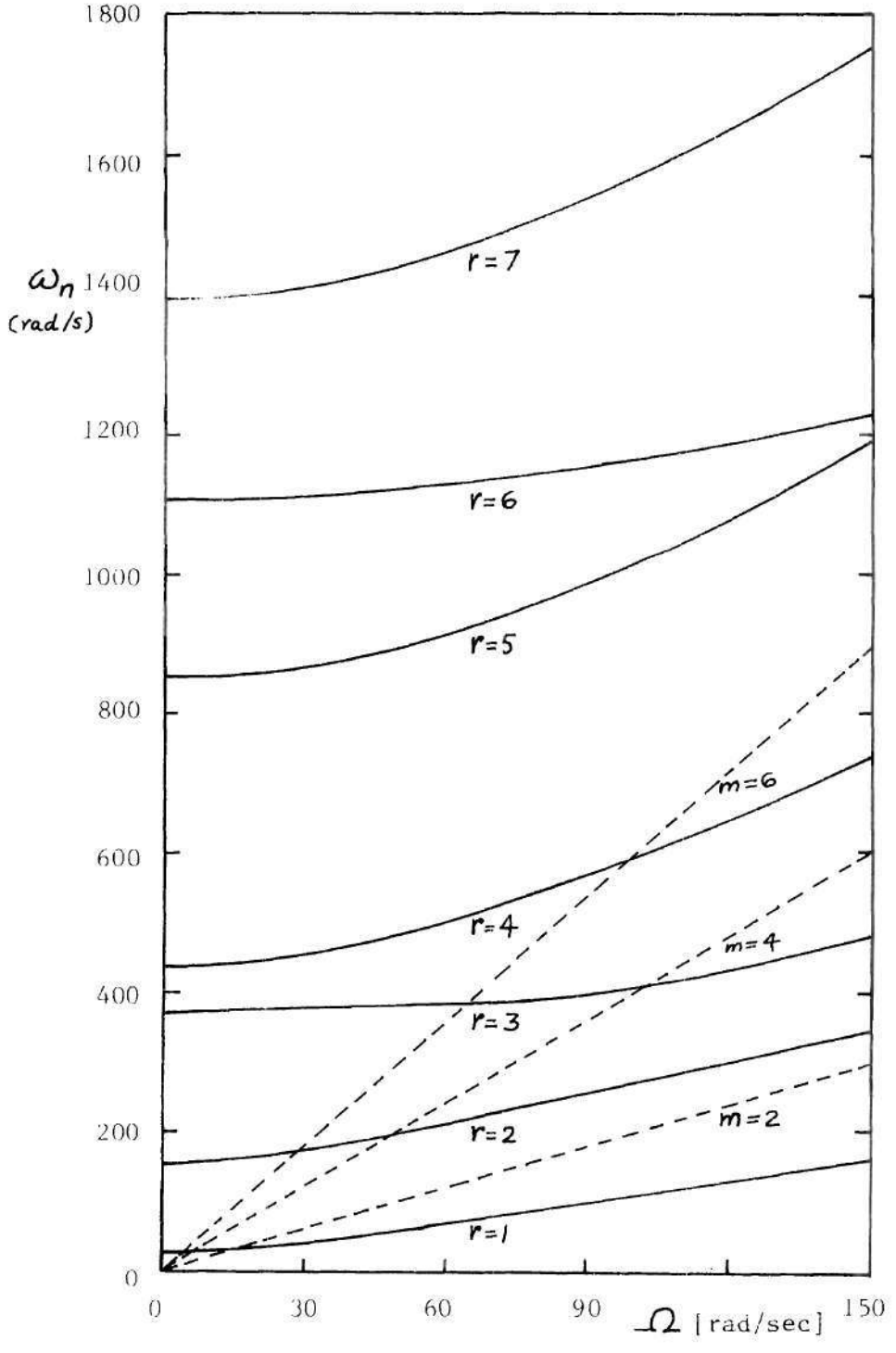

Figure 4. Variation of the Natural Frequencies of Blade No. 2 (Cantilevered Root) With Rotor Speed.

monotonic increase of the natural frequencies with rotor speed. All the points lying on a straight line though the origin in these two Figures, are such that they have the same value for the ratio of natural frequency to rotor speed. It is conventional to draw these fan lines because the frequency ratio can then be readily seen at any point of interest.

Figures 5(a) through 5(h) illustrate the first seven mode shapes of Blade No. 1 at $\Omega^* = 0$ and $\Omega^* = 12.53$. Figures 6(a) through 6(g) illustrate the first seven mode shapes of Blade No. 2 at $\Omega^* = 0$ and $\Omega^* = 12.53$.

Figure 5(a) shows that the first mode of Blade No. 1 is essentially a flapping mode with no torsional deflection at $\Omega^* = 0$ and very small torsional deflection at $\Omega^* = 12.53$. Figure 3 shows that the natural frequency of this mode is essentially the same as that of the rotor speed. The graph of the first mode shape of Blade No. 2 can be seen in Figure 6(a). The bending part is the first cantilever mode and there is little torsional deflection. For $\Omega > 30$ rad/sec., the frequency of this mode is only slightly higher than the rotor speed.

Figure 5(b) shows the second mode shape of Blade No. 1. This is predominantly a bending mode at lower rotor speeds. Figure 3 shows the considerable influence of rotor speed in increasing the natural frequency of this mode. Figure 6(b) is the graph of the second mode shape of Blade No. 2; this is also a predominantly bending mode at low rotor speeds.

It is generally observed that modes exhibiting predominantly torsional deflections are relatively unaffected by rotor speed in terms of changes in natural frequency. Figures 3 and 4 show small increases

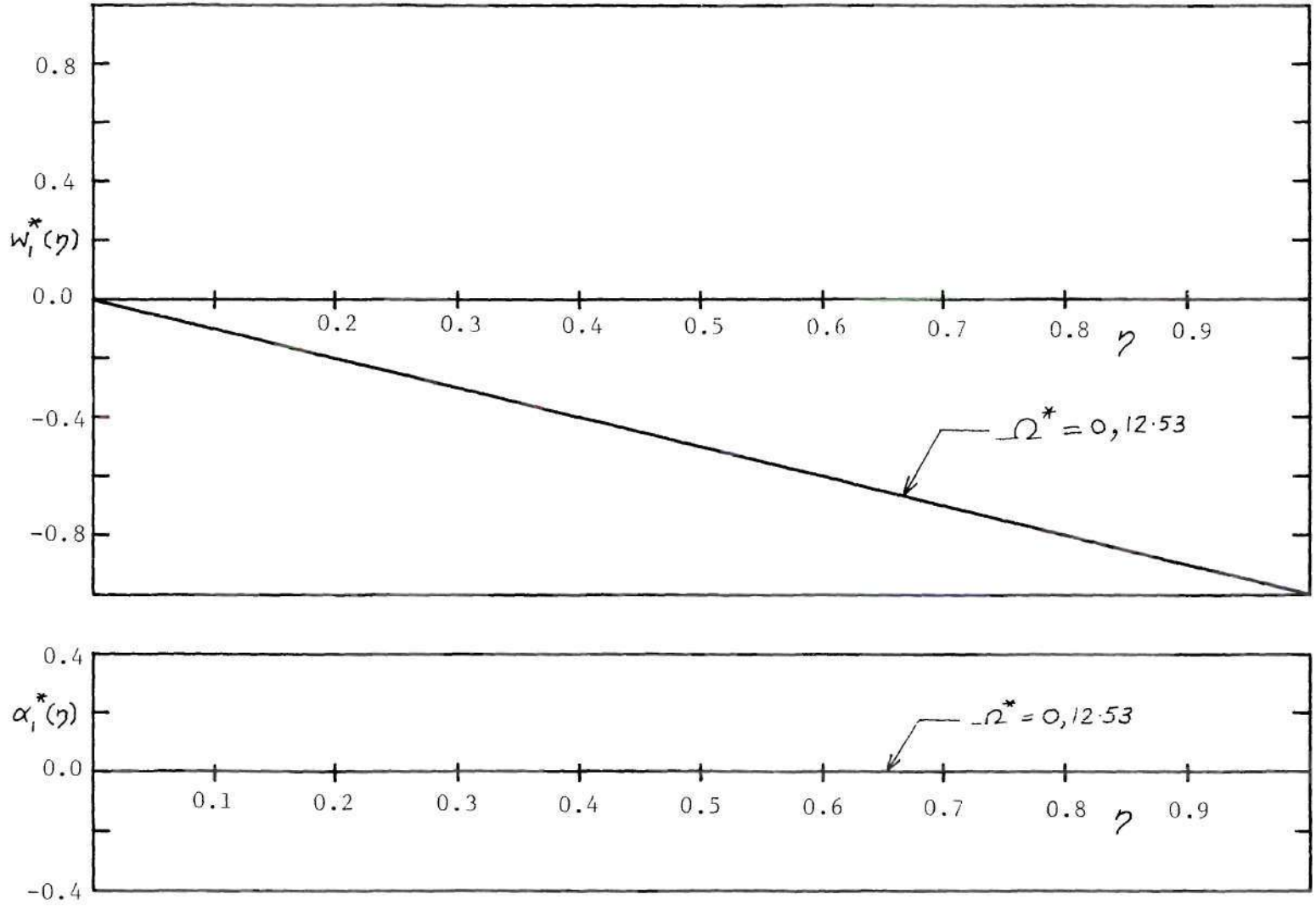

Figure 5a. The First Mode Shape of Blade No. 1.

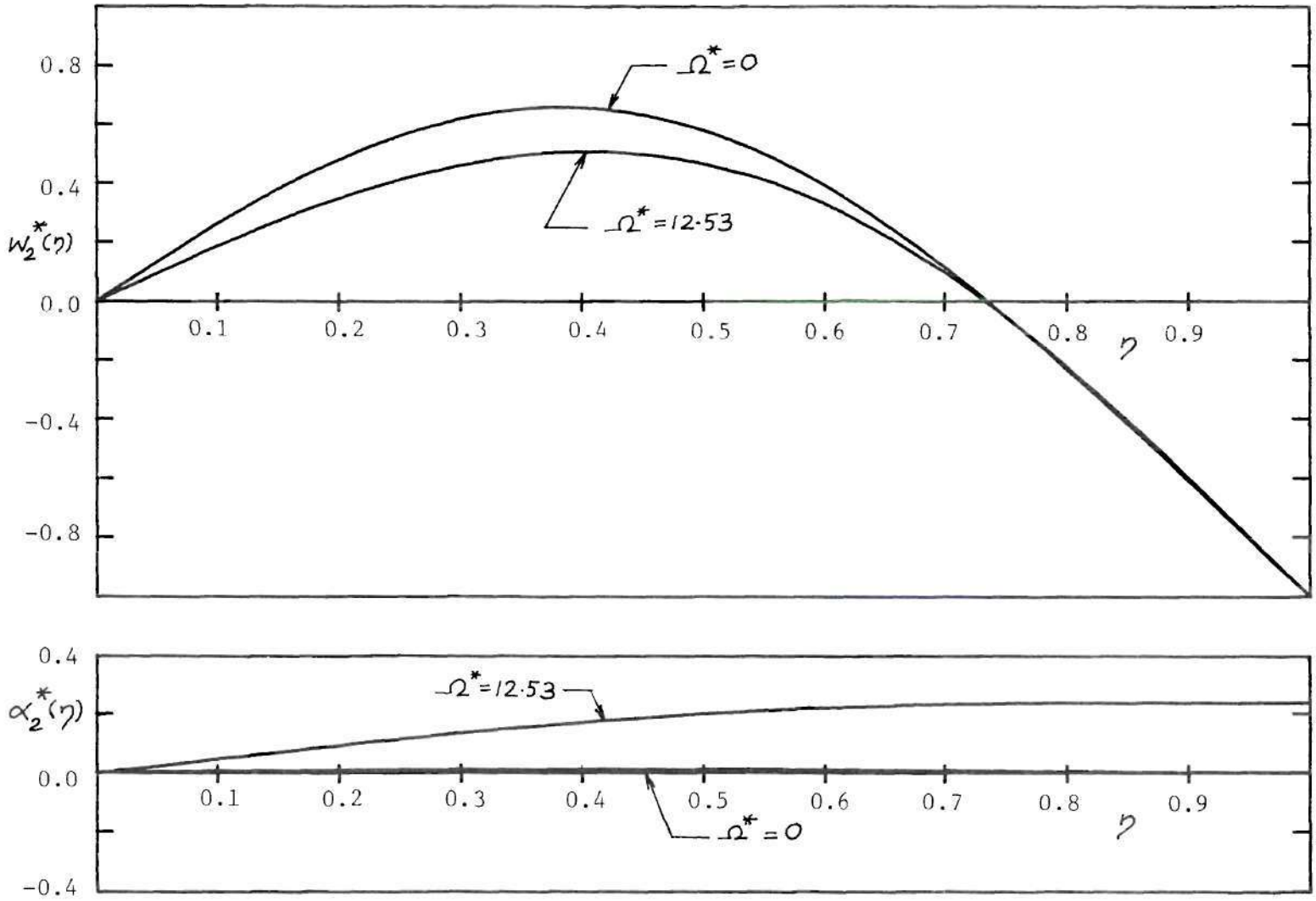

Figure 5b. The Second Mode Shape of Blade No. 1.

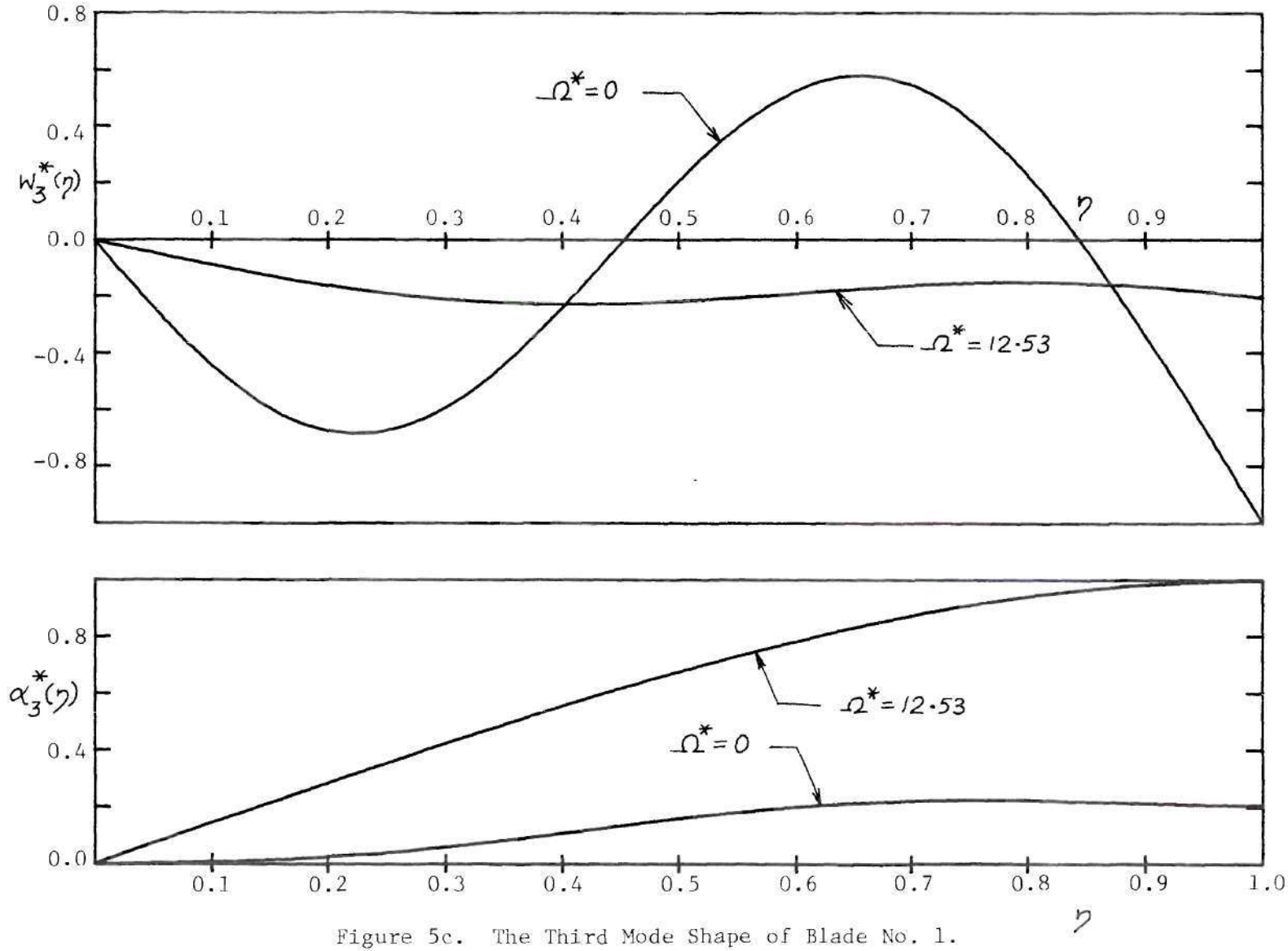

Figure 5c. The Third Mode Shape of Blade No. 1.

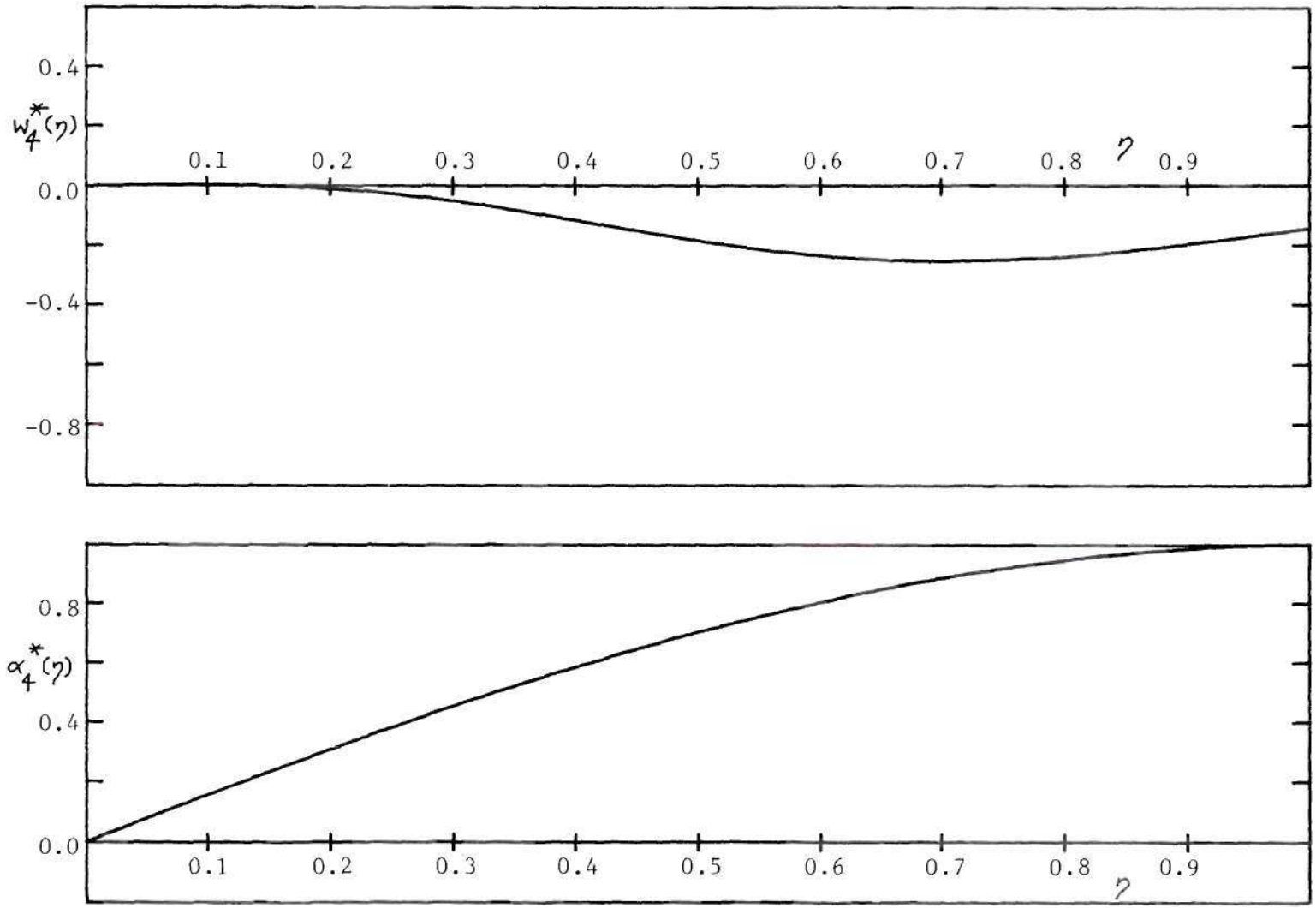

Figure 5d. The Fourth Mode Shape of Blade No. 1 at $\Omega^* = 0$.

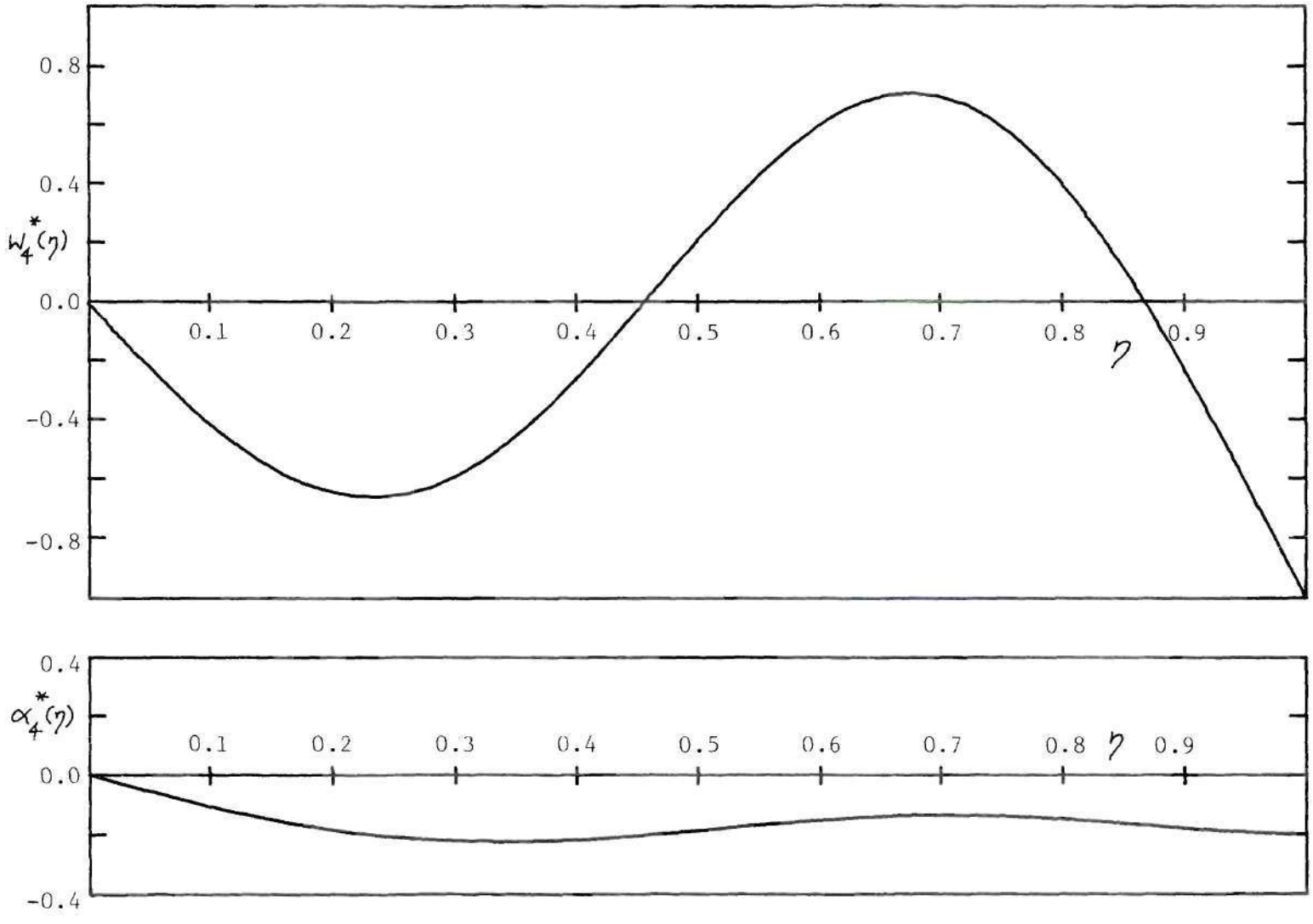

Figure 5e. The Fourth Mode Shape of Blade No. 1 at $\Omega^* = 12.53$.

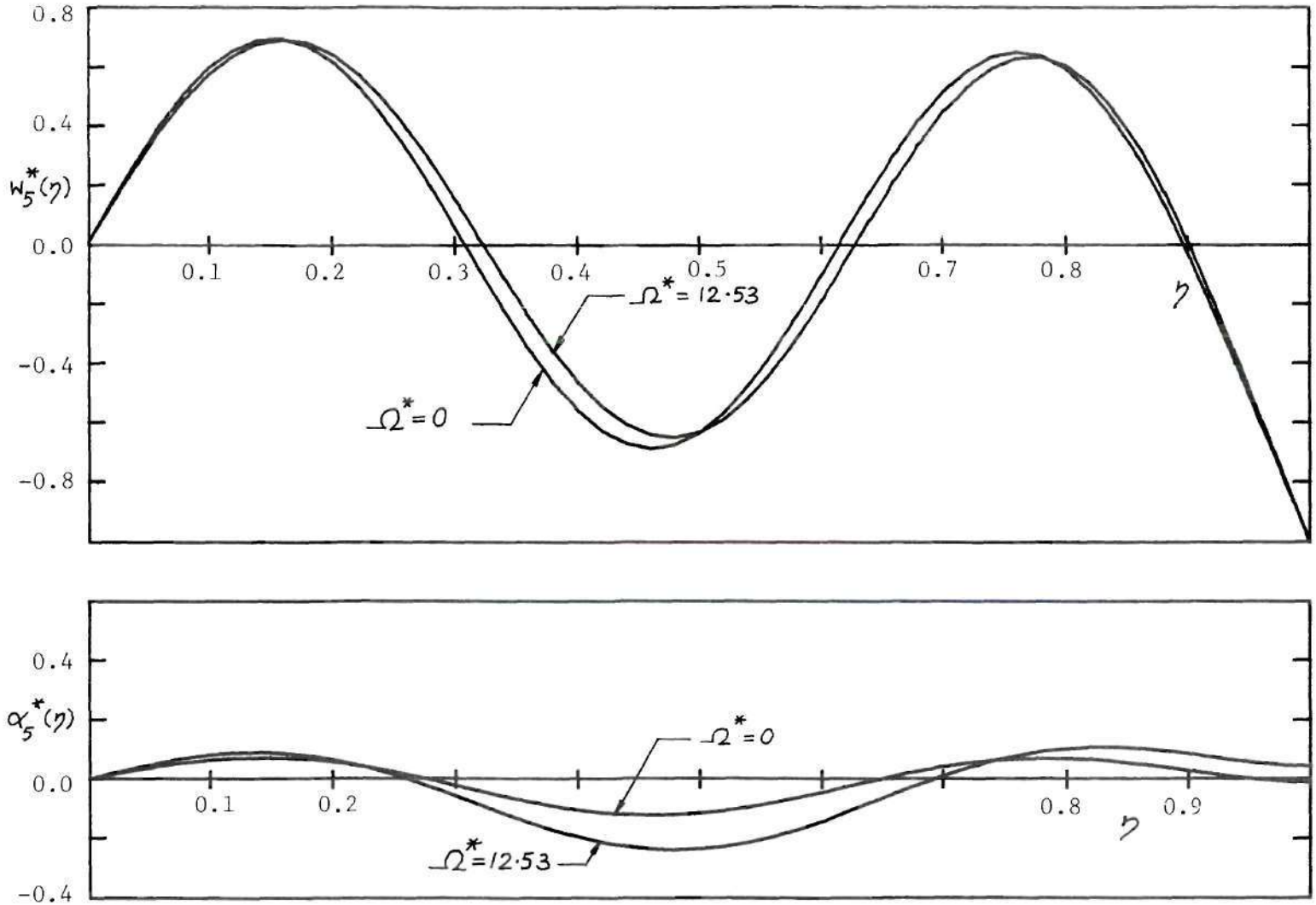

Figure 5f. The Fifth Mode Shape of Blade No. 1.

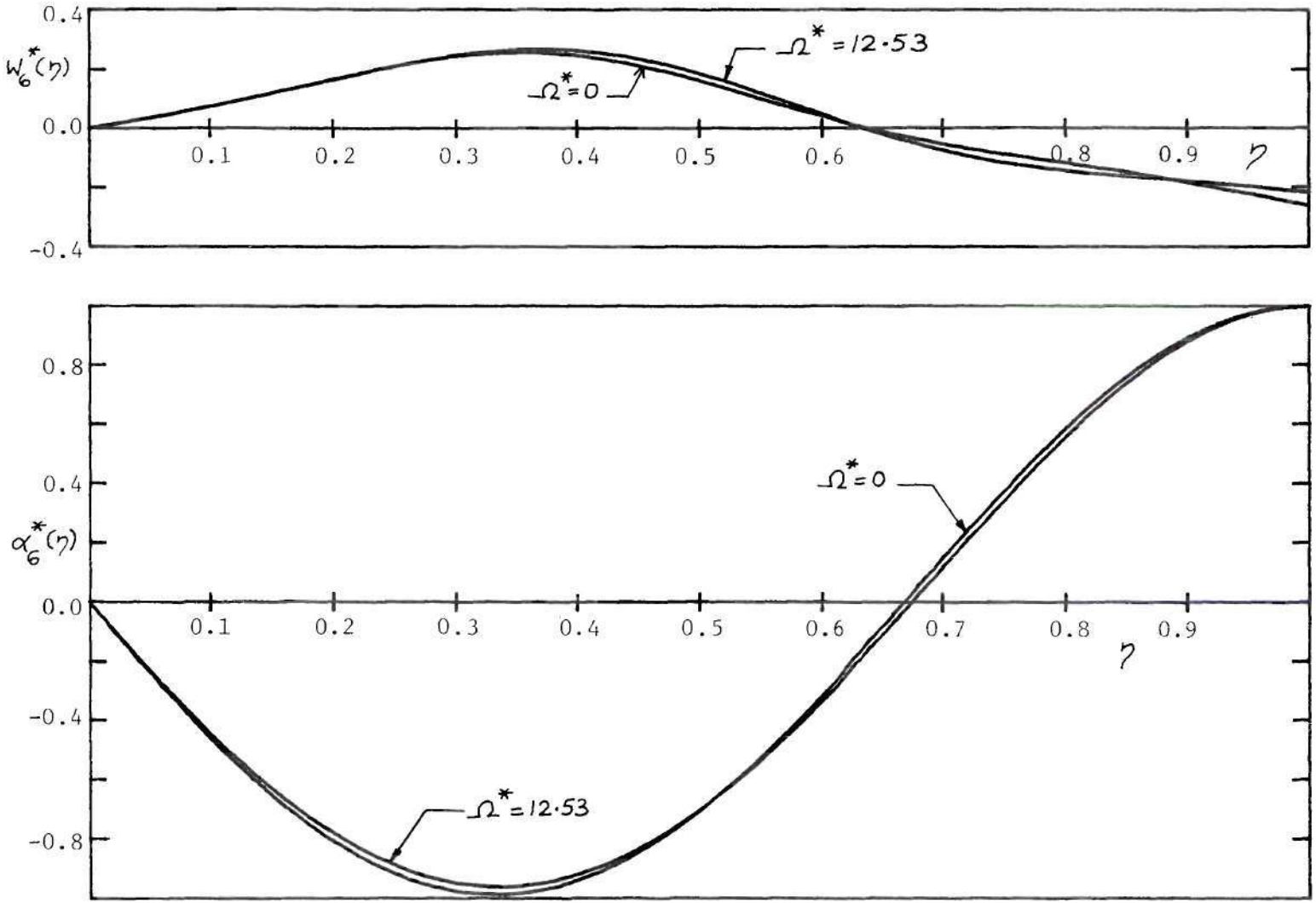

Figure 5g. The Sixth Mode Shape of Blade No. 1.

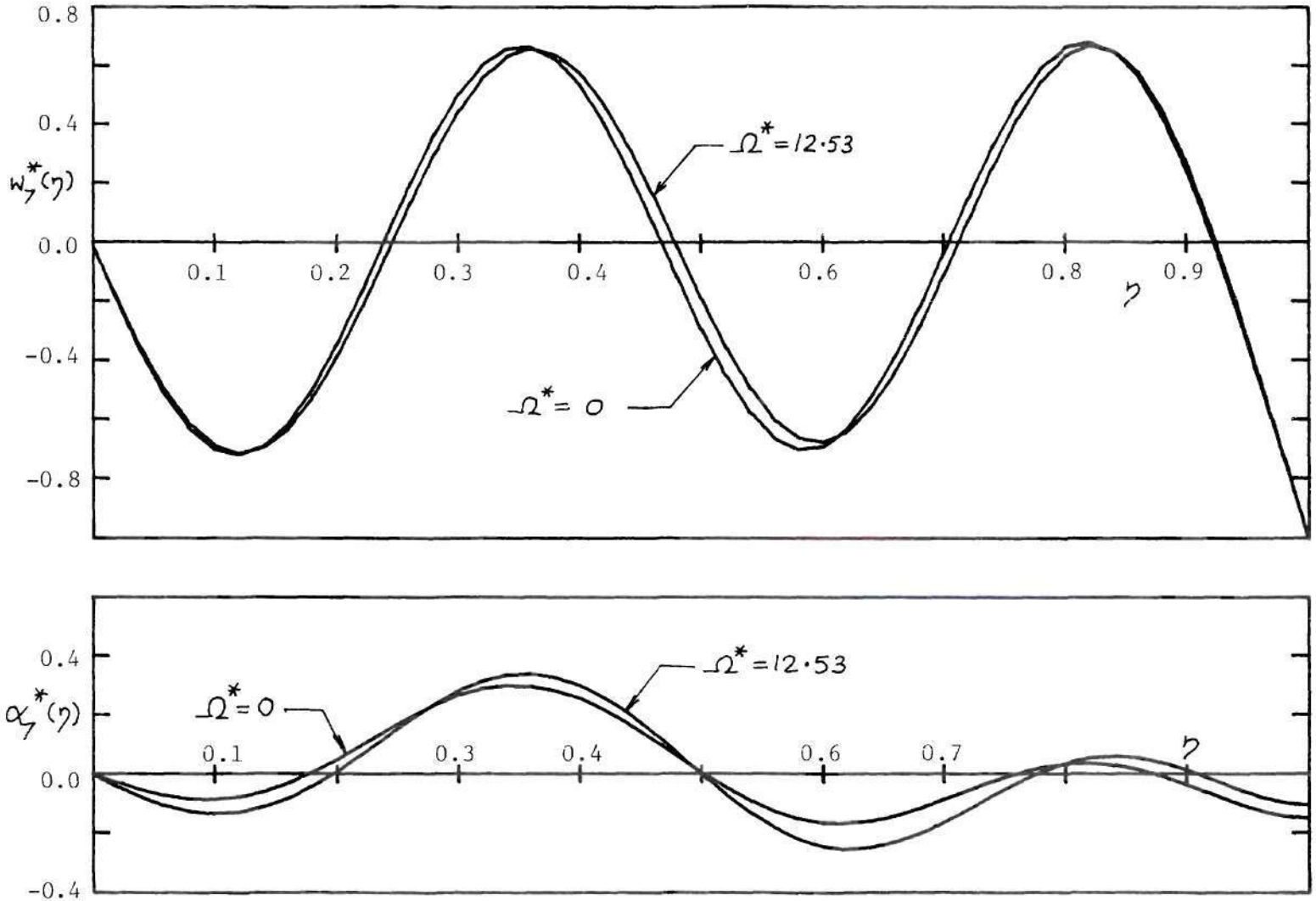

Figure 5h. The Seventh Mode Shape of Blade No. 1.

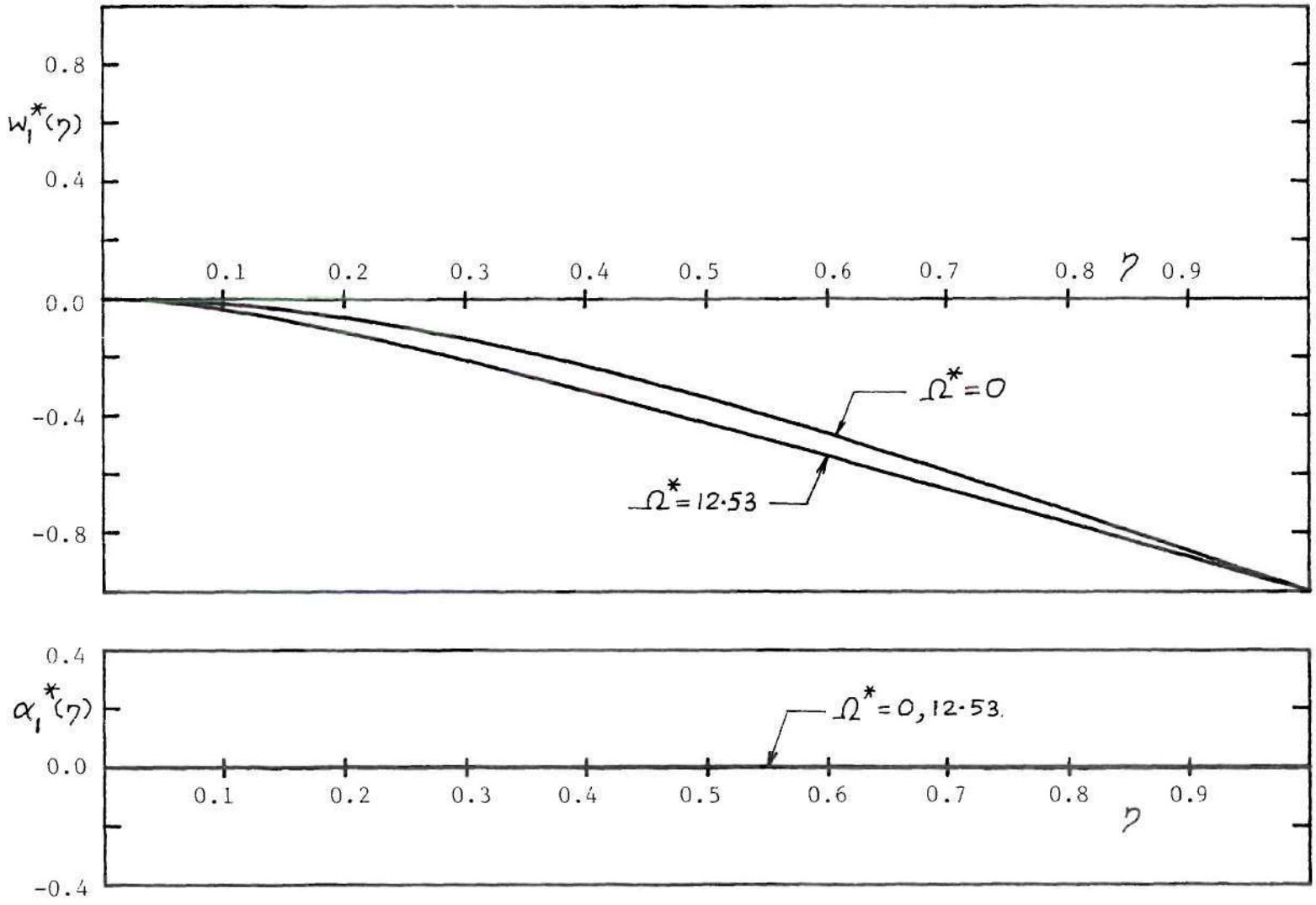

Figure 6a. The First Mode Shape of Blade No. 2.

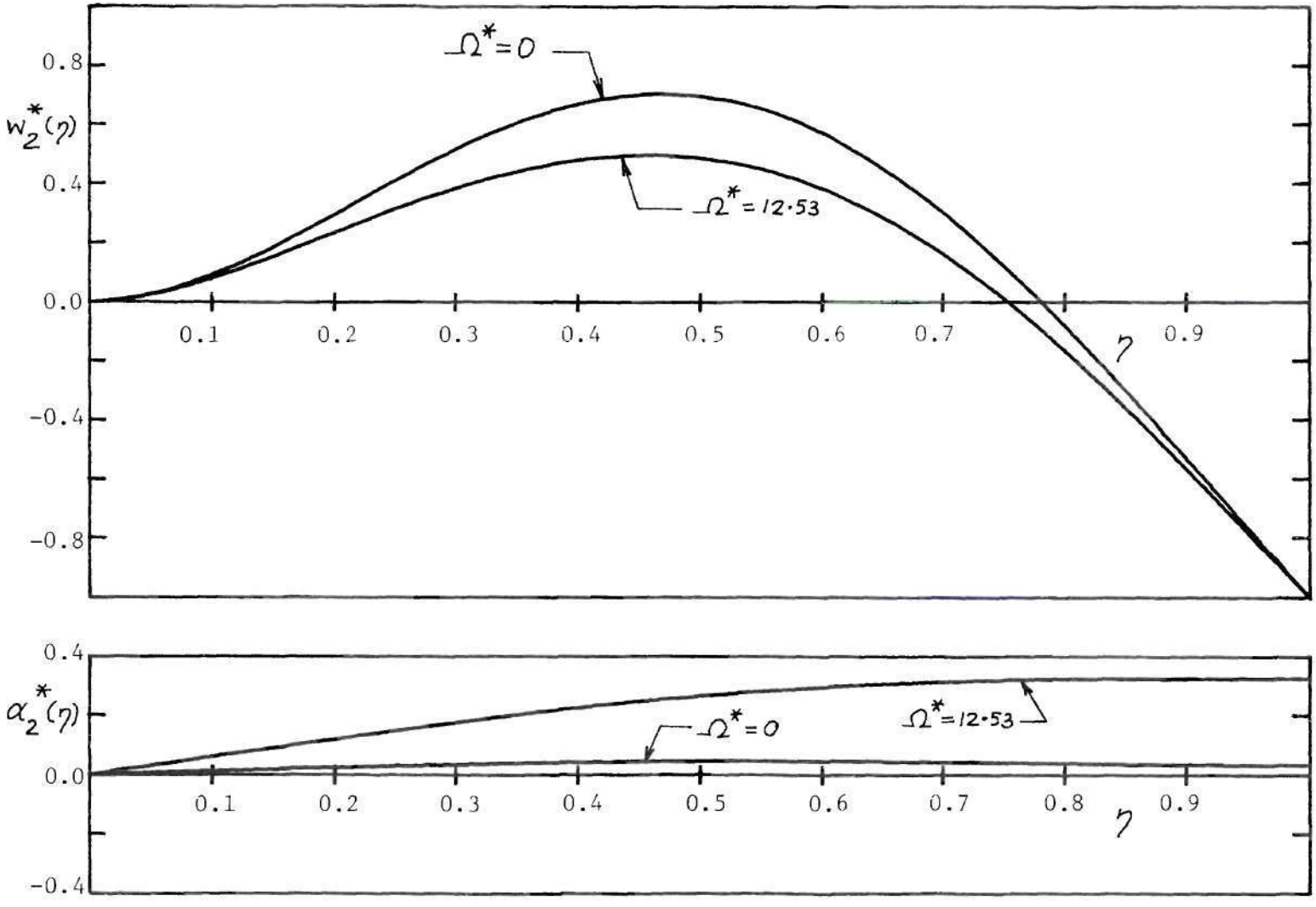

Figure 6b. The Second Mode Shape of Blade No. 2.

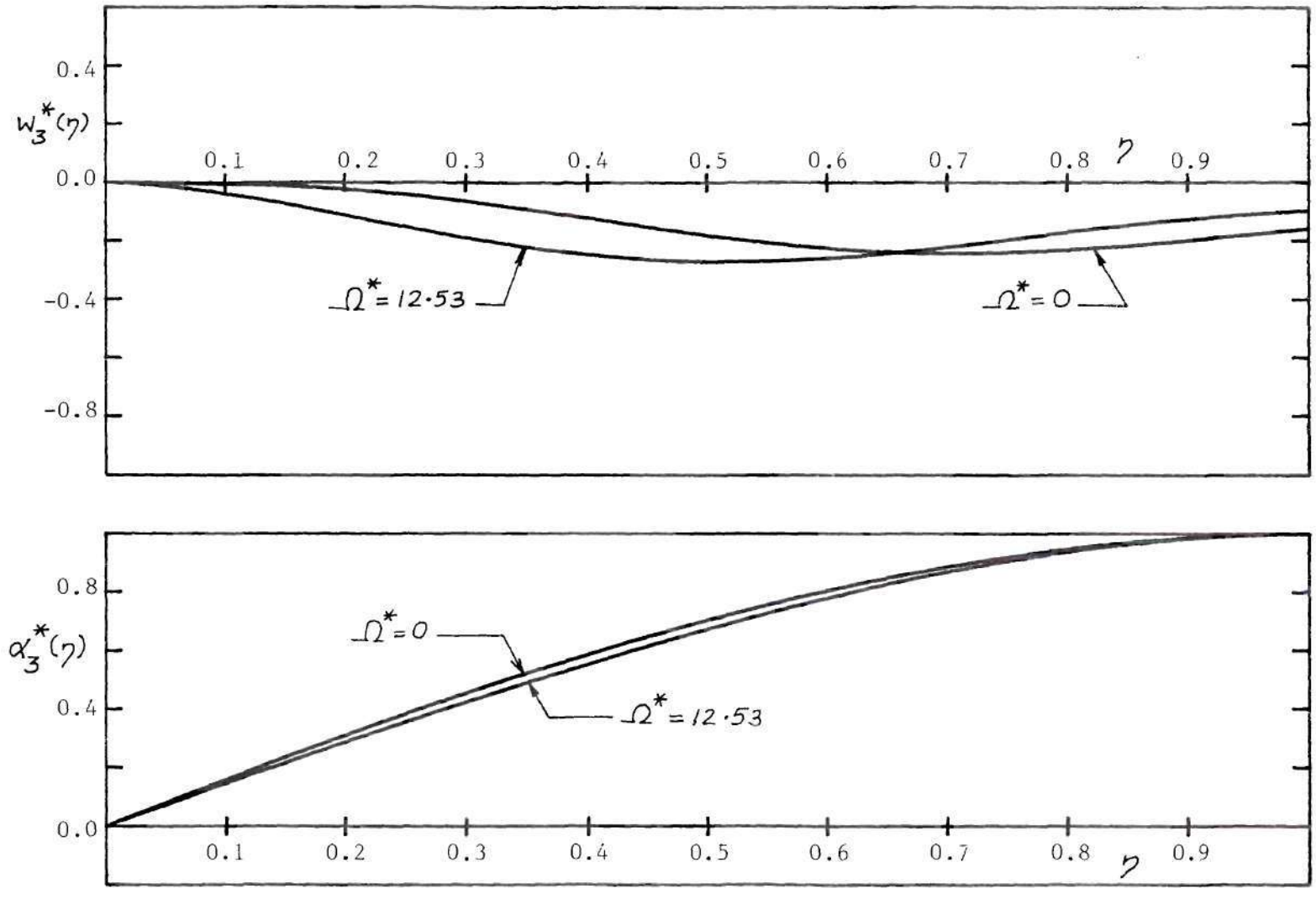

Figure 6c. The Third Mode Shape of Blade No. 2.

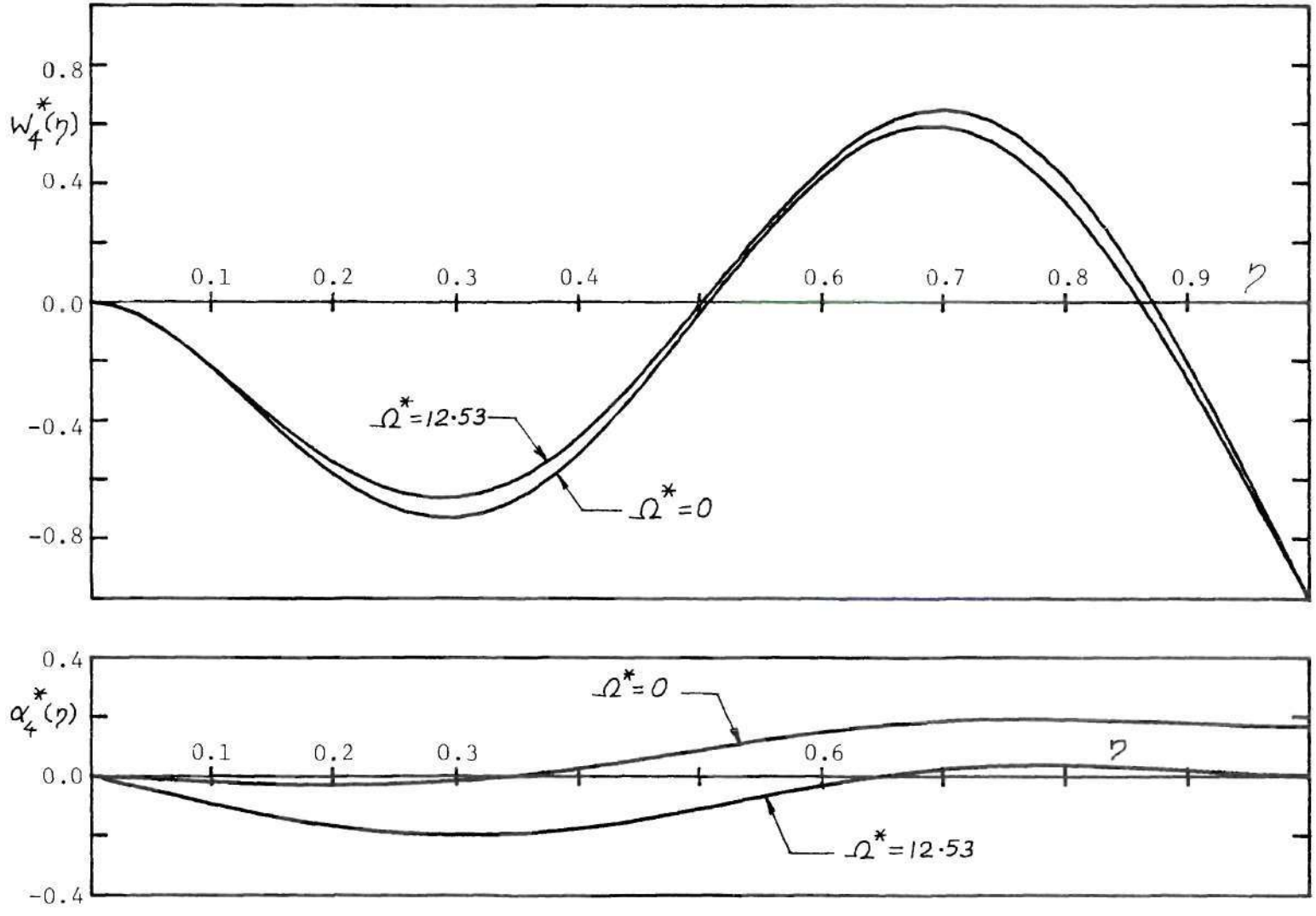

Figure 6d. The Fourth Mode Shape of Blade No. 2.

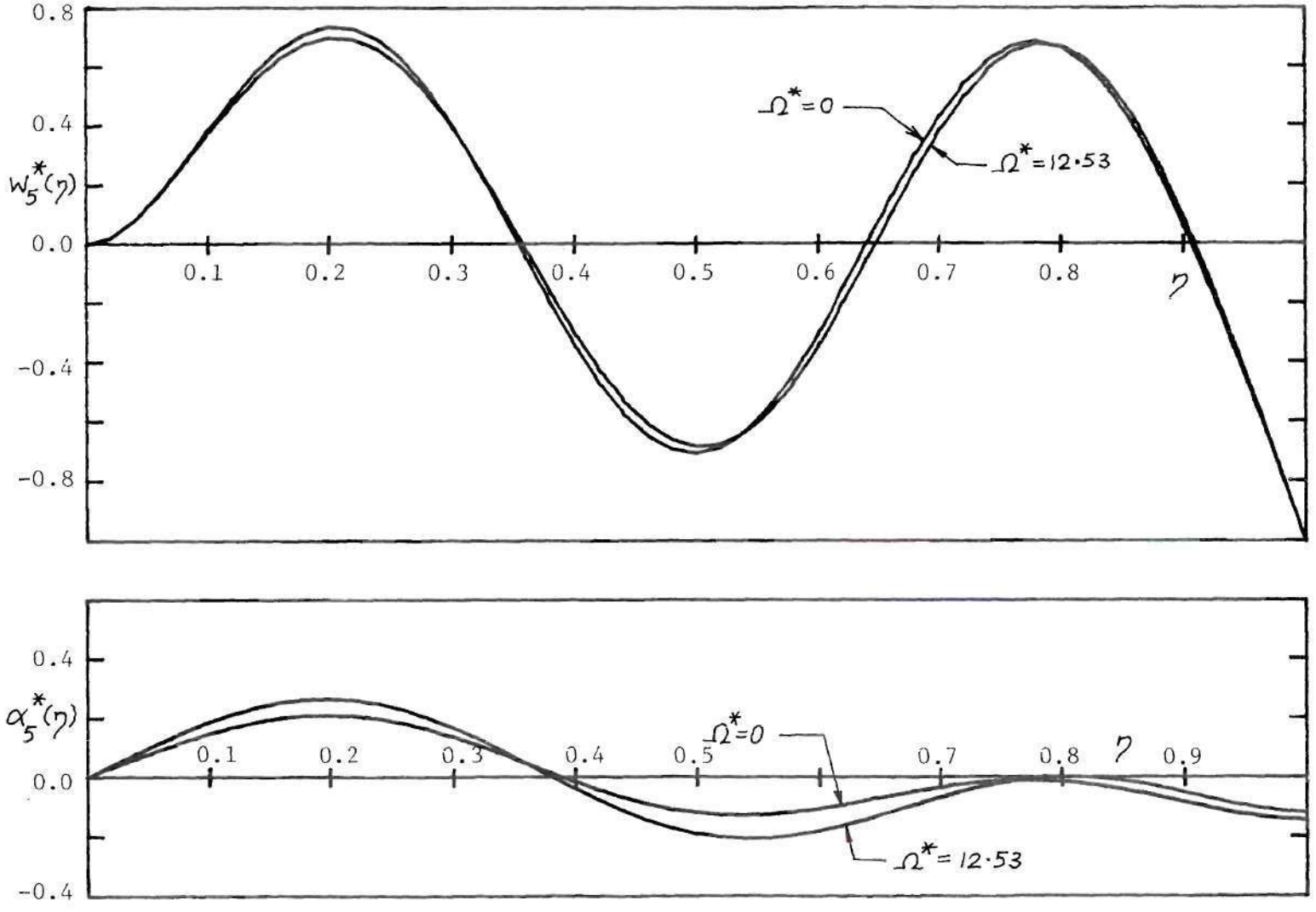

Figure 6e. The Fifth Mode Shape of Blade No. 2.

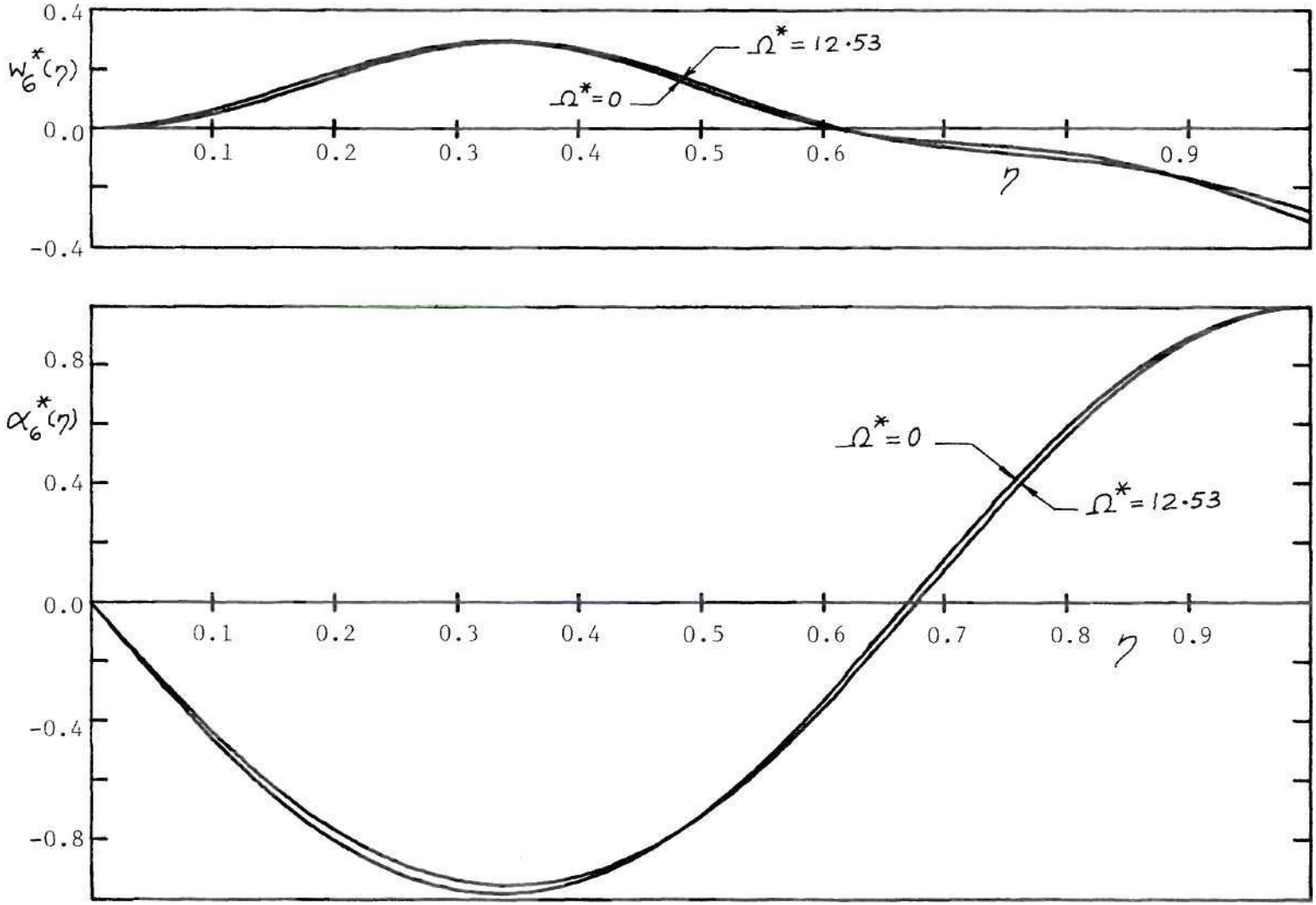

Figure 6f. The Sixth Mode Shape of Blade No. 2.

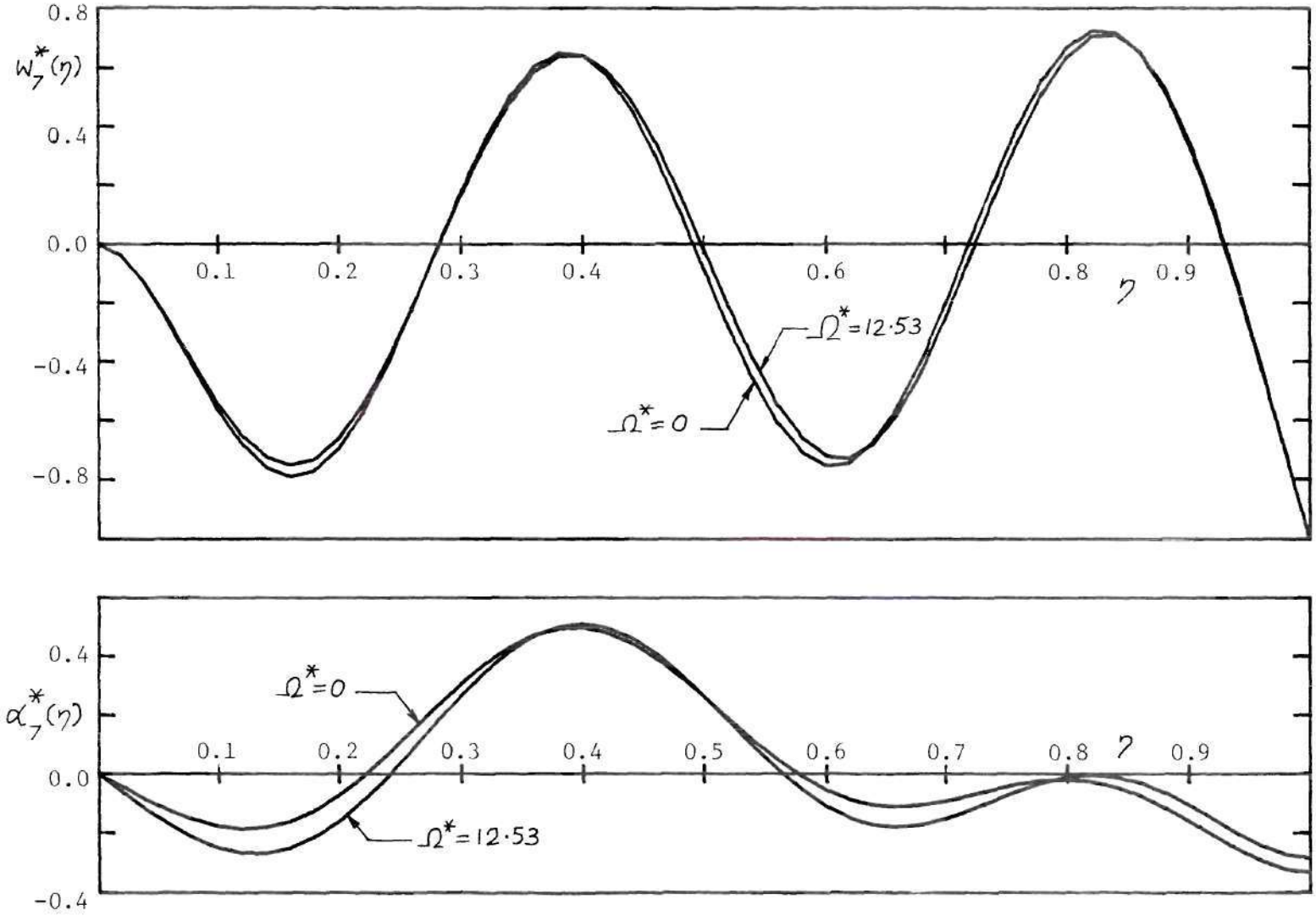

Figure 6g. The Seventh Mode Shape of Blade No. 2.

for the natural frequencies of the third mode whereas large changes are observed for the fourth mode of both blades. At $\Omega^* = 0$, because of the close vicinity of third and fourth modes, the third mode exhibits considerable bending (see Figure 5(c)). But at $\Omega^* = 12.53$, the bending part of this mode loses both the nodal points and the mode becomes predominantly torsional. This demonstrates the complex interaction of centrifugal forces and bending-torsion coupling effects. However, the third mode shape of Blade No. 2 as can be seen plotted in Figure 6(c) is predominantly torsional. There is also a considerable separation in the natural frequencies of the third and fourth modes for this blade even at low rotor speeds.

For Blade No. 1, the fourth mode also has a drastic change in the mode shape as the rotor speed changes from $\Omega^* = 0$ to $\Omega^* = 12.53$ (see Figure 5(d)). But Blade No. 2 (see Figure 6(d)) exhibits predominant bending oscillations in the fourth mode. The natural frequencies of the fourth mode for both blades increase considerably with rotor speed (Figures 3 and 4).

The fifth and seventh modes of both the blades are predominantly bending and their natural frequencies are highly dependent on rotor speed (see Figures 3,4,5(f),5(h),6(e) and 6(g)). It can also be noted that the mode shapes of the fifth and seventh modes of one blade are similar to those of the other blade. Comparing the plots in Figures 3 and 4, it is seen that the fixed root results in higher frequencies than hinged root, in case of predominantly bending modes.

The sixth mode for either blade is predominantly torsional as shown in Figures 5(g) and 6(f). As can be expected, the difference in

the root boundary condition has not affected either the frequency or the mode shape (see Figures 3 and 4). This is because of the fact that as far as torsional deformation goes, hinged as well as fixed roots provide only a fixed boundary condition. The frequencies of the third mode for both the blades are approximately equal at all rotor speeds; this is another indication that this mode is also predominantly torsional.

For both the blades, the bending deflections of the fifth, sixth and seventh modes show respectively 3, 1, and 4 nodal points. Although generally an ordered increase in the number of nodal points can be expected with increasing mode number, it is believed that this need not always happen. The frequency determinant was examined carefully at some high rotor speeds and the behaviour of the determinant function was found to be satisfactory. It is further believed that the seven modes shown in the graphs for each blade are free of significant numerical errors.

A final remark is made regarding the effect of rotor speed on mode shapes. For the fifth, sixth and seventh modes of either blade, the mode shapes are not very different for $\Omega^* = 0$ and $\Omega^* = 12.53$. For the Blade No. 2 it can be said that for $0 \leq \Omega^* \leq 12.53$, all the mode shapes are similar at least in "pattern," but for Blade No. 1, the third and fourth modes are considerably different at different rotor speeds. These factors must be considered if an attempt is made to use non-rotating mode shapes in a dynamic response analysis of a rotating beam.

Orthogonality and the Generalized Equations of Motion

The mode shape of the r-th mode, $\alpha_r(y)$ and $w_r(y)$, and the frequency

ω_r, satisfy the differential equations (10) and (11) and boundary conditions (8). An orthogonality property can be derived which states that for $\omega_r \neq \omega_s$, i.e., for the r-th and s-th modes possessing distinct frequencies,

$$\int_o^R \bar{m}\{w_r w_s + k_m^2 \alpha_r \alpha_s - e(w_r \alpha_s + w_s \alpha_r)\}dy = 0 \tag{21}$$

If a solution is sought of the form

$$\begin{aligned} \alpha(y,t) &= \sum_{r=1}^{\infty} \alpha_r(y)\xi_r(t) \\ w(y,t) &= \sum_{r=1}^{\infty} w_r(y)\xi_r(t) \end{aligned} \tag{22}$$

for the differential equations (7), then the normal coordinates $\xi_r(t)$ are obtained by solving

$$M_r \ddot{\xi}_r(t) + \omega_r^2 M_r \xi_r(t) = \Xi_r(t), \quad r = 1,2,3,... \tag{23}$$

where

$$M_r = \int_o^R \bar{m}\{w_r^2 + k_m^2 \alpha_r^2 - 2e w_r \alpha_r\}dy \tag{24}$$

and

$$\Xi_r(t) = \int_o^R f(y,t)w_r(y)dy + \int_o^R q(y,t)\alpha_r(y)dy \tag{25}$$

When f and q are known, $\Xi_r(t)$ can be computed and $\xi_r(t)$ can be determined from Equation (23). Then the response of the beam is obtained from the modal series of Equation (22).

For the uniform example blades, Equation (21) implies that

$$\int_0^1 \{w_r^* w_s^* + r_\alpha^2 \alpha_r^* \alpha_s^* - (\frac{e}{b})[w_r^* \alpha_s^* + w_s^* \alpha_r^*]\}\, d\eta = \tilde{M}_{rs} = \tilde{M}_{sr} = \begin{cases} 0 & \text{if } r \neq s \\ \dfrac{M_r}{mb^2R} & \text{if } r = s \end{cases} \tag{26}$$

$\tilde{M}_{rs}$ has been evaluated for Blades No. 1 and 2 at several rotor speeds. It has been observed to form an almost diagonal matrix at every rotor speed. Tables 1 and 2 illustrate the 7 x 7 $\tilde{M}_{rs}$ matrix for both the blades at $\Omega^* = 12.53$. The nonvanishing of the off-diagonal elements is due to the numerical inaccuracy of the normal modes shown in Figures 5(a) through 5(h) and 6(a) through 6(g). However, the results can be considered quite satisfactory.

Table 1. $\tilde{M}_{rs}$ Matrix for Blade No. 1 at $\Omega^* = 12.53$

r \ s	1	2	3	4	5	6	7
1	0.33333						
2	-0.033×10^{-6}	0.19320					
3	-0.051×10^{-6}	-0.074×10^{-6}	0.096265			$\tilde{M}_{rs} = \tilde{M}_{sr}$	
4	-0.137×10^{-6}	0.208×10^{-6}	0.341×10^{-6}	0.26371			
5	-0.302×10^{-6}	-0.330×10^{-6}	0.357×10^{-6}	0.330×10^{-6}	0.25211		
6	-0.062×10^{-6}	-0.098×10^{-6}	-0.010×10^{-6}	-0.327×10^{-6}	-1.223×10^{-6}	0.091576	
7	-1.072×10^{-6}	-0.384×10^{-6}	0.351×10^{-6}	-1.652×10^{-6}	-2.394×10^{-6}	2.677×10^{-6}	0.27620

Table 2. $\tilde{M}_{rs}$ Matrix for Blade No. 2 at $\Omega^* = 12.53$

r \ s	1	2	3	4	5	6	7
1	0.29036						
2	-0.248×10^{-6}	0.18344				$\tilde{M}_{rs} = \tilde{M}_{sr}$	
3	-0.017×10^{-6}	-0.228×10^{-6}	0.097163				
4	0.059×10^{-6}	-0.268×10^{-6}	0.389×10^{-6}	0.23654			
5	-0.761×10^{-6}	0.483×10^{-6}	0.148×10^{-6}	-1.885×10^{-6}	0.26795		
6	-0.162×10^{-6}	0.017×10^{-6}	-0.016×10^{-6}	-0.869×10^{-6}	-0.536×10^{-6}	0.092588	
7	-0.697×10^{-6}	-1.714×10^{-6}	0.919×10^{-6}	1.482×10^{-6}	-10.0×10^{-6}	2.182×10^{-6}	0.30184

CHAPTER III

UNSTEADY AERODYNAMICS AND FLUTTER EQUATIONS

In this chapter, the flow about a rotor operating at a steady mean inflow with small simple harmonic perturbations in flow parameters is briefly discussed, and some theories available to determine the unsteady forces are reviewed. A simple example is used to illustrate the importance of considering the wakes below the rotor. The flutter equations with this flow phenomenon are derived.

Unsteady Rotor Flow Field

A rotor in hovering or ascending vertical flight trails a tip vortex which is blown axially downward so that, if otherwise undisturbed, it would form a contracting helix as shown in Figure 7(a). For simplicity, consider that the inflow over the disc, u, is constant; then, the fluid that comes off the trailing edge of the blades makes a helical surface with horizontal radial elements (see Figure 7(b)).

Now, if there is an oscillation in blade effective angle of attack, blade lift will alternate also, and as a result of these changes in lift, vortices will be shed continuously at the blade trailing edge. These vortices fall along the horizontal radial elements of the helical surface shown in Figure 7(b), so long as the oscillations in angle of attack are small. Figure 7(c) shows this helical sheet of shed vorticity. Vorticity is considered to be on the helical surface and the vertical displacements from that surface (as in Figure 7(c)) represent the strength

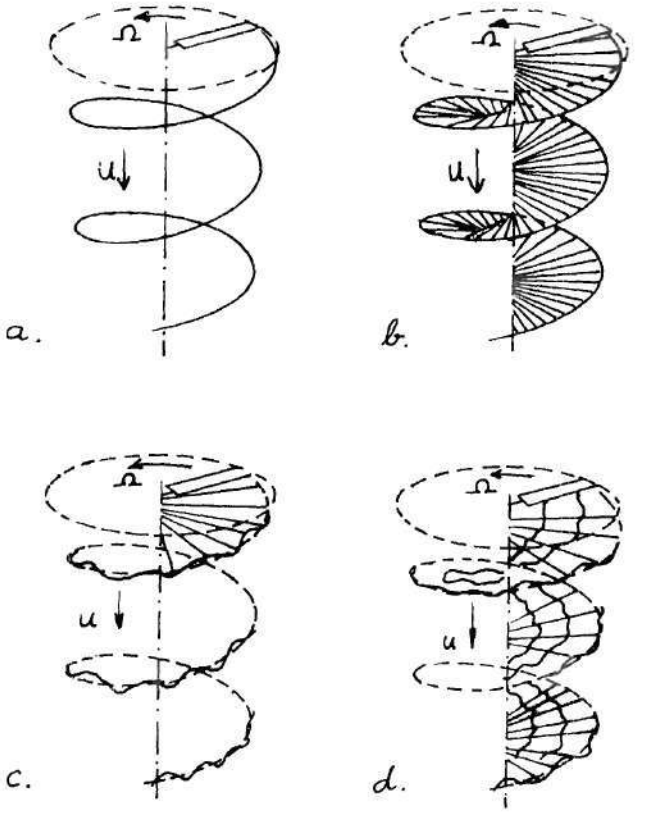

Figure 7. Schematic Elements of Unsteady Rotor Flow Field.

of the vorticity at a particular azimuthal and radial position. The variation in the vortex strength around the azimuth corresponds to the history of the motion of a given blade element at a fixed radius; the variation of the shed vortex strength in the radial direction at any fixed azimuth angle is a function of the variation with the blade span of 1) blade chord, 2) amplitude of the oscillation in effective angle of attack and 3) relative air velocity. A variation of shed vorticity in the radial direction implies the existence of trailing vortices at constant radii similar to and inboard of the tip vortex. These trailing vortices have been included in Figure 7(d).

The schematic drawings of Figure 7(a) through 7(d) indicate pictorially the complexities of attempting to obtain a complete representation of unsteady rotor aerodynamics. When $2\pi u/Q\Omega$, the vertical spacing between adjacent helical surfaces of shed vorticity, is very large, then one would expect that all shed vorticity beyond a small fraction of a revolution would be too far below the blade in question to have an effect on the blade loading. Under these conditions, it would be sufficient to account for only the attached vortex sheet within that fraction of a revolution, as in Figure 8(a). On the other hand, when $2\pi u/Q\Omega$ is very small, all the sheets of shed vorticity tend to pile up on each other, and the effect of that vorticity close to the blade in question (shed by the several previous blades and/or in the several previous revolutions) is of more importance than that which exists beyond a small aximuth angle on either side of the blade. This situation is depicted in Figure 8(b).

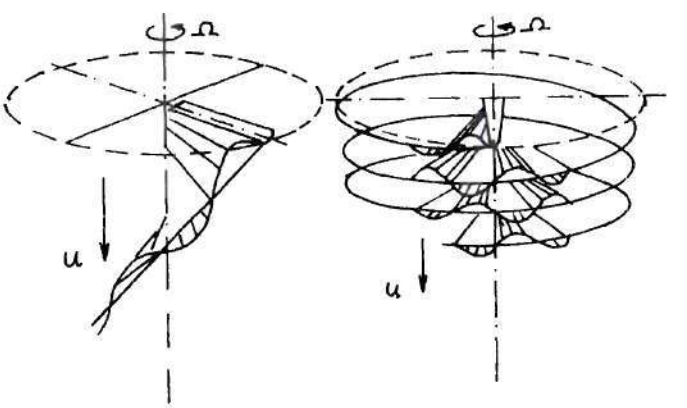

a. High Inflow b. Low Inflow

Figure 8. Schematic Representation of Unsteady Rotor Flow Field.

The first condition exists at high rotor thrust coefficients; the second condition is associated with low thrust coefficients and is encountered in "wake-flutter." Only the case of low inflow flutter is considered in this thesis. Henceforth, the aerodynamic models that are explained and used are for low inflow cases.

Loewy's Incompressible Aerodynamic Model

In arriving at a model which is mathematically tractable for the case of low inflow, it is assumed that only the vorticity contained within a small double azimuth angle straddling the blade is of real consequence. The flow problem at a given blade radius is considered two dimensional and this theory can then be applied in a strip theory fashion to a three-dimensional rotor. The portion of the circular cylindrical surface which is determined by 1) a particular blade radius, 2) the azimuth angle on either side of the blade section (within which the shed vorticity is of importance), and 3) the vertical distance spanned by a given number of rows of vorticity, can be developed and projected on to a plane - one in which the two-dimensional unsteady aerodynamic problem may be attacked. The above considerations form the basis for the incompressible flow model suggested by Loewy [10]. This model is shown in Figure 9. The aerodynamic lift and moment acting on the airfoil are evaluated in terms of nondimensional coefficients which are functions of reduced frequency, frequency ratio, inflow ratio, number of blades and the phase differences in the oscillation of other blades in the rotor with respect to the reference blade. In the case of compressible theories, the Mach number would also be included in the list of parameters on which the aerodynamic coefficients depend.

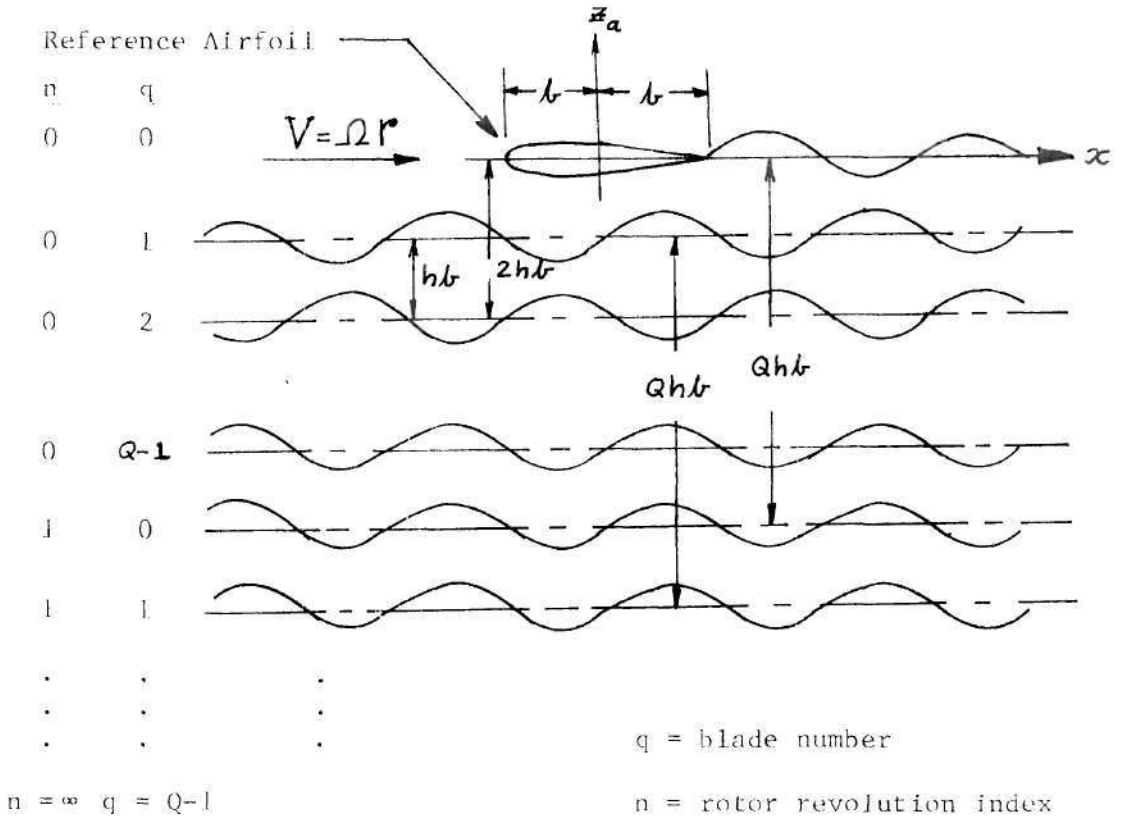

Figure 9. Loewy's Incompressible Aerodynamic Model.

Two Compressible Aerodynamic Theories

Jones and Rao [11] have solved the above problem for compressible flow utilizing a model very similar to that of Loewy [10]. Their analysis of the problem follows a technique developed earlier by Jones [12] for a two-dimensional fixed wing oscillating in subsonic flow.

Coincident with the work of Jones and Rao, Hammond and Pierce [13] independently analyzed a slightly different model of the two dimensional compressible problem. Their model is illustrated in Figure 10. By introducing the acceleration potential, the governing integral equation for the flow and its attendant downwash boundary condition are developed and solved numerically using a pressure mode assumption and a collocation technique. Hammond and Pierce [13] have shown that for small values of the frequency ratios near and above 1, the aerodynamic coefficients are in good agreement.

Pierce and White [1] employed the two compressible theories mentioned above, to predict the flutter speed of a model which had been flutter tested by Brooks and Baker [9]. Both the theories predicted flutter speeds which agreed well with the experimental results of Brooks and Baker. Frequency ratio is a dominant factor in the flutter analysis at low inflow. The flutter frequency ratio for the above case was 2.3 and corresponding to this value, the two theories are in close agreement. White [14] concluded from some theoretical flutter calculations that the theories of Jones and Rao [11] and Hammond and Pierce [13] predict essentially the same flutter speeds but the former theory requires significantly less computer time. For the flutter calculations of this thesis, the theory of Jones and Rao [11] will be used.

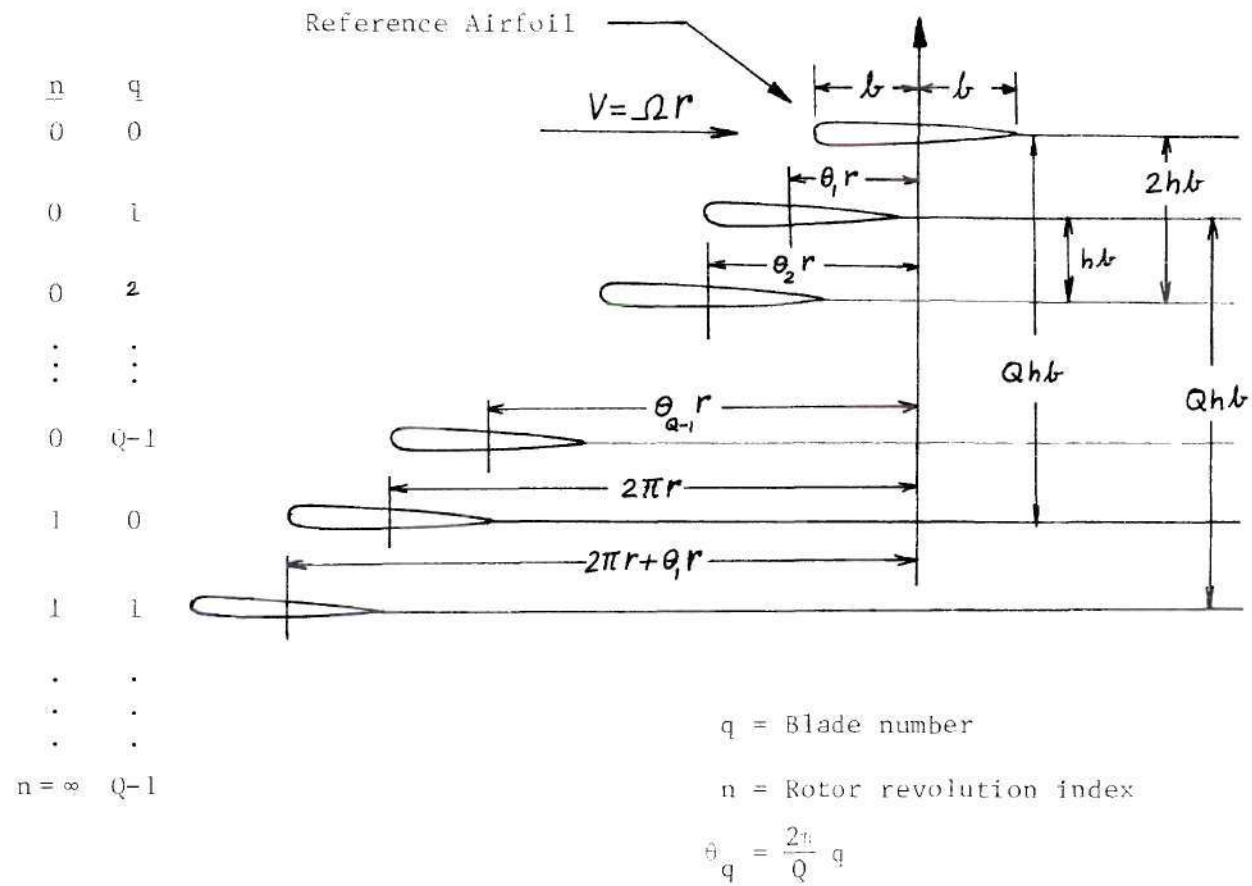

Figure 10. Compressible Aerodynamic Model of Hammond and Pierce [13] for a Multibladed Rotor.

Importance of Wake Effects

A simple example is given to show the importance of having to take into account the velocity induced by the vortex sheets that lie in the wake of the rotor.

Consider a single bladed rotor with uniform blade section properties along the span and with infinitely large bending and torsional stiffness. Let it be provided with a flapping hinge at the root and let $\beta(t)$ denote the flapping response in radians at time t. The equation of motion of this single degree of freedom system can be written as

$$I_f\ddot{\beta} + \Omega^2 I_f\beta = T(t) + \int_o^R \frac{dL}{dr}\, rdr \tag{27}$$

where

$$I_f = \int_o^R \bar{m}\, r^2 dr = \bar{m}\, R^3/3 \tag{28}$$

$T(t)$ is the externally applied moment about the flapping hinge in same sense as $\beta(t)$ and dL/dr is the lift per unit span at blade section r caused by the flapping motion. Equation (27) can be viewed as the balance of inertial moment, centrifugal restoring moment, externally applied moment and aerodynamic damping moment about the flapping hinge.

Consistent with the theory of the vibration of single degree of freedom damped systems, a damping ratio, ζ, can be defined through

$$\int_o^R \frac{dL}{dr} \cdot rdr = -2I_f\Omega\zeta\dot{\beta} \tag{29}$$

Since the aerodynamic moment is known to be not completely in phase with the velocity, a real number ζ cannot satisfy the above equation. In this example, a simple harmonic motion for flapping response is considered. Thus ζ as defined by Equation (29) will turn out to be a time invariant complex number denoting the phase and magnitude relationship of $\dot{\beta}$ with respect to aerodynamic moment.

Corresponding to

$$\beta = \beta_o \exp(i\omega t) \tag{30}$$

unsteady aerodynamic "strip" theory yields

$$dL/dr = \pi\rho_\infty \omega^2 b^2 L_h r \beta_o \exp(i\omega t) \tag{31}$$

where the aerodynamic coefficient $L_h(r)$ is symbolically written as

$$L_h(r) = L_h(k(r), m, h(r), M_\infty(r)) \tag{32}$$

It can now be shown that

$$\zeta = 1{\cdot}5 \ \mathrm{im}\left(\int_o^1 \bar{L}_h(\eta)\eta^2 d\eta \right)/\mu \tag{33}$$

where

μ = density ratio = $\bar{m}/\pi\rho_\infty b^2$

Since the reduced frequency and Mach number at any specified spanwise

station are known from the frequency ratio, the blade planform and Mach number at the tip, it can be written that

$$\zeta = \zeta(m, R/b, M_{\infty tip}, h, \mu) \tag{34}$$

In this example, $R/b = 23$, $M_{\infty tip} = 0.7$, h is constant over the rotor disc at 3, $\mu = 80$. ζ, then, is only a function of the frequency ratio, this function being determined by the aerodynamic theory used. In Figure 11, the modulus of ζ is shown plotted against frequency ratio, according to four different aerodynamic theories.

Curve 1 was generated by employing the compressible theory of Jones and Rao [11]. This is one of the most comprehensive theories available at the moment. Curve 2 was generated by the same theory except that M_{tip} was deliberately set equal to zero, so the differences between curves 1 and 2 can be considered to indicate the compressibility effects. In the interest of clarity, curve 1 is not shown for $m > 2.75$, but the general relationship between curves 1 and 2 remains the same for $m > 2.75$. Curve 3 was obtained by employing fixed wing compressible, unsteady aerodynamics [12] in a strip theory fashion. Curve 4 was obtained by assuming fixed wing steady aerodynamic strip theory to this unsteady case wherein the ratio of the velocity induced by flapping to the equivalent forward speed (Ωr) is considered to constitute the angle of attack. Compressibility is accounted for by employing Prandtl-Glauert correction. In this case, L_h is given by

$$L_h = -2i/(k\sqrt{1 - M_\infty^2}) \tag{35}$$

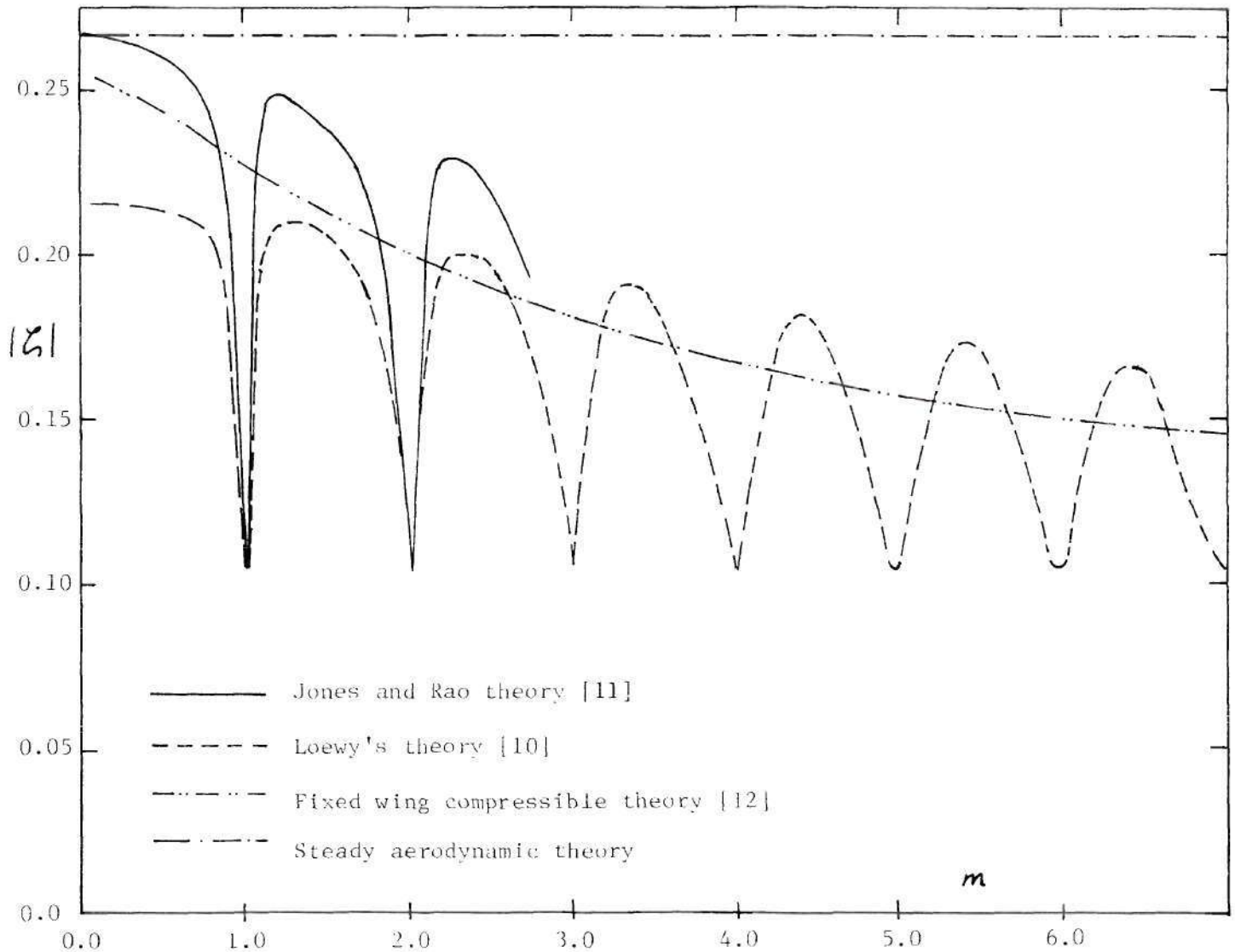

Figure 11. Variation of the Modulus of Damping Ratio with Frequency Ratio for a Pure Flapping Blade.

According to the theory of Jones and Rao, which is believed to be sufficiently accurate, there is a very significant drop in the aerodynamic damping moment at integer values of frequency ratio. At low integral values of m, this drop is confined to a small neighborhood near the integral values, but at higher values of m, this width of low damping increases. In as far as this feature is concerned, curves 1 and 2 predict the same, i.e., compressibility effects do not change this behavior. The striking difference between curves 1 and 2 is that curve 2 always shows a lower aerodynamic moment. This is intuitively expectable since for steady flow, the Prandtl-Glauert similarity rule predicts increased lift at higher Mach numbers for the same angle of attack.

Although curve 3 shows values for ζ in the same range as shown by curves 1 and 2, the fixed wing theory completely fails to predict loss of damping at integer values of m, because it ignores the helical vortex surface lying in the wake of the rotor. As such, fixed wing theory should be considered unsuitable for unsteady rotor flow problems at low inflow conditions.

The steady theory predicts a constant value of $|\zeta|$ at 0.266. As seen in Figure 11, this theory is apparently satisfactory for $m \leq 0.75$ in this example. It is interesting to note that the model chosen in this example shows considerable damping at low frequency of flapping.

Figure 12 shows the phase angle, ϕ, by which the aerodynamic moment, $\int_0^R \frac{dL}{dr}\, r\, dr$, leads the flapping deflection, β. Compressible as well as incompressible rotor aerodynamic theories predict that at integer values of frequency ratio, the phase angle is close to $-90°$,

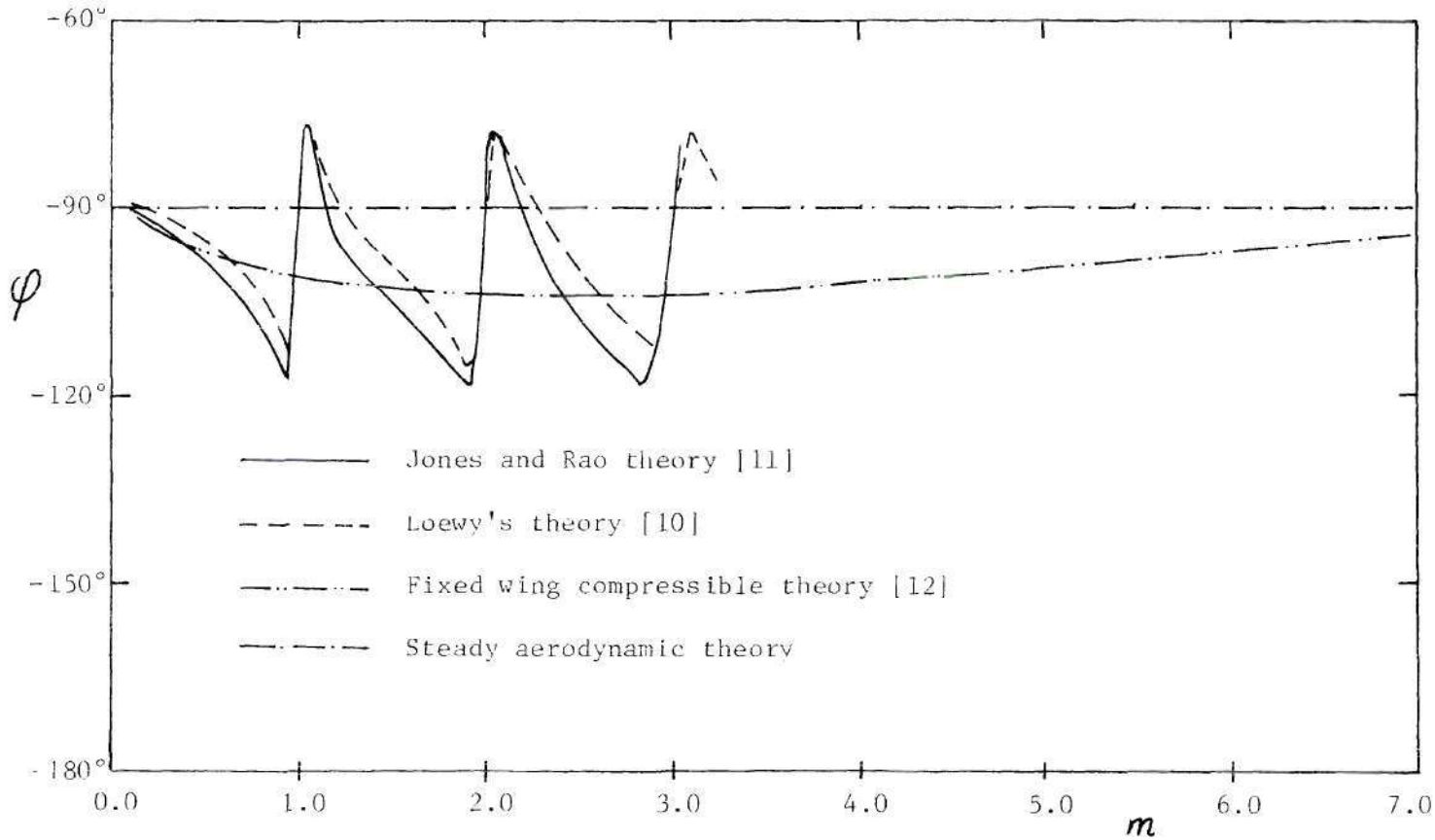

Figure 12. Variation of the Phase Angle of the Aerodynamic Moment with Frequency Ratio for a Pure Flapping Blade.

i.e., the damping moment is approximately 180° out of phase with velocity of flapping. However, away from integral values of m, the phase angle differs considerably from -90°. Again fixed wing unsteady theory and steady theory do not predict such an oscillatory behavior for the phase angle. Though not shown in Figure 12, curves 1 and 2 exhibit the same kind of oscillatory behavior for higher values of m.

White [14] conducted flutter analyses of a model rotor by employing the compressible theory of Jones and Rao [11] once with the wake terms included and another time without including the wake terms. The latter case yielded a flutter speed which was considerably higher than the reported experimental result of Brooks and Baker [9]. This case was for a blade pitch angle of 7.2° and lower pitch angles may produce even larger errors when the wake is neglected.

Experimental results of Ham, Moser and Zvara [15] and Daughaday, Du Waldt and Gates [16] also show considerably decreased aerodynamic damping at integer values of the frequency ratio.

Derivation of the Flutter Equations

Flutter is the phenomenon where the lifting surface undergoes undamped simple harmonic oscillations without the application of any external forces. At this frequency of vibration, the elastic restoring forces, the inertial forces, and the internal structural damping forces are in equilibrium with the aerodynamic forces which are created solely because of the oscillation of the surface. Flutter is a stability boundary. The subsequent response of the aeroelastic system to a disturbance either decays or grows depending upon whether the speed is below or above the

flutter boundary. The problem is treated as linear and homogeneous; the amplitude of vibration is arbitrary.

The expression "flutter mode" means the mode of oscillation in which flutter takes place. One interesting difference between a normal mode and a flutter mode is the following: when the system vibrates in a normal mode, at one instant of time, the entire energy of the system will be kinetic; one fourth of the time period later, the energy is completely potential. But in general, for the system vibrating in flutter mode, neither the potential nor the kinetic energy completely vanishes at any instant of time. The mass points in flutter mode vibrate in different phases and hence to describe the flutter mode graphically we need to show the deflected configuration at several instances of time within one cycle.

At the end of Chapter II, equations were derived in terms of the normal coordinates, $\xi_r(t)$, to obtain the response due to externally applied arbitrary forces. It is now assumed that the flutter mode can be represented by a series of the first several normal modes with undetermined coefficients of the form

$$\begin{aligned} \alpha(y,t) &= \sum_{r=1}^{N} \alpha_r(y)\xi_r(t) \\ w(y,t) &= \sum_{r=1}^{N} w_r(y)\xi_r(t) \end{aligned} \tag{36}$$

It is further assumed that $\xi_r(t)$ can be obtained by solving the following N coupled differential equations:

$$M_r\ddot{\xi}_r(t) + (1 + ig_r)\omega_r^2 M_r\xi_r(t) = \Xi_r(t), \quad r = 1,2,3,\ldots,N \tag{37}$$

where g_r is the structural damping constant of the r-th mode and

$$\Xi_r(t) = -\int_o^R L(y,t)w_r(y)dy + \int_o^R M_{ea}(y,t)\alpha_r(y)dy \qquad (38)$$

In Equation (38), $L(y,t)$ is the lift per unit span and $M_{ea}(y,t)$ is the aerodynamic moment per unit span, and these loadings are the result of the motion of the surface defined by Equation (36). The positive sign convention used in the unsteady aerodynamic analysis is shown in Figure 13.

Let the motion be simple harmonic with ω as the frequency. Then,

$$\begin{aligned} \alpha(y,t) &= \bar{\alpha}(y)\ \exp(i\omega t) \\ w(y,t) &= \bar{w}(y)\exp(i\omega t) \\ \xi_r(t) &= \bar{\xi}_r\ \exp(i\omega t),\ r = 1,2,3,\ldots,N \end{aligned} \qquad (39)$$

and

$$\begin{aligned} L(y,t) &= \bar{L}(y)\ \exp(i\omega t) \\ M_{ea}(y,t) &= \bar{M}_{ea}(y)\ \exp(i\omega t) \\ \Xi_r(t) &= \bar{\Xi}_r\ \exp(i\omega t) \end{aligned} \qquad (40)$$

$\bar{\alpha}$, $\bar{w}$, $\bar{\xi}_r$, $\bar{L}(y)$, $\bar{M}_{ea}(y)$ and $\bar{\Xi}_r$ are complex quantities and their phases are thus defined with respect to some reference vector.

From unsteady aerodynamic theory,

$$\begin{aligned} \bar{L}(y) &= L_1(y)\bar{w}(y)/b(y) + L_2(y)\bar{\alpha}(y) \\ \bar{M}_{ea}(y) &= M_1(y)\bar{w}(y)/b(y) + M_2(y)\bar{\alpha}(y) \end{aligned} \qquad (41)$$

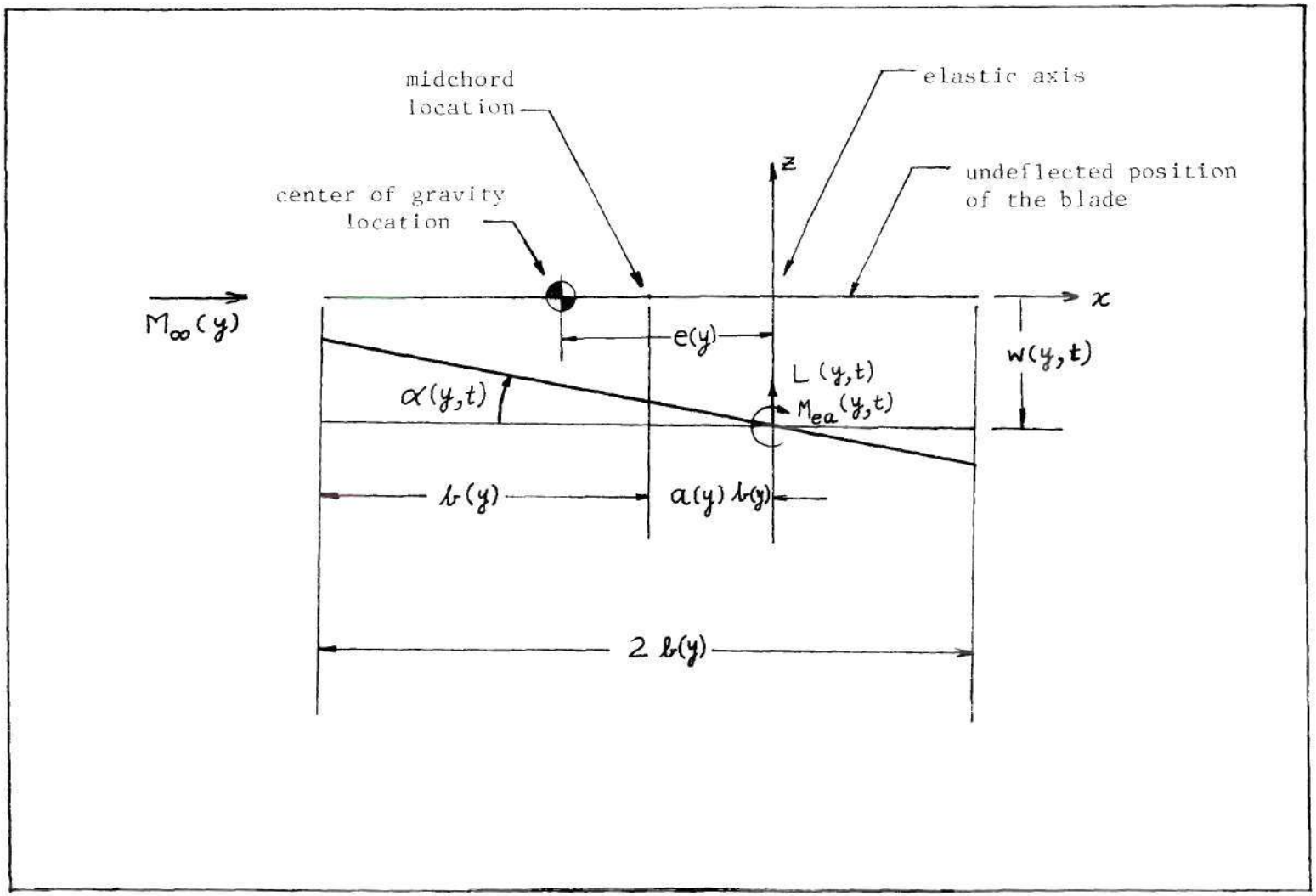

Figure 13. Positive Sign Convention for Unsteady Aerodynamic Program.

where

$$\begin{Bmatrix} L_1(y) \\ L_2(y) \\ M_1(y) \\ M_2(y) \end{Bmatrix} = -\pi\rho_\infty \omega^2 b^4(y) \begin{Bmatrix} L_h(y)/b(y) \\ [L_\alpha(y) - L_h(y)\varepsilon(y)]/b(y) \\ -M_h(y) + L_h(y)\varepsilon(y) \\ -M_\alpha(y) + [L_\alpha(y) + M_h(y)]\varepsilon(y) \\ -L_h(y)\varepsilon^2 \end{Bmatrix} \tag{42}$$

and

$$\varepsilon(y) = \frac{1}{2} + a(y) \tag{43}$$

The nondimensional aerodynamic coefficients L_h, L_α, M_h and M_α are functions of the reduced frequency, frequency ratio, inflow ratio and Mach number at the spanwise station y and in case of a multibladed rotor they also depend on the number of blades and the phase difference between the oscillations of the blades. In this thesis, only equivalent single bladed rotor flutter is considered. This implies that for multibladed rotor systems, all blades are vibrating in some known interblade mode.

Using Equations (36), (38), (39), (40), (41) and (42), it can now be shown that

$$\bar{\Xi}_r = \pi\rho_\infty \omega^2 R\, b_{ref}^4 \sum_{n=1}^{N} \bar{\xi}_n A_{rn} \tag{44}$$

where

$$A_{rn} = \int_0^1 [\beta^2 L_h w_r^* w_n^* + \beta^3 (L_\alpha - L_h \varepsilon) w_r^* \alpha_n^* + \beta^3 (M_h - L_h \varepsilon) \alpha_r^* w_n^* + \beta^4 \{M_\alpha - (L_\alpha + M_h)\varepsilon + L_h \varepsilon^2\} \alpha_r^* \alpha_n^*] d\eta \tag{45}$$

and

$$\beta = b(\eta)/b_{ref} = \beta(\eta) \tag{46}$$

and the nondimensional r-th mode shape is defined by

$$w_r^* = w_r/b_{ref}$$
$$\alpha_r^* = \alpha_r \tag{47}$$

Now the equation of motion (37) can be written as

$$[-\omega^2 + (1 + ig_r)\omega_r^2] M_r \bar{\xi}_r = \pi \rho_\infty \omega^2 R\, b_{ref}^4 \sum_{n=1}^{N} \bar{\xi}_n A_{rn} \tag{48}$$

With the introduction of the nondimensional generalized mass M_r^* defined by $M_r^* = M_r/(\pi \rho_\infty b_{ref}^4 R)$ or,

$$M_r^* = \left(\frac{\bar{m}_{ref}}{\pi \rho_\infty b_{ref}^2}\right) \int_0^1 \frac{\bar{m}(\eta)}{\bar{m}_{ref}} \{w_r^{*2} + \left(\frac{k_m(\eta)}{b_{ref}}\right)^2 \alpha_r^{*2} - 2\left(\frac{e(\eta)}{b_{ref}}\right) w_r^* \alpha_r^*\} d\eta \tag{49}$$

Equation (48) can be written in the completely nondimensional matrix form as

$$\left[[-1 + (1 + ig_r)(\frac{\omega_r}{\omega})^2]M_r^*\right] \{\bar{\xi}\} = [A] \{\bar{\xi}\} \qquad (50)$$

$$(N \times N) \text{ diagonal} \qquad (Nx1)\ (NxN)\ (Nx1)$$

Equation (50) is the matrix equation representing a system of N linear, homogeneous, algebraic equations for the response vector $\{\bar{\xi}\}$. For the given angle of incidence at the root and the steady aerodynamic operating conditions corresponding to a given rotor speed, a structural dynamic investigation can be carried out which will yield ω_r and M_r^*. Values of g_r are provided either by estimation or from experiments. If we then assume a certain frequency of oscillation ω, then the unsteady aerodynamic flow field is completely specified and the matrix [A], can be evaluated. But since Equation (50) is homogeneous, there arise two cases: 1) if the determinant of the coefficient matrix is nonzero, then $\{\bar{\xi}\} \equiv \{0\}$ is the only solution and this means the system cannot possess a self excited steady state vibration of this frequency ω. 2) if the determinant of the coefficient matrix is zero, then there exists a nontrivial solution for $\{\bar{\xi}\}$, but the amplitude is arbitrary. The lifting surface then experiences flutter.

CHAPTER IV

THE k-METHOD OF FLUTTER SOLUTION

Statement of the Problem

It was shown in the last chapter that the matrix equation governing the flutter phenomenon is given by

$$\{ \left[[-1 + (1 + ig_r)(\omega_r/\omega)^2] M_r^* \right] - [A] \} \{\bar{\xi}\} = \{0\} \tag{51}$$

g_r, ω_r and M_r^* for r = 1 to N are known for a blade if the rotor speed, density of the fluid medium and collective pitch are specified. All the elements of [A] are determined after ω and Ω are selected. Since the terms involved are complicated functions of their arguments, the flutter solution requires choosing a certain value for Ω, scanning through various appropriate values of ω and verifying for each such pair (Ω,ω) whether Equation (51) can be satisfied to yield (Ω_f,ω_f).

Determinant Method of Solution

This method is based on the fact that for a nontrivial solution of $\{\bar{\xi}\}$ to exist at flutter, the determinant

$$\Delta(\Omega_f, \omega_f) = 0 \tag{52}$$

where

$$\Delta(\Omega, \omega) = \left| \left[[-1 + (1 + ig_r)(\omega_r/\omega)^2] M_r^* \right] - [A] \right| \tag{53}$$

The coefficient matrix whose determinant is written in Equation (53) is in general a non-Hermitian matrix and hence Δ is complex valued. The procedure begins with choosing a certain value for rotor speed, say Ω_1. Then a set of scanning frequencies ω are used such that the interval of frequency scanning is small near integral values of frequency ratio. Then the determinant, $\Delta(\Omega_1,\omega)$, is calculated for each case and plotted in the Argand diagram. If the curve does not pass through the origin, then $\Omega_1 \neq \Omega_f$, and a higher trial rotor speed is chosen and the process repeated.

Figure 14(a) shows one such plot. If the obtained plot is of this nature, then it is simple to organize a computer program that will interpolate for the flutter point (Ω_f, ω_f). Unfortunately, for an example rotor flutter problem worked out numerically, invariably only a typical plot as shown in Figure 14(b) was obtained. Such an irregular behavior of the determinant makes it totally impossible to predict the flutter point by interpolation and hence requires excessive computer time. The nature of rotor blade flutter under low inflow conditions seems to be such that even if (Ω_1,ω) is close to (Ω_f, ω_f), the determinant value does not appear to approach the origin. In view of such a numerical difficulty, this method is abandoned as impracticable.

The Conventional V - g Method or the k Method

This method assumes that for a given rotor speed Ω, there exist several aeroelastic modes. The blade, when disturbed and let free, is capable of decaying purely in any of these aeroelastic modes, if the initial conditions are suitable. Each aeroelastic mode is characterized by (ω, g) where ω is the damped natural frequency and g is the additional structural damping required by each of the vacuum normal modes to constitute

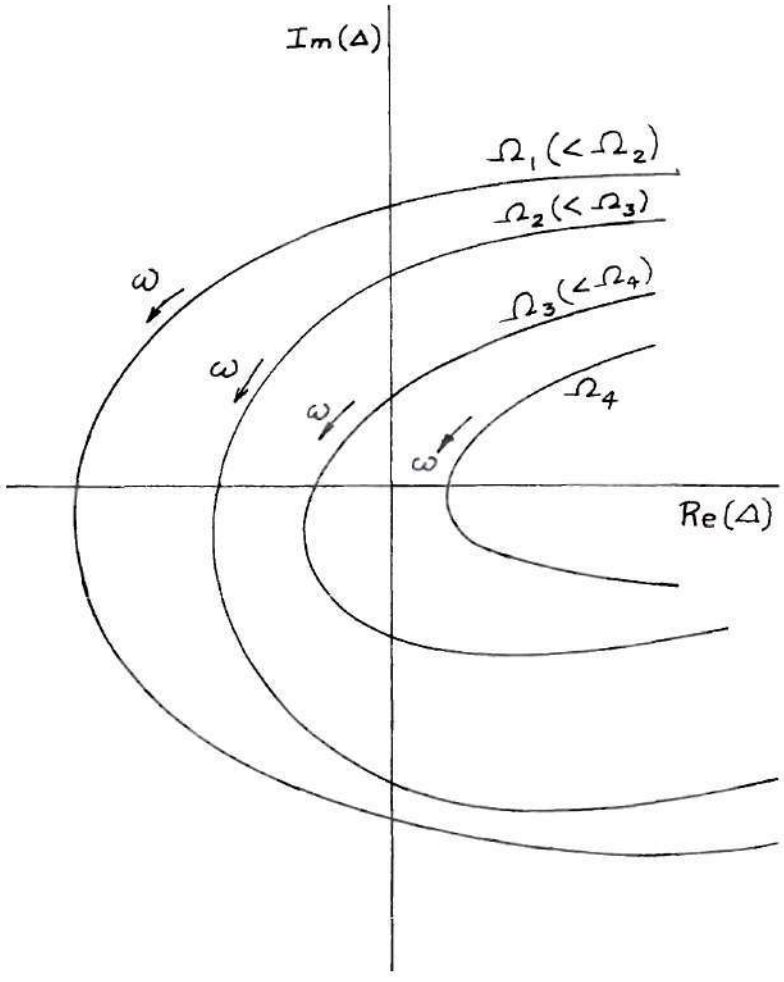

Figure 14(a)

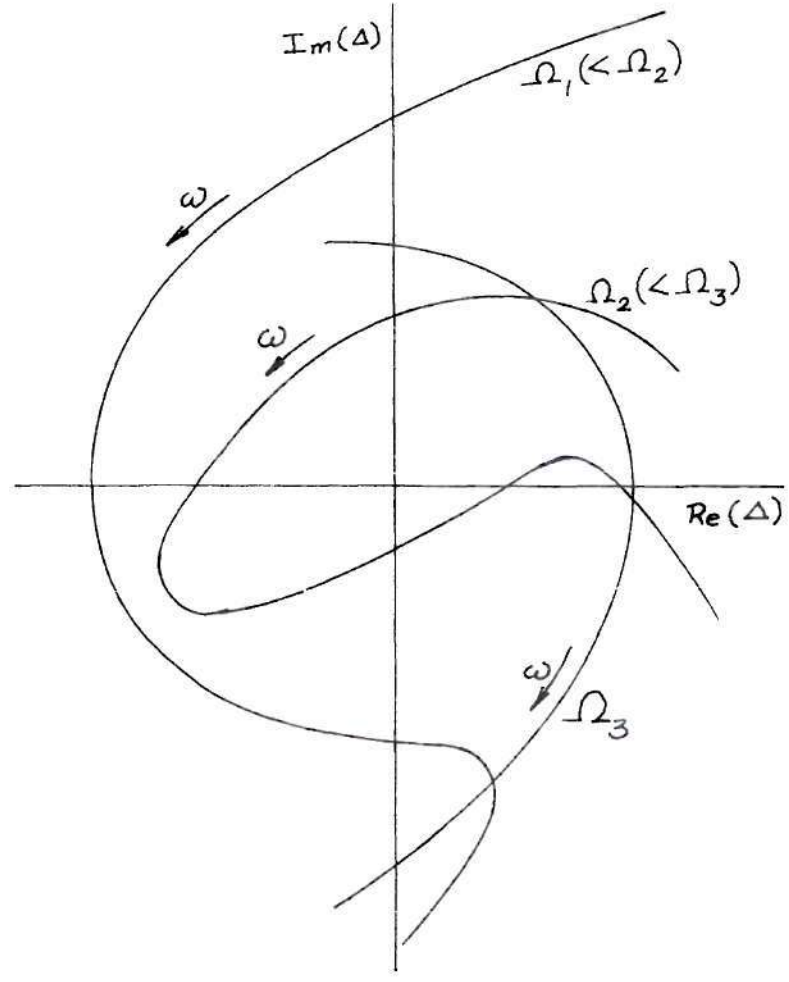

Figure 14(b)

Figure 14. Plot of the Flutter Determinant on the Argand Diagram.

this aeroelastic mode. It is proposed from elementary theory that πg is equal to the logarithmic decrement of that aeroelastic mode.

The above principle is mathematically modeled below. But since the subcritical aeroelastic damping cannot be expressed completely through structural damping, this method cannot predict the damping accurately.

In the flutter equations (51), replace g_r by $(g_r + g)$. Then approximate $(1 + ig_r + ig)$ by $(1 + ig)\,(1 + ig_r)$ since g and g_r are small compared to 1 and also the error vanishes as g goes to zero. The flutter equations now become

$$\{[A] + \left[M_r^*\right] + - \left[(1 + ig_r)(1 + ig)(\omega_r/\omega)^2 M_r^*\right]\}\{\bar{\xi}\} = \{0\} \tag{54}$$

If $\omega_1 \neq 0$, premultiply Equation (54) by

$$\left[[(\omega_{ref}/\omega_r)^2]/[(1 + ig_r)M_r^*]\right]$$

to obtain

$$\left\{\left[\frac{(\omega_{ref}/\omega_r)^2}{(1+ig_r)M_r^*}\right]([A] + \left[M_r^*\right]) - \lambda[I]\right\}\{\bar{\xi}\} = \{0\} \tag{55}$$

where

$$\lambda = (1 + ig)\,(\omega_{ref}/\omega)^2 \tag{56}$$

The conventional V - g method used in fixed wing flutter analyses in the technical literature is modified in this thesis for the rotary wing analysis. The procedure is as follows:

1. Specify the desired value for collective pitch and density of the fluid medium.

2. Choose a trial rotor speed Ω_1 and conduct a structural dynamic investigation to yield ω_r and M_r^*. Provide g_r as an estimate or as experimental data.

3. Choose a suitable set of frequency ratios $m_1, m_2, m_3, \ldots, m_\ell$ as described previously.

4. Corresponding to each of the frequency ratios, do the following: Let the frequency ratio be m_j $(1 \leq j \leq \ell)$. Note that Equation (55) is in the form of a standard eigenvalue problem. Now each of the N x N complex elements of the eigenvalue matrix (coefficient matrix) can be evaluated. The N complex eigenvalues, namely, $\lambda_1^{(j)}, \lambda_2^{(j)}, \ldots, \lambda_N^{(j)}$ can be obtained. From each complex eigenvalue $\lambda_i^{(j)}$, $1 \leq i \leq N$, ω and g are obtained from Equation (56) as

$$\omega_i^{(j)} = \omega_{ref} / \sqrt{Re(\lambda_i^{(j)})} \tag{57a}$$

$$g_i^{(j)} = I_m(\lambda_i^{(j)}) / Re(\lambda_i^{(j)}) \tag{57b}$$

since

$$\lambda_i^{(j)} = (1 + ig_i^{(j)})(\omega_{ref}/\omega_i^{(j)})^2 \tag{57c}$$

A value for rotor speed is inferred from

$$\Omega_i^{(j)} = \omega_i^{(j)}/m_j \tag{58}$$

The above procedure is graphically shown below:

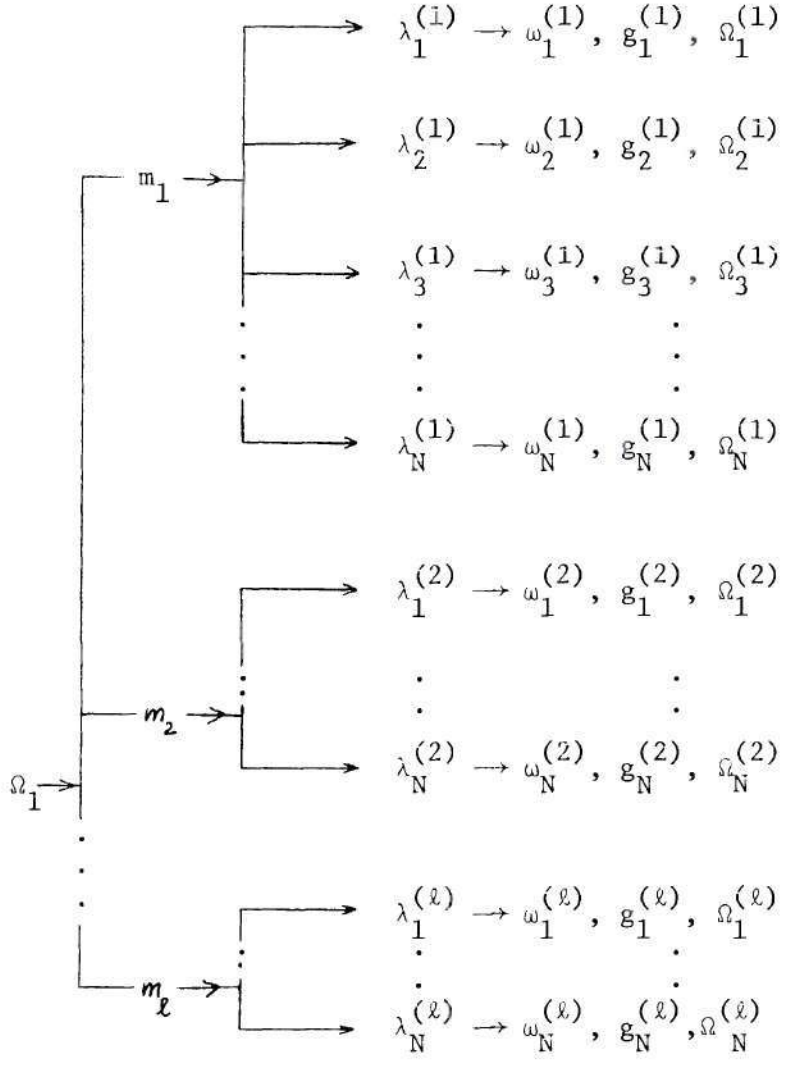

For convenience, the frequency ratios m_j, $1 \leq j \leq \ell$, should be chosen in a monotonically decreasing fashion. For a typical rotor problem, one list of m could be 7.00, 6.95, 6.90, 6.85,..., 3.00, 2.98, 2.96, 2.94,..., 0.70. For low inflow ratios, scanning should be made with intervals as low as $\Delta m = -0.02$, near integral values for the frequency ratio. A case of wake excited flutter has been reported [17] with frequency ratio as large as 20.0 and if an instability is expected at high frequencies, suitable values of m must be included in the scanning list.

Numbering the Aeroelastic Modes

Through the experience gained, it has been observed that when m_1 is chosen to be high like 7 (with Q = 1), $\omega_1^{(1)}$, $\omega_2^{(1)}$ $\omega_3^{(1)}$,...,$\omega_N^{(1)}$ turn out to be close to the vacuum natural frequencies of the N fundamental modes chosen. The eigenvalues $\lambda_1^{(1)}$, $\lambda_2^{(1)}$, $\lambda_3^{(1)}$,...,$\lambda_N^{(1)}$ are then rearranged if necessary, so that the modes can be numbered 1 through N, closely following the vacuum frequency pattern.

The eigenvalues for $m = m_2$, may be disordered compared to the eigenvalues for $m = m_1$. For example, let N = 4, and let $\lambda_1^{(1)}$ through $\lambda_N^{(1)}$ be (200 - 2i), (150 - 1.8i), (132 - 1.65i) and (100 - 0.8i). Let $\lambda_1^{(2)}$ through $\lambda_N^{(2)}$ be (199 - 1.95i), (131.8 - 1.66i), (100.1 - 0.81i) and (150.8 - 1.82i). It is clear that the eigenvalues $\lambda_1^{(2)}$ through $\lambda_N^{(2)}$ must be reordered to read (199 - 1.95i), (150.8 - 1.82i), (131.8 - 1.66i) and (100.1 - 0.81i). The new set of eigenvalues $\lambda_i^{(j)}$ can be reordered, (in many cases it will not be necessary), on the basis of damped natural frequency $\omega_i^{(j)}$ or the damping $g_i^{(j)}$ or both.

Desmarais and Bennett [18] have developed a procedure that can be used to automatically sort the eigenvalues. Basically, they [18] have introduced a method of determining the eigenvalues of a complex matrix by iterating on approximate input eigenvalues. They have also discussed in detail the application of their method to fixed wing flutter problems. The eigenvalue routine is briefly described in Appendix A. It has been applied in this thesis to the case of rotor flutter as follows:

1) For m_1, m_2 and m_3, any eigenvalue routine like Francis' QR Transform [19], can be used to obtain the eigenvalues, $\lambda_i^{(j)}$. (These $\lambda_i^{(j)}$ can be further processed through the Desmarais - Bennett subroutine and refined, if necessary).

2) By inspecting the frequencies obtained above, the eigenvalues should be ordered, if necessary. The frequencies are generally close to the undamped natural frequencies.

3) $\omega_i^{(1)}$, $\omega_i^{(2)}$, $\omega_i^{(3)}$, $(1 \leq i \leq N)$, are parabolically extrapolated to provide an estimate for $\omega_i^{(4)}$ at $m = m_4$. A similar extrapolated estimate is also available for $g_i^{(4)}$. Thus the column of eigenvalues which approximate $\lambda_i^{(4)}$ is prepared as input to the Desmarais - Bennett subroutine along with the eigenvalue matrix for $m = m_4$ as given by Equation (55). Then the user selected number of iterations are carried out and the output eigenvalues are considered to be sufficiently accurate for the aeroelastic eigenvalues, $\lambda_i^{(4)}$. Usually five iterations are found to be sufficient.

4) For obtaining the eigenvalues corresponding to m_j, first the elements of the eigenvalue matrix are evaluated (Equation (55)). Then

the eigenvalues approximate to $\lambda_i^{(j)}$ are obtained by parabolically extrapolating $\lambda_i^{(j-3)}$, $\lambda_i^{(j-2)}$ and $\lambda_i^{(j-1)}$. Then the trial input eigenvalues are refined by the Desmarais - Bennett subroutine and $\omega_i^{(j)}$, $g_i^{(j)}$ and $\Omega_i^{(j)}$ are evaluated as explained previously.

5) Now the frequency - damping - rotor speed plots can be prepared for all the N aeroelastic modes. The points $(\omega_i^{(1)}, \Omega_i^{(1)})$, $(\omega_i^{(2)}, \Omega_i^{(2)}) \ldots, (\omega_i^{(\ell)}, \Omega_i^{(\ell)})$ can be joined in the $\omega - \Omega$ plane to yield the plot of the damped natural frequency of the i-th aeroelastic mode against the rotor speed, $(1 \leq i \leq N)$. By joining the points $(g_i^{(1)}, \Omega_i^{(1)})$, $(g_i^{(2)}, \Omega_i^{(2)}), \ldots, (g_i^{(\ell)}, \Omega_i^{(\ell)})$ on the $g - \Omega$ plane, the damping of the i-th mode is plotted against rotor speed, $(1 \leq i \leq N)$.

It should be recognized that the rotor speed that is inferred after the eigenvalue problem is solved, does not necessarily match the rotor speed that was assumed initially in carrying out the vibrational analysis. Hence even if one condition for $g = 0$ was indicated by the analysis, it may not be a flutter condition since the rotor speed assumed initially may not match the rotor speed indicated for flutter. The following procedure is suggested and used in this thesis:

1. Choose a rotor speed $\Omega = \Omega_a$. Go through the entire procedure, to obtain the frequency-damping-rotor speed plots.

2. Let the indicated rotor speed for flutter be Ω_b, as determined by the point corresponding to $g = 0$. In general, $\Omega_b \neq \Omega_a$. Now choose a rotor speed $\Omega = \Omega_b$ and repeat the analysis for the frequency - damping - rotor speed plots.

3. Continue this procedure until the rotor speed assumed equals the indicated rotor speed for flutter.

In practice, about 3 or 4 trials will be sufficient for the trial rotor speed to converge to the flutter speed for unbalanced rotor blades, where the mass axis is aft of the quarter chord axis. This rotor speed corresponds to a point on the flutter boundary and is called a "matched" flutter point since compressibility effects in aerodynamics as well as the centrifugal force effects on the structural dynamic properties have been correctly taken into account. The resulting rotor speed (flutter speed) and the frequency of oscillation (flutter frequency) are the exact "coupled eigenvalues" of Equation (51). ($\Omega_f = \Omega$ and $\omega_f = \omega$ are considered "coupled eigenvalues" here because they together give rise to a nontrivial solution for $\{\bar{\xi}\}$, the flutter mode shape vector.)

It is very useful to program the technique in such a way as to obtain along with the computer output the above mentioned plots, through a device like the CALCOMP plotter.

The incorporation of the Desmarais-Bennett subroutine makes the flutter solution automated. When the eigenvalues are obtained in the fashion mentioned above, a certain amount of computer time is saved compared to the case where only the QR transform is used all the time. But more importantly, the eigenvalues obtained are almost always ordered in the desired sequence and hence the frequency - damping - rotor speed plots can be rapidly prepared. Numerical difficulty and also difficulty in ordering are expected if any two eigenvalues come close to each other. But often, when the frequencies become close, the value of damping are well separated and thus the difficulty does not generally arise. An extensive computer program was prepared based on this method and a wrong ordering

of the eigenvalues took place only once in about a thousand times. Such places, in general, can be easily located by an inspection of the computer plot output.

In the case of fixed wing aeroelastic analysis, the generalized aerodynamic forces, namely the elements of the [A] matrix, change relatively little from one reduced frequency to another at a given forward speed. On the other hand, in the case of the low inflow rotor aeroelastic analysis at a given rotor speed, the elements of the generalized aerodynamic matrix generally change very rapidly with frequency ratio, especially near integral values of frequency ratio. It is now a standard practice [18] for the fixed wing analysis to compute the [A] matrix for only a few reduced frequency values, and for intermediate reduced frequencies, the matrix is obtained by interpolation. Because of the reason mentioned above, interpolation for the [A] matrix was not resorted to, in this work.

The Desmarais - Bennett procedure has greatly helped in tracking the g curves as the frequency ratio is incremented. Thus, in a given trial, the rotor speed corresponding to $g = 0$ is automatically computed by interpolating between the two values of frequency ratio between which g changes sign. Thus the iteration for the flutter boundary of the rotor is facilitated, and this is the way an automated matched flutter point computer program has been developed. This program has been used to solve several example problems to be discussed later.

A similar procedure for fixed wing fiutter can also be formulated.

The flight Mach number and atmospheric density are assumed. The flutter analysis is carried out for a set of reference reduced frequencies, and conventional V - g plots are generated to indicate a point (g = 0) on the flutter boundary. In an incompressible flow, this speed at g = 0 is the matched flutter point. But in compressible flow, this speed may not be consistent with the chosen values of density and Mach number for a standard atmosphere. Now recompute the Mach number according to the indicated flutter speed and specified density. The entire procedure is repeated until convergence. In the case of rotor flutter, the dependence of the structural dynamic properties on the rotor speed has resulted in an additional dimension of complexity when compared to the fixed wing flutter analysis.

An Example Problem

In Chapter II, the properties of two example blades numbered 1 and 2 were described and their structural dynamic properties were illustrated. The flutter characteristics of these uniform blades will now be considered. The k-method as described in the previous section was used to determine the flutter boundary. The first five normal modes were used in the flutter analysis. Structural damping coefficients in the vacuum modes were assumed to be zero.

Hovering flight ($V_\infty = 0$) is assumed for a single bladed model rotor with

$$\rho_\infty = 0.002378 \text{ slug/ft}^3$$

$$a_\infty = 1117.0 \text{ ft/sec.}$$

$$\alpha_s(o) = 4 \text{ degrees}$$

$$a = -0.46.$$

The blade built-in twist is zero. The blade chord is four inches and uniform along the span. The radius of the rotor is 46.0 inches.

The Mach number at each radial station is given by $\Omega y/a_\infty$. The inflow ratio variation along the radius is given by the combined simple momentum and blade element analysis:

$$h(\eta) = \frac{2}{\sigma}\left\{ \left(\frac{V_\infty}{\Omega R} - \frac{\bar{a}(\eta)\sigma}{8}\right) + \sqrt{\left(\frac{V_\infty}{\Omega R} - \frac{\bar{a}(\eta)\sigma}{8}\right)^2 + \frac{\bar{a}(\eta)\alpha_s(\eta)\eta\sigma}{2}} \right\} \quad (59)$$

where

$$\sigma = 2bQ/(\pi R)$$

and

$$\bar{a}(\eta) = \bar{a}_{inc}(\eta)/\sqrt{1 - M_\infty^2(\eta)} \quad (60)$$

$a_{inc}(\eta)$ is taken as 5.75. Figure 15 shows the inflow ratio as a function of radius for Ω = 90 rad/sec.

The frequency ratio, m, remains the same for all spanwise stations. But the reduced frequency at any station y is given by k = mb/y. 130 values of frequency ratio were scanned ranging from 12.5 to 0.6 with an average interval of $\Delta m = -0.1$ in $7.5 > m > 3.0$ and with $\Delta m = -0.05$ in $3.0 > m > 0.6$. The interval was reduced near integer values of m.

The output of the flutter analysis for Blade No. 1 is summarized below:

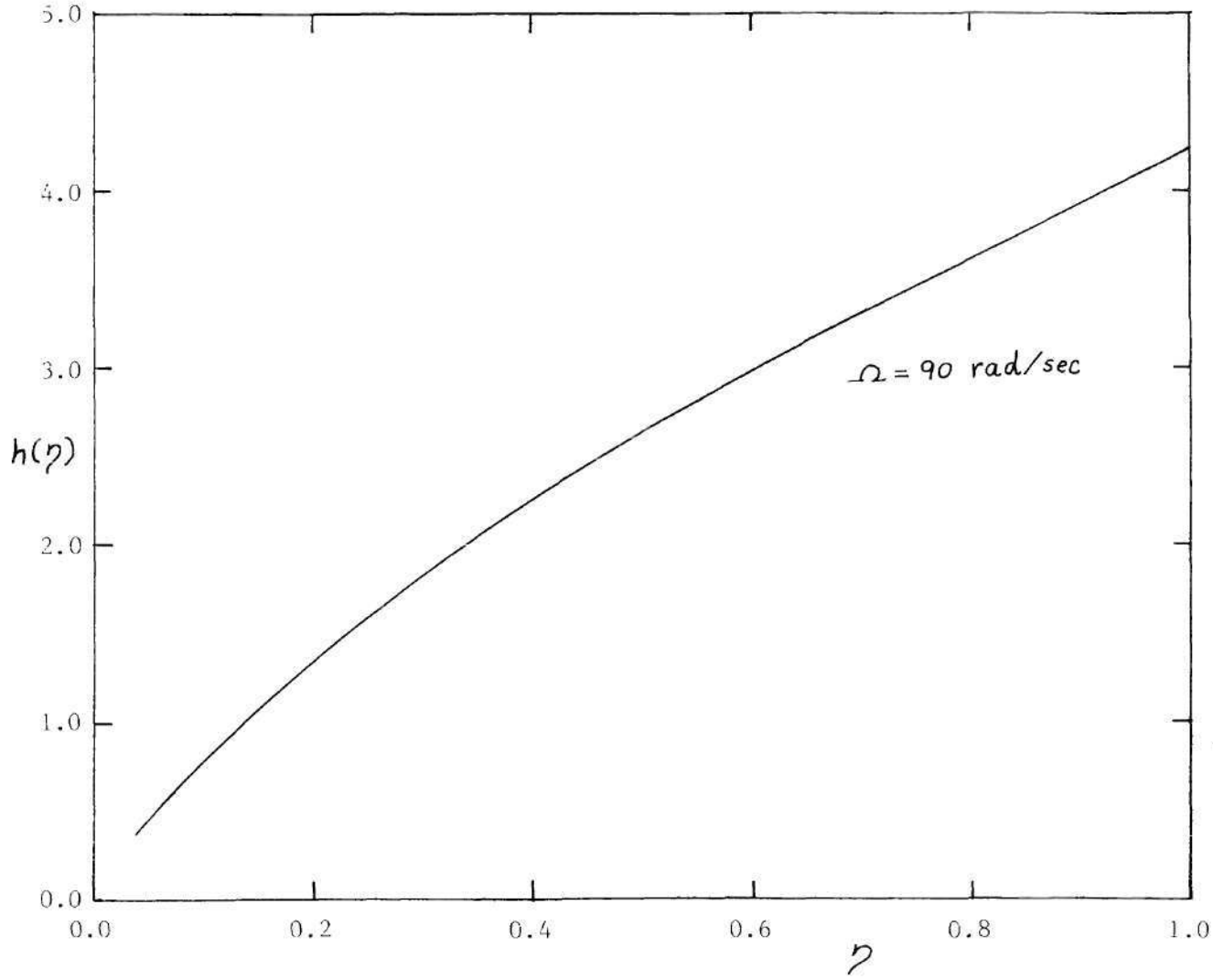

Figure 15. Variation of Inflow Ratio with Blade Radius.

Trial Number	Trial Rotor Speed	Indicated Flutter Rotor Speed
1	40.0 rad/sec.	100.9 rad/sec.
2	70.5 rad/sec.	96.8 rad/sec.
3	96.8 rad/sec.	90.3 rad/sec.
4	90.3 rad/sec.	90.1 rad/sec.

The flutter boundary rotor speed is concluded to be 90.1 rad/sec. since convergence is satisfactory. The frequencies and vacuum mode shapes of this blade at this speed can be approximately seen from Figures 3, and 5(a) through 5(h) of Chapter II.

The flutter frequency is ω_f = 195.8 rad/sec. which corresponds to the frequency ratio of m_f = 2.17. The flutter mode shape has been determined to be the eigenvector in Equation (51).

$$\{\bar{\xi}\} = \left\{ \begin{array}{l} 1.0 \\ -0.8262 + 0.3476\ i \\ -0.2220 + 0.05798\ i \\ -0.01212 + 0.007233\ i \\ -0.0002294 + 0.0002815\ i \end{array} \right\} = \left\{ \begin{array}{l} 1.0 \\ 0.8963 \exp(157.18^\circ\ i) \\ 0.2294 \exp(165.4^\circ\ i) \\ 0.01411 \exp(30.85^\circ\ i) \\ 0.0003631 \exp(129.2^\circ\ i) \end{array} \right\}$$

Figures 16(a), 17(a), 18(a), and 19(a) show the variation of the damped natural frequencies of the first four aeroelastic modes as function of rotor speed. Figures 16(b), 17(b), 18(b) and 19(b) show the variation of the damping present in the first four modes as a function of rotor speed. These figures will also be used to compare the prediction

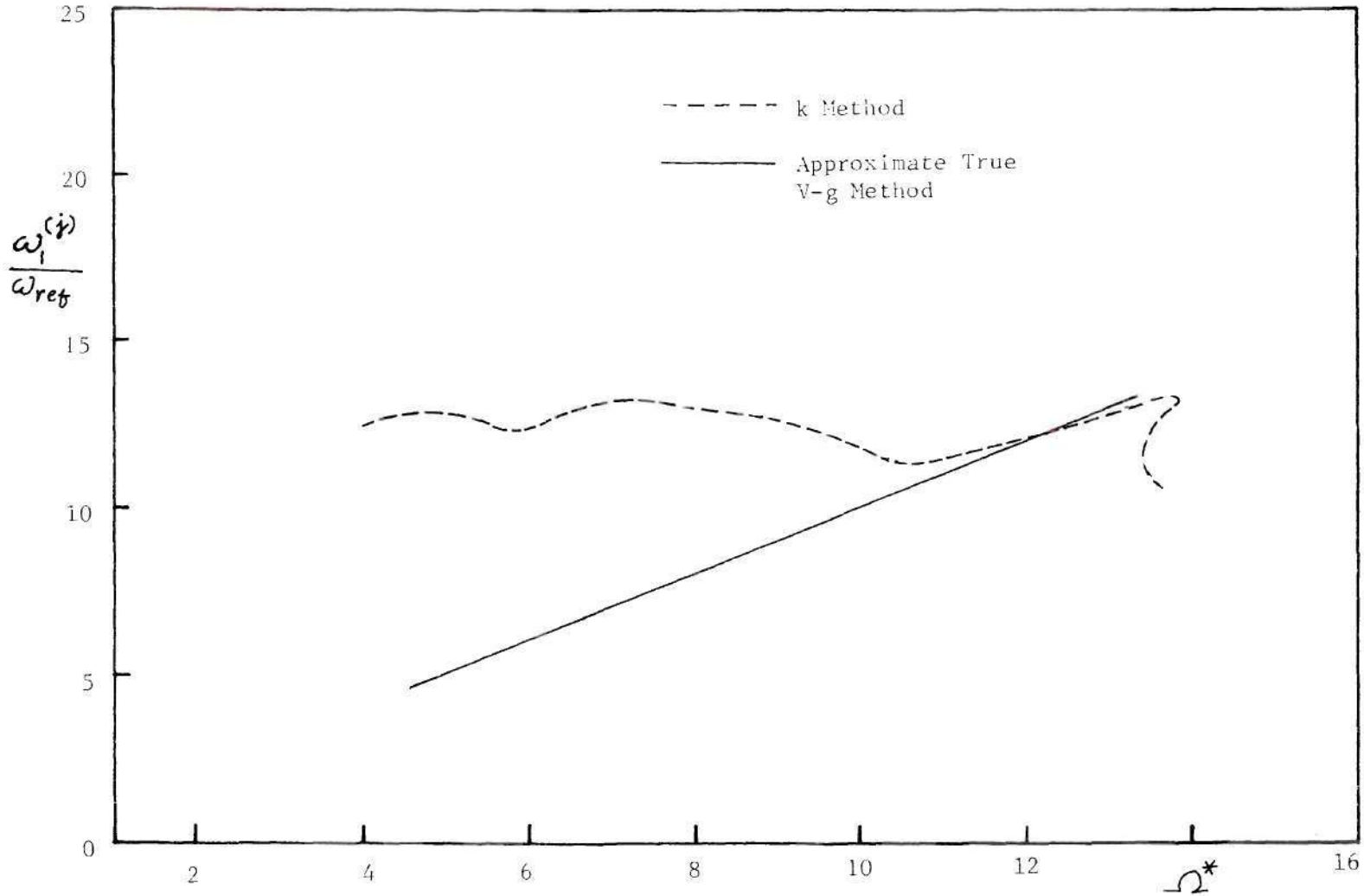

Figure 16a. Frequency-Rotor Speed Plot of the First Mode.

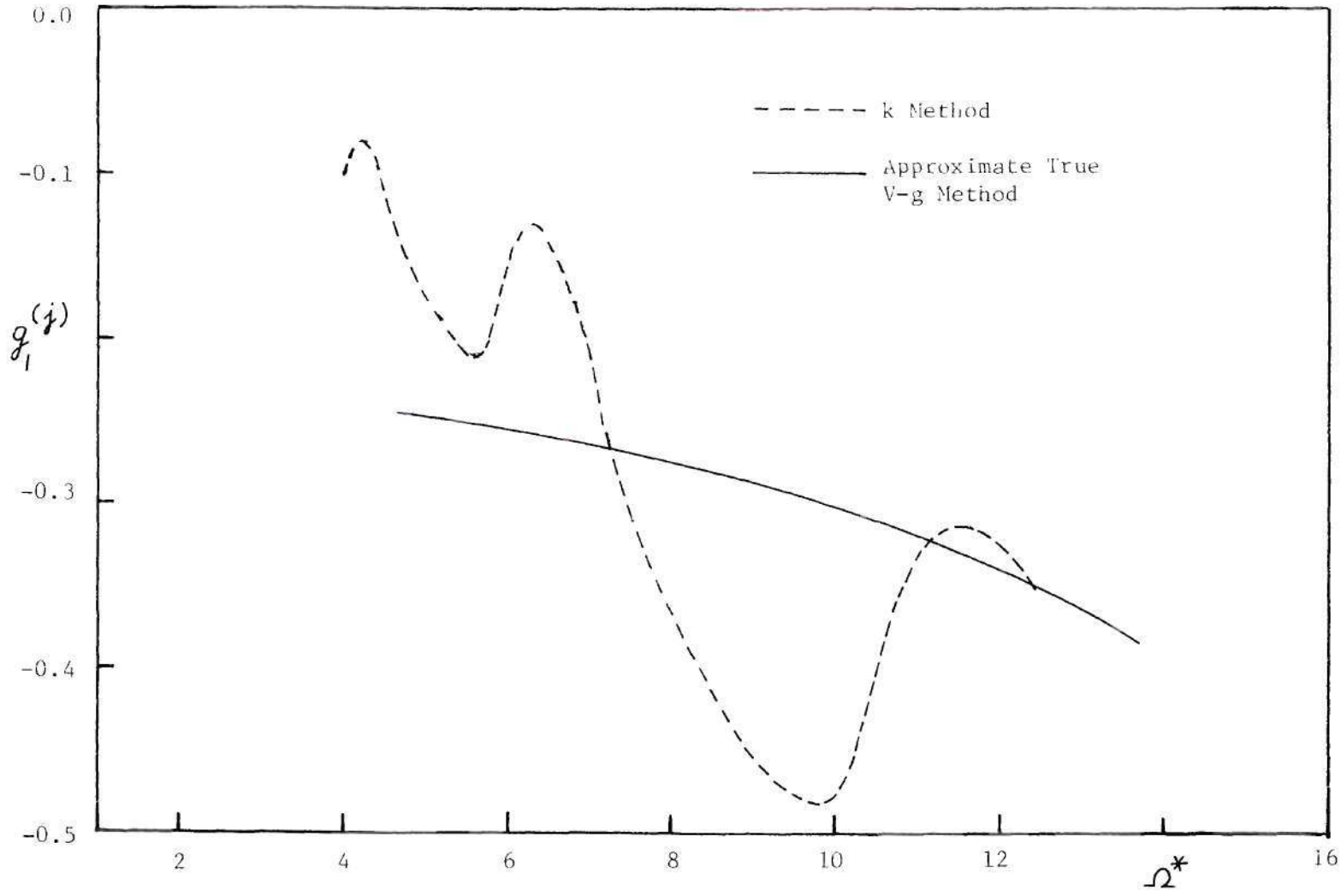

Figure 16b. Damping-Rotor Speed Plot of the First Mode.

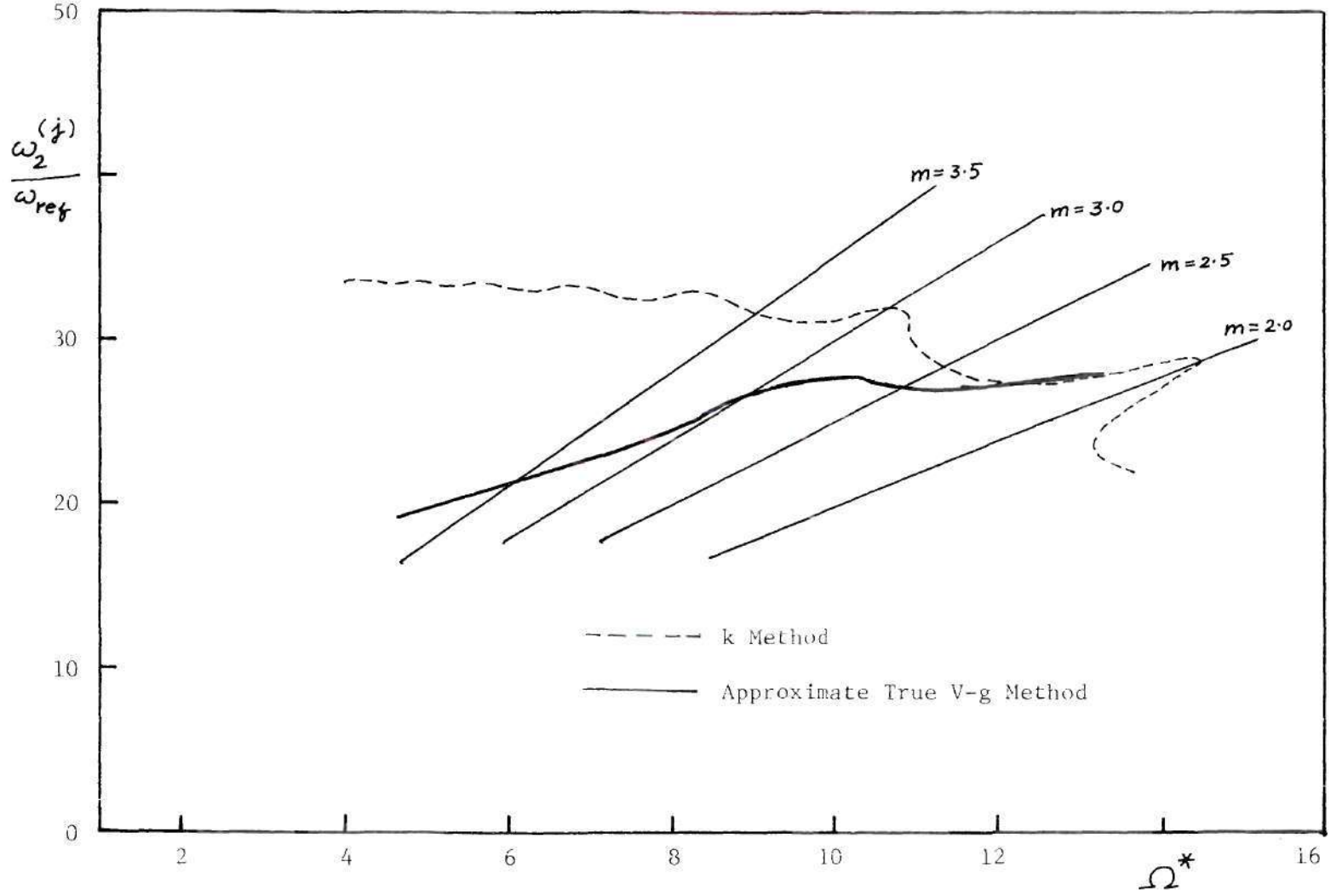

Figure 17a. Frequency-Rotor Speed Plot of the Second Mode.

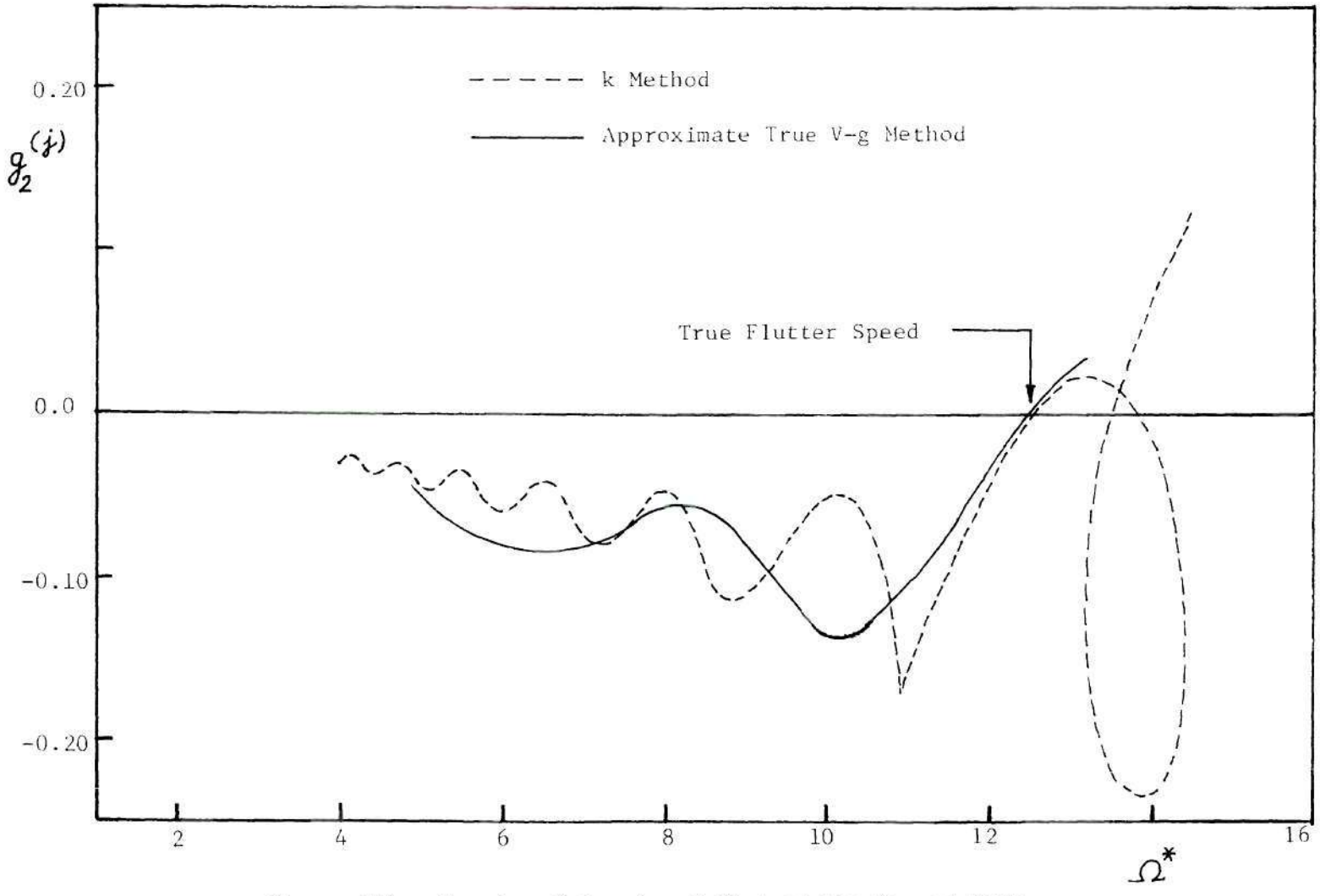

Figure 17b. Damping-Rotor Speed Plot of the Second Mode.

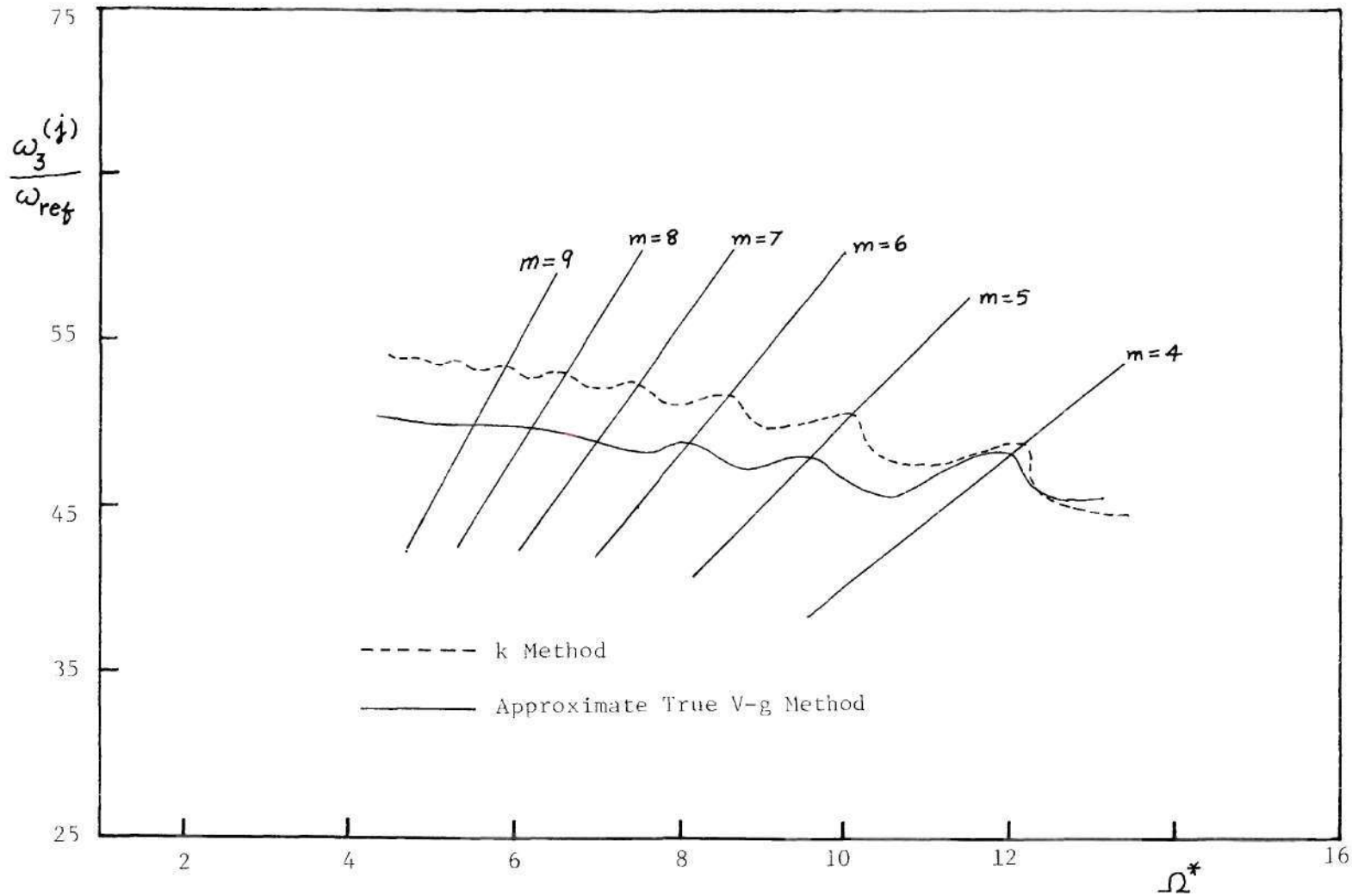

Figure 18a. Frequency-Rotor Speed Plot of the Third Mode.

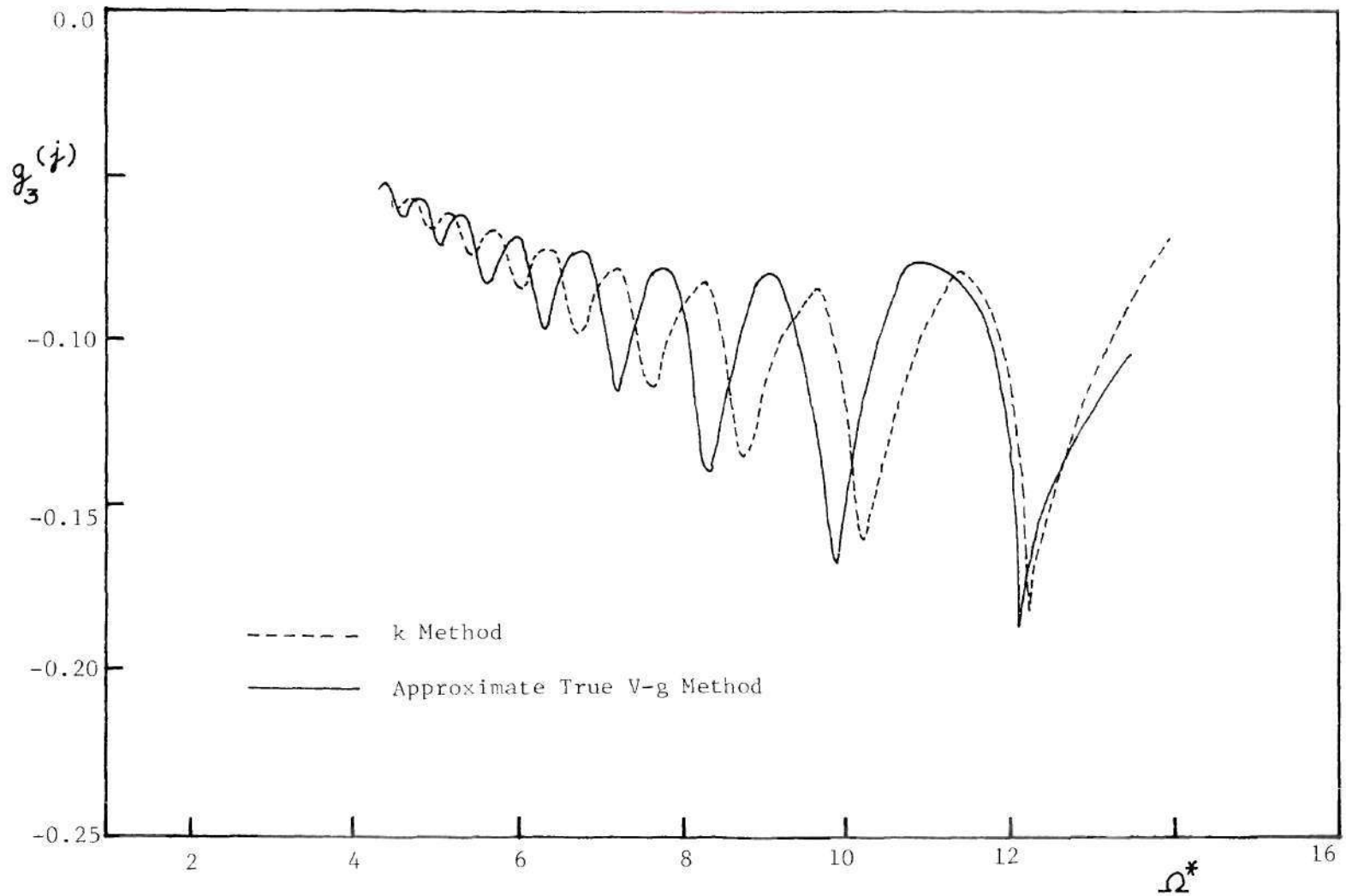

Figure 18b. Damping-Rotor Speed Plot of the Third Mode.

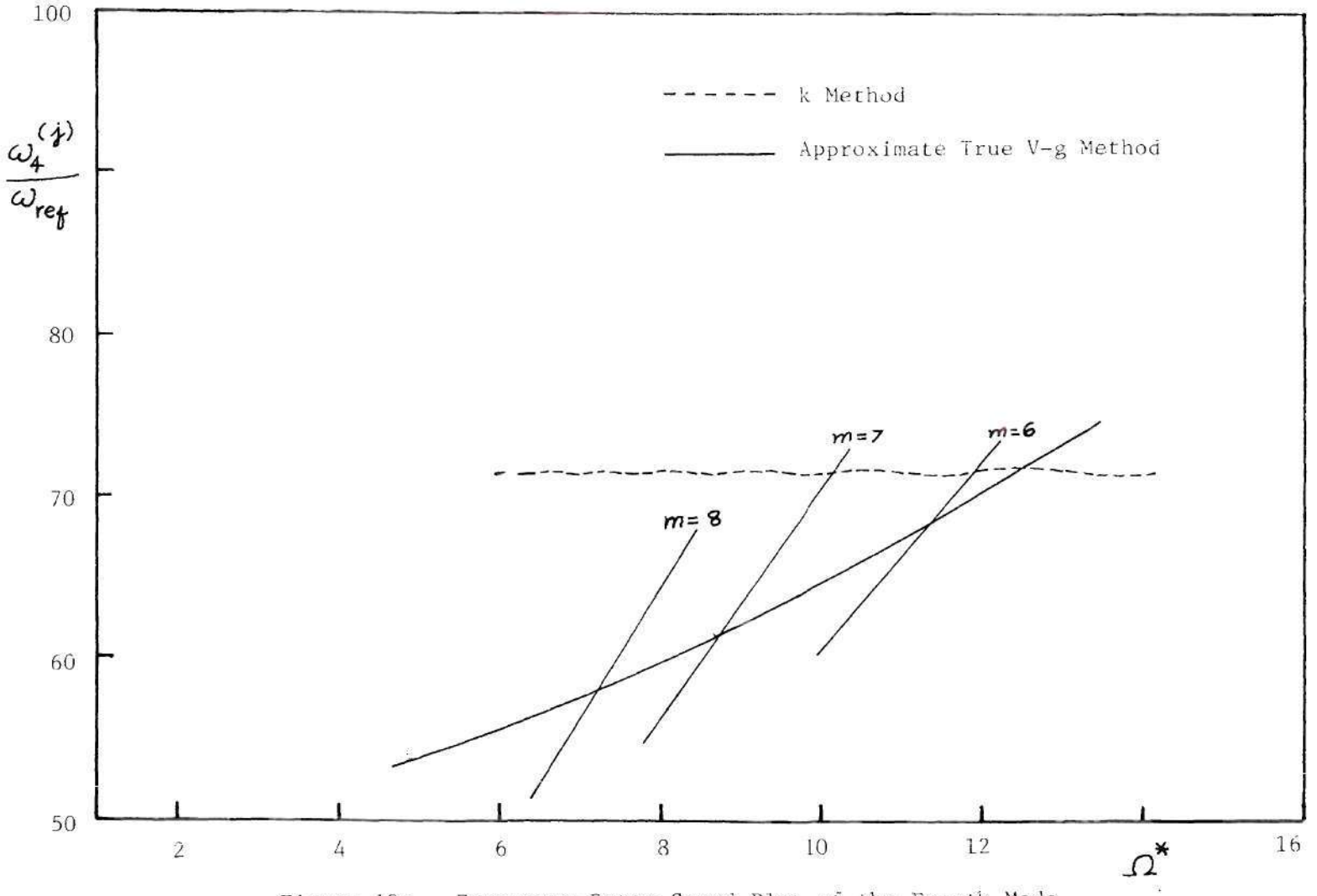

Figure 19a. Frequency-Rotor Speed Plot of the Fourth Mode.

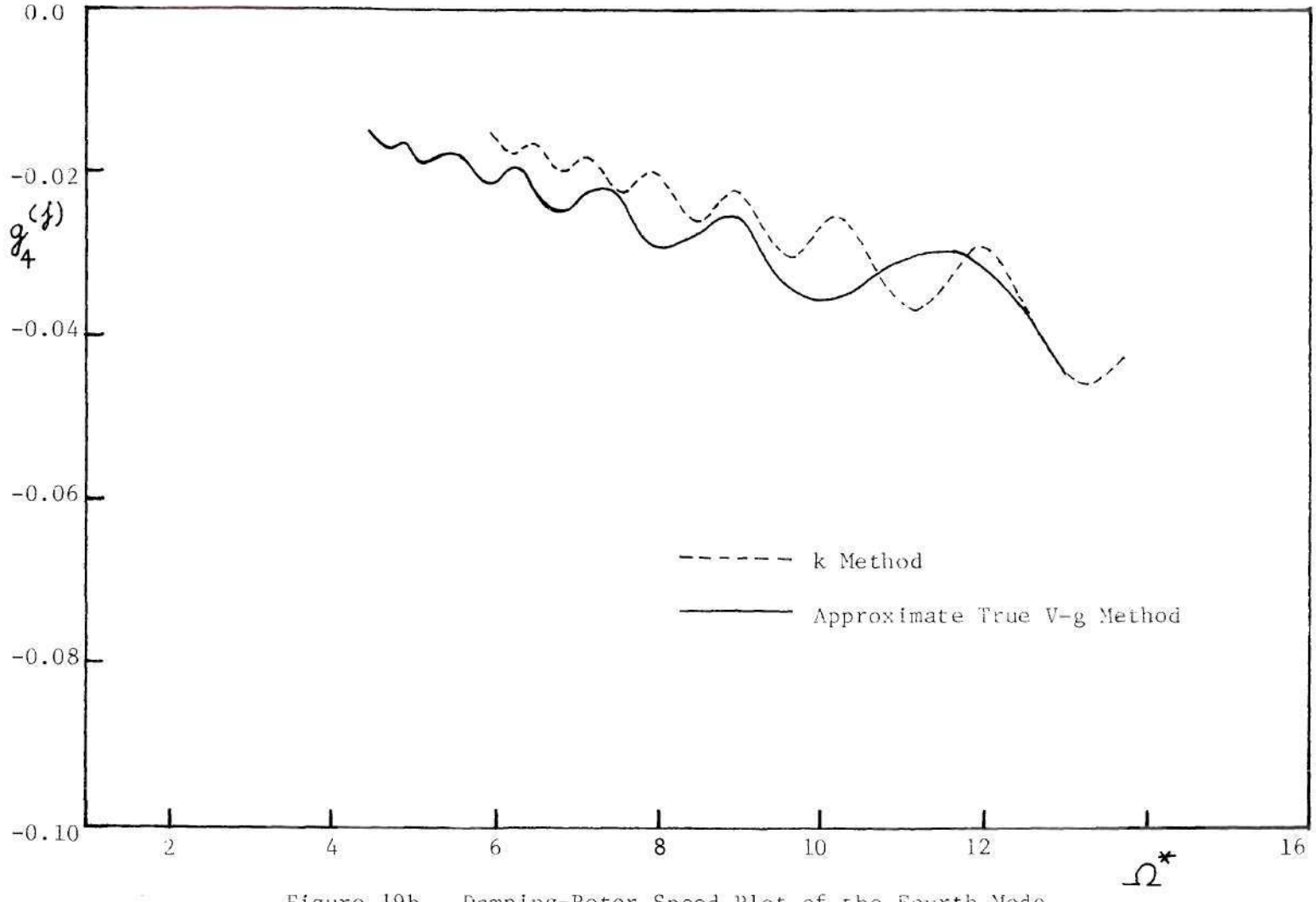

Figure 19b. Damping-Rotor Speed Plot of the Fourth Mode.

of the corresponding quantities by the approximate true V - g method and the p - k method.

Figures 20(a) and 20(b) illustrate the bending and torsional deformations of the blade while undergoing flutter at various instants of time. They were obtained from

$$w_f^*(\eta,t) = \text{Re}\left[\sum_{r=1}^{N} w_r^*(\eta)\bar{\xi}_r \exp(i\omega_f t)\right]$$
$$\alpha_f^*(\eta,t) = \text{Re}\left[\sum_{r=1}^{N} \alpha_r^*(\eta)\bar{\xi}_r \exp(i\omega_f t)\right] \qquad (61)$$

Since the modal response vector $\{\bar{\xi}\}$ is composed of vectors making different angles with the real axis in the Argand Diagram, (different relative phase angles), it follows that when the blade undergoes a flutter oscillation with constant amplitude some part of the blade is always in motion. At no instant of time does the kinetic energy or the potential energy of the system completely vanish. The radial location of the node point (point at which the instantaneous deflection is zero) continuously changes with time. The bending and torsional deformations at each radial station are simple harmonics of a certain amplitude and phase at a frequency equal to the flutter frequency. Since the phase angle at each radial station has in general a different value, it is necessary to draw the shape time histories as shown in Figures 20(a) and 20(b) to completely describe the flutter motion.

The flutter frequency, ω_f, is 195.8 rad/sec. at the rotor speed, Ω_f, of 90.1 rad/sec., while the first three vacuum natural frequencies are 90.1, 243.6 and 397.4 rad/sec. The first of these natural frequencies

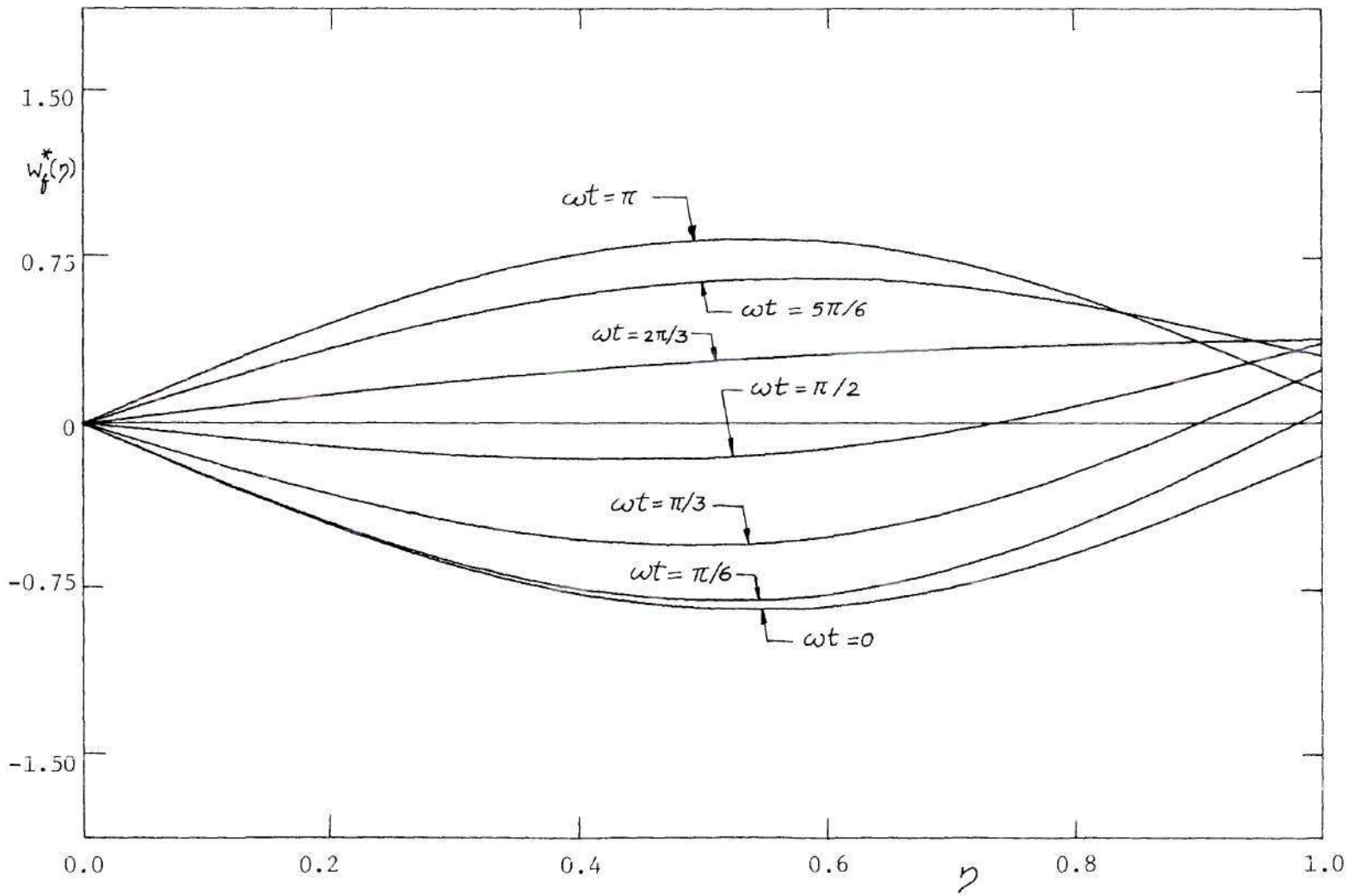

Figure 20a. Bending Deformation of the Fluttering Blade No. 1.

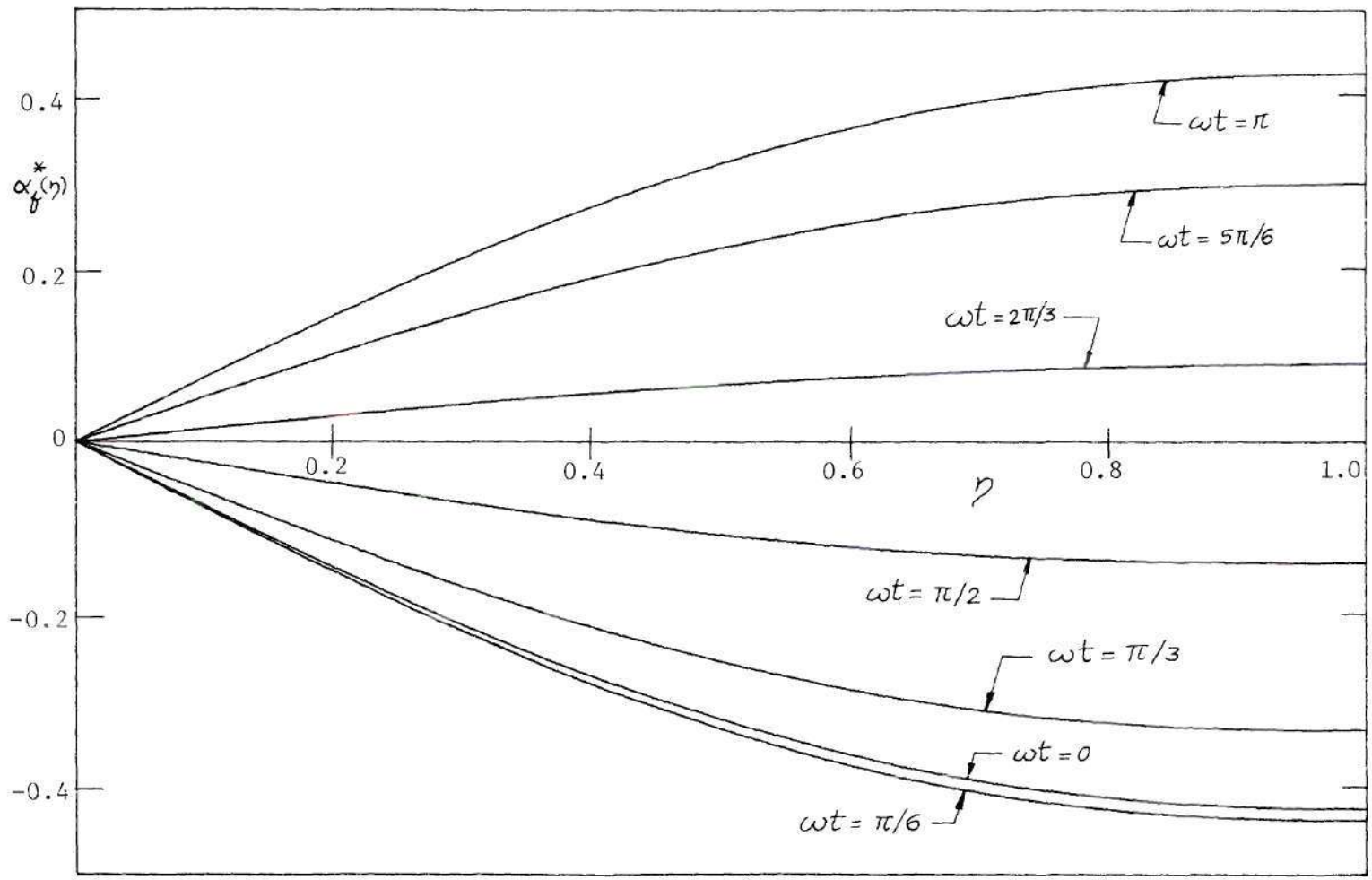

Figure 20b. Torsional Deformation of the Fluttering Blade No. 1.

corresponds to the flapping mode, the second is predominantly the first out-of-plane elastic bending mode, and the third is predominantly the first torsional mode. The flutter mode shape vector consists primarily of these three modes while the contributions from the fourth and fifth modes appear almost negligible.

The scales for Figures 20(a) and 20(b) were chosen so as to give the impression that in this flutter mode, torsional deflection is considerably larger than bending. It is difficult to compare these two descriptions of the deformed blade. The maximum amplitude of torsional deflection occurs approximately at the tip of the blade. The flapping angle (slope of the bending deflection at the root) is considered the appropriate quantity in comparing the relative magnitudes of bending and torsion. The amplitudes of the flutter deformations are arbitrary to a multiplicative constant, since they are the nontrivial solutions to a homogeneous problem. The ratio of the maximum amplitude of torsional oscillation to the flapping oscillation is about 4.36. It is interesting to note that although the vacuum torsional frequency is 397.4 rad/sec., this mode is a prime contributor to flutter which occurs with a frequency as low as 195.8 rad/sec. This emphasizes the importance of including a torsional mode in a flutter analysis.

The variation of the flutter speed for Blades No. 1 and No. 2 was studied for various positions of the center of gravity axis. All of the other dynamic and aerodynamic parameters were left unchanged from the previously specified values. Figure 21 illustrates the results. This study confirms the well known result that the flutter speed considerably

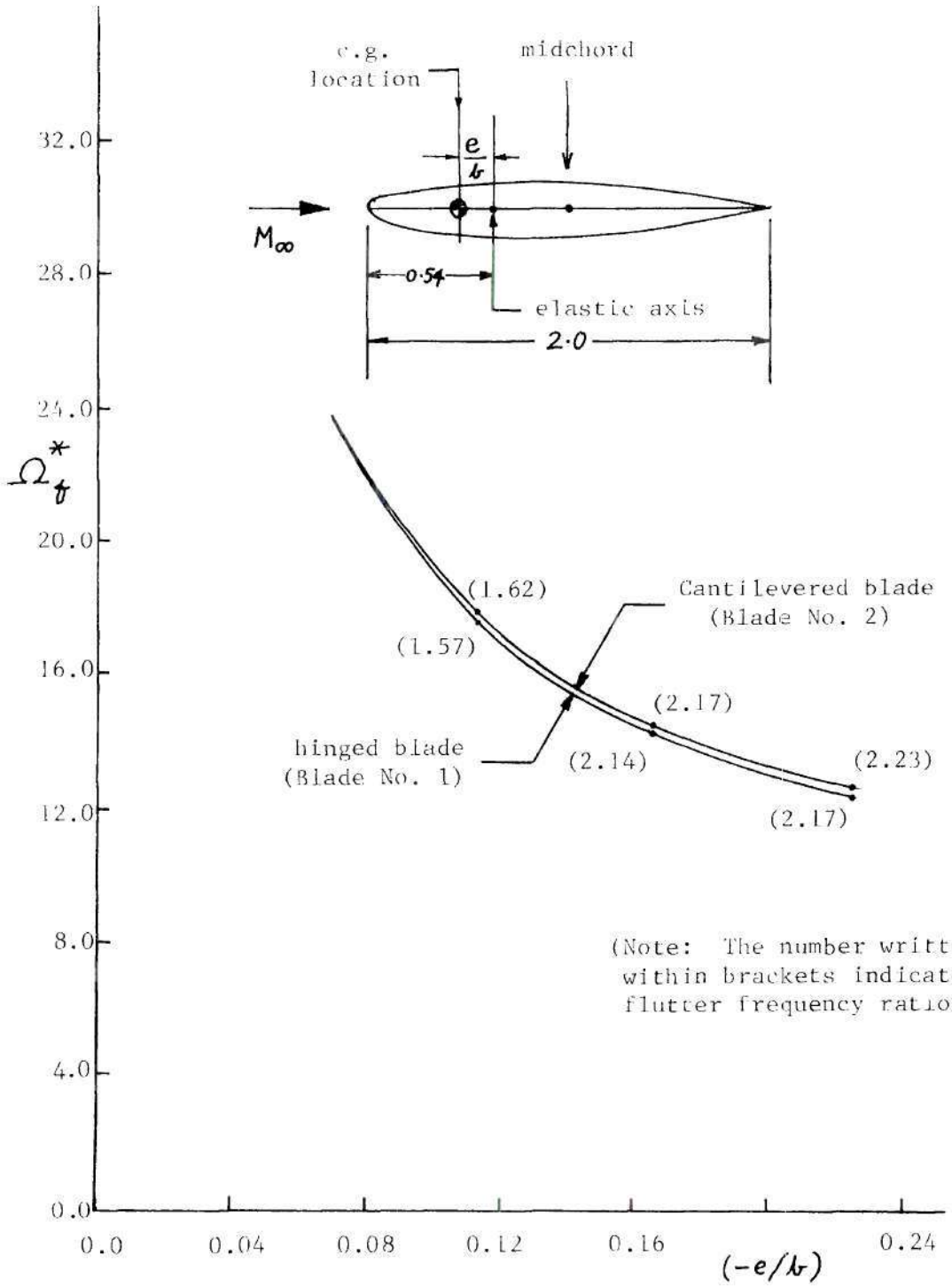

Figure 21. Variation of Flutter Speed with Chordwise Center of Gravity Location.

increases with forward movement of the center of gravity axis. The flutter speeds (as well as flutter frequencies) of the hinged and fixed blades are approximately equal.

Because of the large number of factors that enter the flutter analysis, such a plot as shown in Figure 21 would vary in shape as well as in magnitude from one rotor system to another. In the case of the single bladed rotors with Blades No. 1 and 2, the flutter boundary rotor speed increases with the forward shift of the center of gravity axis. Experiments conducted by Brooks and Baker [9] showed that forward movement of the blade chordwise center of gravity location generally raised the flutter speeds at low pitch angles but had no appreciable effect at high pitch angles.

An Approximate True V - g Solution

It has been mentioned in the previous sections that when the conventional V - g method is used in a rotor flutter analysis, the indicated flutter rotor speed does not, in general, match with the chosen trial rotor speed. This necessitates an iterative procedure so that the indicated flutter speed and trial rotor speed are equal. The frequency - damping - rotor speed plots of an example problem were shown when the trial rotor speed (90.27 rad/sec) matched acceptably with the indicated flutter speed (90.1 rad/sec.).

It can be assumed then, that at Ω = 90.1 rad/sec., the second aeroelastic mode will undergo flutter at ω = 195.8 rad/sec. The flutter mode shape $\{\bar{\xi}\}$ as plotted in Figure 20(a) and 20(b) together with these two eigenvalues satisfy the flutter equations of motion, expressed by Equation

(51) exactly. This solution is emphasized to be exact because this solution is totally independent of the method of solution and the motion is truly simple harmonic with zero damping in this aeroelastic mode.

At all speeds below this speed, every aeroelastic mode possesses positive damping and hence it can never exhibit simple harmonic motion. But it is of interest for the blade designer to have some knowledge about the logarithmic decrement with which each mode will decay at subcritical rotor speeds. Hence the damping should also be predicted by the flutter analysis.

The conventional V - g method fails to accomplish this. As is clear from the analysis, for speeds below the flutter speed, the structural dynamic description as well as the aerodynamic description are inaccurate because of the lack of matching of the assumed rotor speed and the rotor speed resulting from the analysis.

If the factor πg is to be used to describe the logarithmic decrement of the aeroelastic mode, then the applicability of the conventional V - g method is restricted to a region of rotor speeds very close to the trial rotor speed. This is the basis for the approximate true V-g method.

A true V - g solution can be considered to be the combination (Ω, ω, g) that exactly satisfies Equation (55). Let the conventional V - g method be carried out for one trial rotor speed Ω_1. Whenever for some $m_j = \omega_j/\Omega_1$ the value $\Omega_i^{(j)}$ inferred from the eigenvalue $\lambda_i^{(j)}$ equals Ω_1, there is obtained a true V - g solution $(\Omega_1, \omega_j, g_i^{(j)})$. For one trial rotor speed, in general, N such true V - g solutions can be obtained. Thus a large number of trial rotor speeds can be selected and by obtaining the N such solutions for each speed, the frequency - damping - rotor speed plots of

the N aeroelastic modes can be generated. This solution is then called the true V - g solution.

But since the computation required to accomplish the above is extensive, a procedure is described below that provides an approximation to the true V - g solution.

A certain rotor speed Ω_1 is chosen and the conventional V - g method is employed to generate the frequency - damping - rotor speed plots. A rotor speed tolerance, $\Delta\Omega_1$, is chosen and only those segments of the frequency - damping - rotor speed plots lying within $\Omega_1 - \Delta\Omega_1 \leqq \Omega \leqq \Omega_1 + \Delta\Omega_1$ are considered sufficiently accurate and useful. Then, a higher rotor speed Ω_2 is chosen along with $\Delta\Omega_2$ and another segment of the plots are generated for $\Omega_2 - \Delta\Omega_2 \leqq \Omega \leqq \Omega_2 + \Delta\Omega_2$. Note $\Omega_2 - \Delta\Omega_2$ is set equal to $\Omega_1 + \Delta\Omega_1$ for continuity in the results.

In the example flutter analysis of Blade No. 1, the rotor speeds chosen were 35, 45, 55, 65, 75 and 85 rad/sec. The $\omega_i^{(j)}$, $g_i^{(j)}$ plots of each rotor speed were considered good for $\Delta\Omega$ = 5 rad/sec. These plot segments obtained from the rotor speeds are faired to provide a continuous and smooth result.

Figure 16(a) compares the frequency-rotor speed plot of the first mode by the k method (conventional V - g method) and the approximate true V - g method. $\Delta\Omega^*$ was chosen to be 0.7. It turns out that the k method always predicts the frequency of this mode to be approximately the same as the chosen rotor speed itself. This is quite expected because this mode is a rigid body flapping mode with vacuum natural frequency being the rotor speed itself. The prediction in the close neighborhood of the matched flutter speed is same by both methods.

Figure 16(b) shows the damping in the almost pure first harmonic rigid body flapping mode.

The erroneous prediction of the frequencies by the k method or the conventional V - g method at the non-matched rotor speeds, prevents it from predicting the unsteady aerodynamic damping accurately since the unsteady aerodynamic forces are highly dependent on the frequency ratio at low inflow conditions.

In the second aeroelastic mode, the conventional k method predicts a rapidly oscillating damping while the approximate true V - g method predicts a more gradual change in damping. For the third mode, both methods predict similar damping characteristics. This mode being predominantly torsion, the frequency remains fairly independent of rotor speed (as predicted by both methods). As the rotor speed increases, the blade damped natural frequency ratio passes through integer values from about 10 to 4.

It has so far been discussed as to how the state of the art in employing the k method has been improved for its automated application in a rotor flutter analysis. The subcritical damping prediction is almost always unsatisfactory. Hence the conventional k method may be concluded to be inadequate for subcritical analyses.

The approximate true V - g method, on the other hand, seems to predict the frequencies and damping well, although comparisons should be made with experimental results. At any chosen rotor speed, the damped natural frequencies in the several sought aeroelastic modes can be estimated as follows. If the chosen rotor speed is small, then these frequencies will be close to the undamped natural frequencies. If the

chosen rotor speed is large, then the aerodynamic forces can be expected to have influenced these frequencies and an approximate estimate must be made by inspecting the frequencies calculated for lower rotor speeds. The frequency ratios to be scanned prior to the eigenvalue problem can be restricted to those values which will give rise to output rotor speeds which are in the desired range, namely slightly above and below the chosen rotor speed. In this manner, the computation time can be considerably reduced and the procedure automated.

CHAPTER V

THE p-k METHOD OF FLUTTER SOLUTION

The Concept of the Decay Rates

It was assumed in Chapter III that the blade motion could be described through the superposition of normal modes as

$$\begin{aligned} \alpha(y,t) &= \sum_{r=1}^{N} \alpha_r(y)\xi_r(t) \\ w(y,t) &= \sum_{r=1}^{N} w_r(y)\xi_r(t) \end{aligned} \tag{62}$$

Utilizing this representation, the equations of blade bending and torsional motion are described by

$$M_r\ddot{\xi}_r + (1 + ig_r)\omega_r^2 M_r \xi_r = \Xi_r(t), \quad r = 1 \text{ to } N \tag{63}$$

where

$$\Xi_r(t) = -\int_0^R L(y,t)w_r(y)dy + \int_0^R M_{ea}(y,t)\alpha_r(y)dy \tag{64}$$

Consider a solution of the form

$$\xi_r(t) = \bar{\xi}_r \exp(pt), \quad r = 1 \text{ to } N \tag{65}$$

where $p = (\gamma\omega + i\omega)$ and $\bar{\xi}_r$ is the complex amplitude of the r-th mode. According to this solution, every point on the lifting surface undergoes a motion of the form

$$D \exp(\gamma\omega t) \cos(\omega t + \phi)$$

The amplitude of the oscillatory motion is $D \exp(\gamma\omega t)$, where D is a function of the y location on the lifting surface. This amplitude decays exponentially when $\gamma < 0$. ω is the damped frequency of the vibration and ϕ is the phase angle with respect to some reference time. It is interesting to note that at every point the motion decays with the same value of the logarithmic decrement, namely $2\pi\gamma$.

Since $L(y,t)$ and $M_{ea}(y,t)$ are linear functions of the normal coordinates, they will also be of the form $\exp(pt)$, but possibly with a phase shift.

$$L(y,t) = L_3(y)\left[\sum_{r=1}^{N} w_r(y)\xi_r(t)\right]/b(y) + \\ + L_4(y)\left(\sum_{r=1}^{N} \alpha_r(y)\xi_r(t)\right) = \bar{L}(y)\exp(pt) \tag{66}$$

Hence,

$$\bar{L}(y) = L_3(y)\left[\sum_{r=1}^{N} w_r(y)\bar{\xi}_r\right]/b(y) + L_4(y)\sum_{r=1}^{N} \alpha_r(y)\bar{\xi}_r \tag{67}$$

and, similarly,

$$\bar{M}_{ea}(y) = M_3(y)\left[\sum_{r=1}^{N} w_r(y)\bar{\xi}_r\right]/b(y) + M_4(y)\sum_{r=1}^{N} \alpha_r(y)\bar{\xi}_r \tag{68}$$

where L_3, L_4, M_3 and M_4 are complex unsteady aerodynamic coefficients, which are functions of p/Ω and other parameters. They can be represented by

$$\begin{Bmatrix} L_3(y) \\ L_4(y) \\ M_3(y) \\ M_4(y) \end{Bmatrix} = -\pi\rho_\infty\omega^2 b^4 \begin{Bmatrix} L_{hp}/b \\ [L_{\alpha p} - L_{hp}\varepsilon]/b \\ -M_{hp} + L_{hp}\varepsilon \\ -M_{\alpha p} + (L_{\alpha p} + M_{hp})\varepsilon + \\ -L_{hp}\varepsilon^2 \end{Bmatrix} \tag{69}$$

where the second subscript, p, denotes that these are p-type aerodynamic coefficients. An aerodynamic theory that is developed for a motion of the form exp (pt) is called p-type. A contrasting aerodynamic theory dealing with simple harmonic motion of the form exp ($i\omega t$) is called k-type, where k is a conventional notation for the reduced frequency associated with ω. The p-k method uses k-type aerodynamics with modifications, to simulate a p-type motion. The generalized aerodynamic forces of Equation (64) can be expressed by

$$\Xi_r(t) = \overline{\Xi}_r \exp(pt), \quad r = 1 \text{ to } N \tag{70}$$

where

$$\overline{\Xi}_r = \pi\rho_\infty\omega^2 b_{ref}^4 R \sum_{n=1}^{N} A_{rnp} \overline{\xi}_n, \quad r = 1 \text{ to } N \tag{71}$$

and

$$A_{rnp} = \int_0^1 [\beta^2 L_{hp}\, w_r^* w_n^* + \beta^3 \{L_{\alpha p} - L_{hp}\varepsilon\}\, w_r^*\, \alpha_n^* + \beta^3 \{M_{hp} - L_{hp}\varepsilon\}\, \alpha_r^*\, w_n^* + \beta^4 \{M_{\alpha p} - (L_{\alpha p} + M_{hp})\varepsilon + L_{hp}\varepsilon^2\}\, \alpha_r^*\, \alpha_n^*]\, d\eta \tag{72}$$

Equation (63) can now be written as

$$p^2 M_r^*\, \bar{\xi}_r + (1 + ig_r)\omega_r^2 M_r^*\, \bar{\xi}_r = \omega^2 \sum_{n=1}^{N} \bar{\xi}_n\, A_{rnp},\quad r = 1 \text{ to } N \tag{73}$$

or in matrix form as

$$\left[[(p/\omega)^2 + (1 + ig_r)(\omega_r/\omega)^2] M_r^*\right] \{\bar{\xi}\} = [A_p]\{\bar{\xi}\} \tag{74}$$

where A_{rnp} is the element on the r-th row and n-th column of matrix $[A_p]$. A_{rnp} can be evaluated after obtaining L_{hp}, $L_{\alpha p}$, M_{hp} and $M_{\alpha p}$ at several points along the radius by knowing the local Mach number, inflow ratio, frequency ratio, reduced frequency, decay rate, the number of blades and the phase angle between blades.

Equation (74) represents the equations of motion that must be satisfied for the blades to undergo a motion of the form described by Equation (65). This relation represents N algebraic equations which are linear, homogeneous, and contain p/ω as an unknown quantity.

The overall problem can be stated as follows: For given operating conditions specified by Ω, ρ_∞, a_∞, $\alpha_s(o)$, etc. is it possible to find a value for p, ω and $\{\bar{\xi}\}$ such that Equation (74) is satisfied? If yes, then this solution constitutes an aeroelastic mode. To demonstrate these aeroelastic modes in a laboratory, the wake must be first perturbed consistent with the blade vibration pattern.

At one rotor speed, there will be N aeroelastic modes. It is interesting to note that just like N normal modes, each of these N aeroelastic modes can be excited independent of each other. Each one is separately identifiable by a mode shape $\{\bar{\xi}\}$, a decay rate γ and a damped natural frequency ω.

Inference of the Decay Rates from Forced Response

The decay rates of the aeroelastic modes provide a means of assessing the amount of damping present in the aeroelastic system. It was pointed out that at each rotor speed, Ω, there in general would exist N aeroelastic modes, each individually characterized by a mode shape, frequency and decay rate. A knowledge of these quantities at sub-flutter rotor speeds provides a measure of the aeroelastic stability of blade motion.

Almost all comprehensive unsteady aerodynamic theories are of the k-type. When a lifting blade surface is acted upon by externally applied simple harmonic forces, the steady state blade response is also simple harmonic. The k-type aerodynamic theory will then predict the simple harmonic airload acting on the blade. From the equations of motion, the resulting response can be obtained at all points of the surface for any

prescribed simple harmonic forcing function. The response amplitudes will be functions of the frequency of excitation. As the forcing frequency is varied, the amplitude response can be evaluated as a function of the forcing frequency, and thus the frequency response function can be obtained.

In the classical theory of single-degree-of-freedom systems, several techniques are available which can be used to predict the decay rate of the system. These techniques are based on quantities like the frequency width of the half power points near resonance, the slope of the phase angle versus frequency at resonance, inference from the in-phase response and so on. These methods are exact.

For multi-degree-of-freedom systems, the above methods yield approximate results. If the damped natural frequencies of the various aeroelastic modes are far apart compared to the frequency width between their half power points, then the single degree of freedom assumption can be used to obtain an approximation to the decay rates.

For continuous systems with numerous degrees of freedom, the shape of the amplitude response curve, namely the plot of the response amplitude versus forcing frequency is dependent on the location of the response measurement and the point (or points) of application, of the forcing function. Consequently, for aeroelastic systems, these methods seem to be somewhat unreliable for predicting the damping. However, experimentally obtained frequency response characteristics are very useful in substantiating a k-type unsteady aerodynamic theory. Such a theory can be used in the p-k method to obtain the decay rates directly.

The Principle of the p-k Method

The p-k method is an approximate technique to obtain the decay rates by employing a k-type aerodynamic theory in a modified fashion for a p-type motion. Employing a comprehensive p-type aerodynamic theory is a highly involved and formidable numerical task in comparison to an equally comprehensive k-type aerodynamic theory. The advantages of the p-k method will be seen in this light. It is a simple, direct, viable and elegant method for damping prediction which employs k-type aerodynamics. The results are also used for determining the flutter boundary.

For a lifting surface undergoing motion of the form exp (pt), Equation (66) describes the instantaneous unsteady lift, as being proportional to the bending and torsional deflections. In the same equation, the lift is also written as $\bar{L}(y)$ exp (pt) which implies that depending on whether the motion grows or decays, the lift also grows or decays and does so at the same rate and frequency as that of the motion. It is assumed that the functions L_3 and L_4 are not strongly dependent on the magnitude of the decay rate, at least for slowly converging or diverging motions. This is the premise of the p - k method.

Mathematically, this assumption then leads to

$$L_{hp} \approx L_h \tag{75}$$

$$L_{\alpha p} \approx L_\alpha$$

$$M_{hp} \approx M_h$$

$$M_{\alpha p} \approx M_\alpha$$

for all values of γ. Hence the equations of motion given by Equation (74) will be approximated by

$$\left[[(p/\omega)^2 + (1 + ig_r)(\omega_r/\omega)^2] M_r^* \right] \{\bar{\xi}\} = [A]\{\bar{\xi}\} \qquad (76)$$

It can be observed that any error introduced due to the assumption of Equation (75) vanishes at flutter where indeed $\gamma = 0$ and k-type aerodynamics are valid. Equation (50) of Chapter III was written for the flutter condition, and it can be verified that Equation (76) is identical to this relation when $\gamma = 0$ (or $p/\omega = i$).

Equation (76) is a system of N linear, homogeneous, algebraic equations. At any chosen rotor speed, Ω, every value of p (if any) is sought that will produce a non-trivial solution for $\{\bar{\xi}\}$. In other words, all possible aeroelastic modes are to be determined.

Substantiation of the p-k Method

Hassig [2] has discussed the p, the k, and the p-k methods of flutter analysis for fixed wing configurations. The p-k method has been employed in an actual flutter analysis by Irwin and Guyett [20]. They presented a graphical method to match the imaginary part of p with the k value of the aerodynamics.

Hassig [2] has also highlighted, through an example problem, the differences in frequency and damping prediction by application of the three methods at various speeds up to flutter. He considered the case of a twin jet transport aircraft. The flutter equations of motion were first formulated for the p-type motion using the p-type aerodynamics formulated by Mazelsky and O'Connell [21].

The damping - frequency - airspeed plots were obtained employing the p, the k and the p-k methods of solution. The differences in the damping predicted by the p method and the k method were considerable.

However, there were virtually no differences between the damping predicted by the p method and the p-k method. In judging the significance of such an example problem, it should be noted that the unsteady aerodynamic theory employed was in a rather simple form. However, it was sophisticated enough to illustrate the validity of the p-k method.

The p-k method shows considerable promise as a tool for damping prediction. It is direct, and except for the implied assumption on the aerodynamic forces, it is an exact method. Furthermore and very importantly, the p-k method illustrates the concept of the aeroelastic modes and their decay rates, by its very formulation. On the contrary, the conventional k method completely fails in the above regard. However, if only flutter speed is of interest and not the decay rates at sub-flutter speeds, then the conventional k method may require significantly less numerical effort than the p-k method.

Two Numerical Schemes for the p-k Method

The Determinant Iteration Method

Hassig [2] has described the determinant iteration method in detail. The objective of this method is to determine the value of $p = \gamma\omega + i\omega$, which satisfy Equation (76) at a selected rotor speed. It is clear that for a nontrivial solution for $\{\bar{\xi}\}$ to exist,

$$\left| \left[[(p/\omega)^2 + (1 + ig_r)(\omega_r/\omega)^2] M_r^* \right] - [A] \right| = 0 \tag{77}$$

The above equation can be written symbolically as

$$\text{Det } (\Omega, p) = 0 \tag{77a}$$

In the case of a multibladed rotor, the phase differences between the various blades must be assumed. After choosing the rotor speed Ω, the value of p is the only unknown in the elements of the determinant of Equation (77a). The procedure is as follows:

1. Choose an estimated p_1 for the desired aeroelastic mode and obtain Det (Ω, p_1). After choosing another estimated p_2, obtain Det (Ω, p_2).

2. The Regula Falsi method gives a first iterated value for p as

$$p_3 = \frac{[p_2 \text{ Det}(\Omega,p_1) - p_1 \text{Det}(\Omega, p_2)]}{[\text{Det}(\Omega, p_1) - \text{Det}(\Omega, p_2)]} \tag{78}$$

3. This process is repeated according to the recurrence formula

$$p_{i+2} = \frac{p_{i+1}\text{Det}(\Omega,p_i) - p_i \text{ Det}(\Omega,p_{i+1})}{[\text{Det}(\Omega,p_i) - \text{Det}(\Omega,p_{i+1})]} \tag{79}$$

until a specified degree of convergence is obtained. From the converged value of p, the frequency and damping are given as

$$\omega = \text{Im } (p) \tag{80}$$

$$\gamma = \text{Re } (p)/\text{Im } (p)$$

4. By repeating the above three steps, obtain the converged values of p for other aeroelastic modes at this same rotor speed Ω.

5. Proceed to the next rotor speed and repeat steps 1 through 4.

6. Construct the frequency - damping - rotor speed plots of the required number of aeroelastic modes up to the desired rotor speed.

In a fixed wing flutter analysis, the generalized aerodynamic force matrix [A] is normally a relatively smooth function of ω. Hence it is acceptable to calculate [A] at several values of ω and utilize its interpolated result at intermediate values of ω. However, in the case of rotor unsteady aerodynamics, the variation in the aerodynamic coefficients is large, especially near integral values of equivalent frequency ratio. While employing the p-k method, this interpolation scheme can be used to save computation time in the process of convergence.

Evaluation of the complex determinant, Det (Ω, p), is not a particularly difficult task, if $N \leq 7$. It may be advantageous to first reduce the matrix to the triangular form.

An Eigenvalue Method of Solution

Equation (76) can be rearranged as

$$\left[\left[1/M_r^*\right] [A] - \left[(1+ig_r)(\omega_r/\omega)^2\right] - (\gamma+i)^2 \left[I\right] \right] \{\bar{\xi}\} = \{0\} \quad (81)$$

The objective of this method is to determine the pairs (γ,ω) that will satisfy Equation (81). It can be observed that Equation (81) is in a standard eigenvalue form. If a certain value for ω is chosen, then the matrix

$$\left[1/M_r^*\right] [A] - \left[(1 + ig_r)(\omega_r/\omega)^2\right]$$

can be evaluated and the N complex eigenvalues, $(\gamma + i)^2$ can be obtained. Note that for a valid ω, the square root of the eigenvalue is $(\gamma + i)$. Based on this observation the procedure is as follows:

1. Select an approximation $\omega = \omega^{(1)}$ for the first aeroelastic mode. Evaluate the above matrix and obtain all the eigenvalues. In general, only one of the eigenvalues will be such that its complex square root will have an imaginary part whose absolute value is close to 1.

2. That particular root may be expected to lead to a converged eigenvalue. A second approximation, $\omega = \omega^{(2)}$, is chosen and the square root of the potentially converging eigenvalue is evaluated.

3. An iteration procedure is set up so that for the chosen frequency ω, the eigenvalue can be expressed as $(\gamma + i)^2$. Thus the solution pair (γ, ω) can be obtained.

4. Repeat steps 1 to 3 for other aeroelastic modes at this rotor speed Ω.

5. Repeat steps 1 to 4 at other rotor speeds and construct the frequency - rotor speed - decay rate plots of all aeroelastic modes desired.

It should be noted that once the potentially converging eigenvalue has been established, the other $(N-1)$ eigenvalues are of no interest. Furthermore, every time a new frequency ω is chosen in the iteration, an approximation for the converging eigenvalue is available from the previous iteration steps. These two observations can be utilized to advantage using the eigenvalue routine of Desmarais and Bennett [18] as explained in Appendix A.

No comparison has been made regarding the computation time required by these two approaches for the p-k method, but they are expected to be comparable. When more than seven degrees of freedom are involved, generally

the eigenvalue approach is better than the determinant approach. In the example rotor aeroelastic problems to be described, both methods have been found to be satisfactory. In the second method only ω is input and γ is inferred from the output. In the determinant iteration procedure, both γ and ω constitute the input and the iteration is aimed at making both the real and imaginary parts of the determinant vanish simultaneously. The eigenvalue method shows promise but more research should be done to exploit the entire potential of the method.

An Example Problem

In Chapter IV, the damped natural frequencies and decay rates of example Blade No. 1 were obtained by the conventional k method and the approximate true V - g method. Now, for the same blade under identical operating conditions, an aeroelastic analysis is carried out by the p - k method.

Figure 22(a) shows that the frequency of the first aeroelastic mode is almost equal to the rotor speed. This should be expected since this is simply the rigid body flapping mode. Figure 22(b) shows that this mode is highly damped. The logarithmic decrement of an aeroelastic mode is equal to πg as well as $2\pi\gamma$. Hence g and γ are related by $g = 2\gamma$. Figure 23(a) illustrates the damped natural frequency of the mode that will exhibit flutter at high rotor speed. Figure 23(b) shows how the damping rate of this mode depends on rotor speed. This mode exhibits a hard flutter point as characterized by the rapidly decreasing damping near the flutter speed. The flutter mode shape was illustrated in Chapter IV.

The frequency and damping plots of the third aeroelastic mode are shown in Figures 24(a) and (b). This is a predominantly torsional mode.

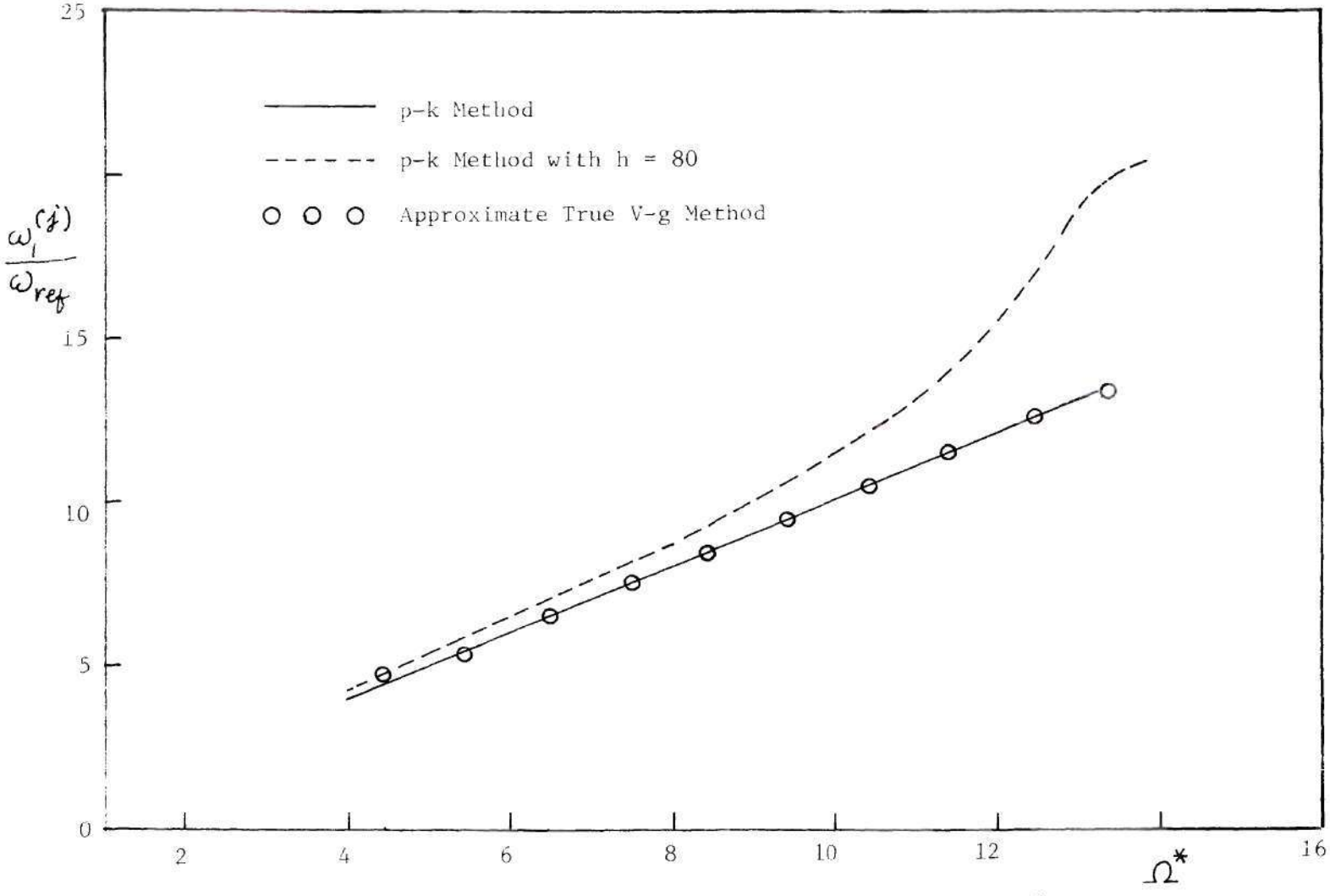

Figure 22a. Frequency-Rotor Speed Plot of the First Mode.

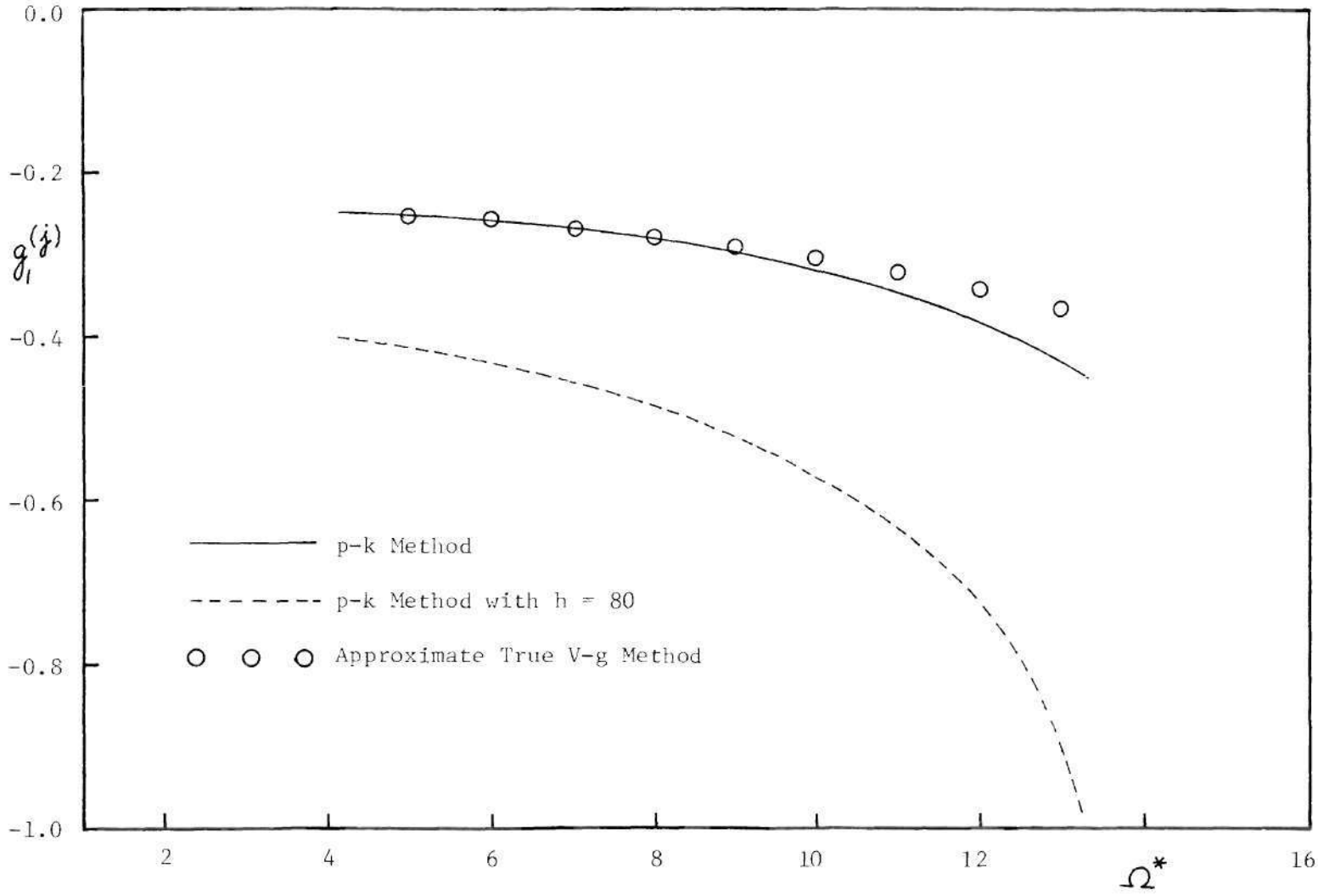

Figure 22b. Damping-Rotor Speed Plot of the First Mode.

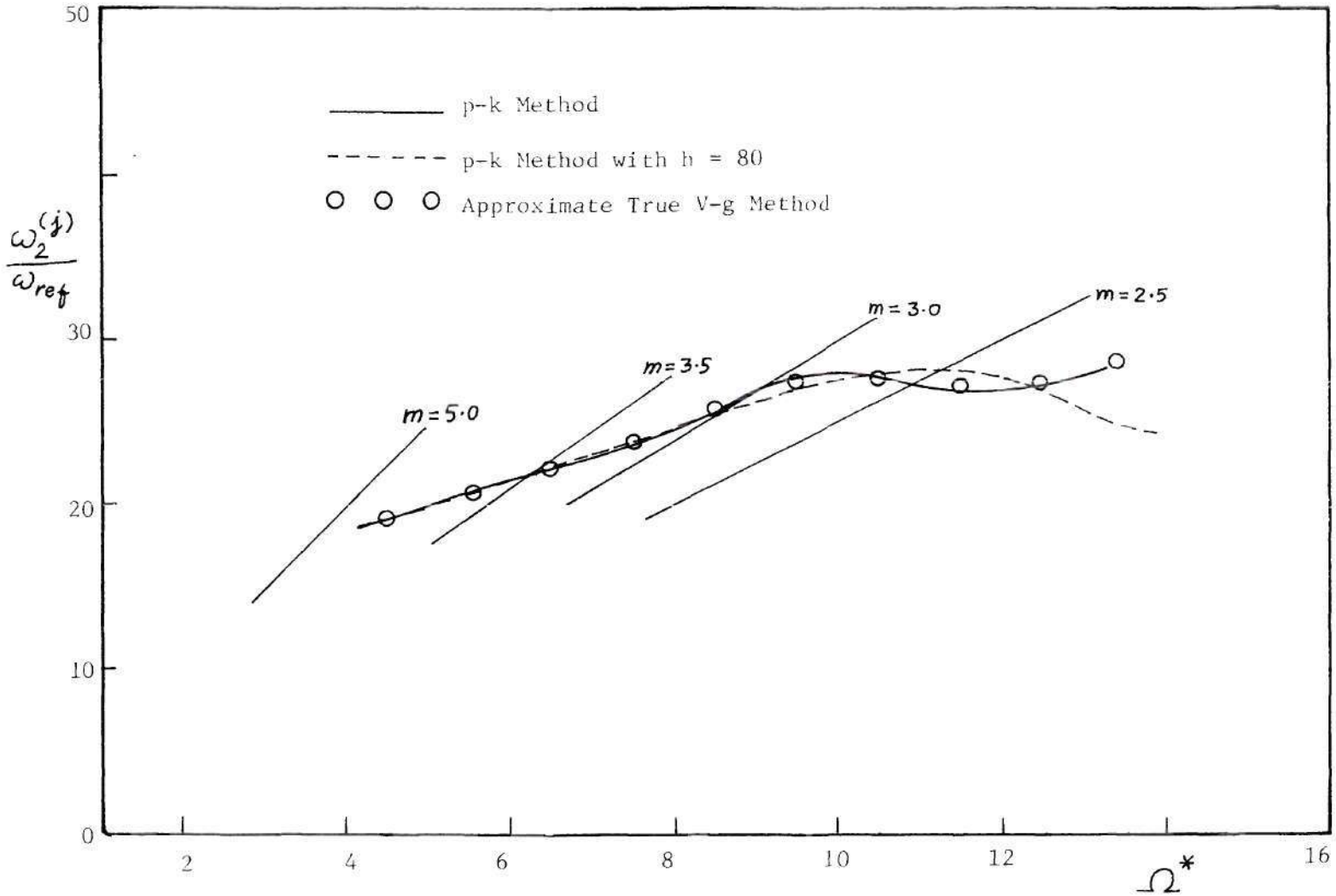

Figure 23a. Frequency-Rotor Speed Plot of the Second Mode.

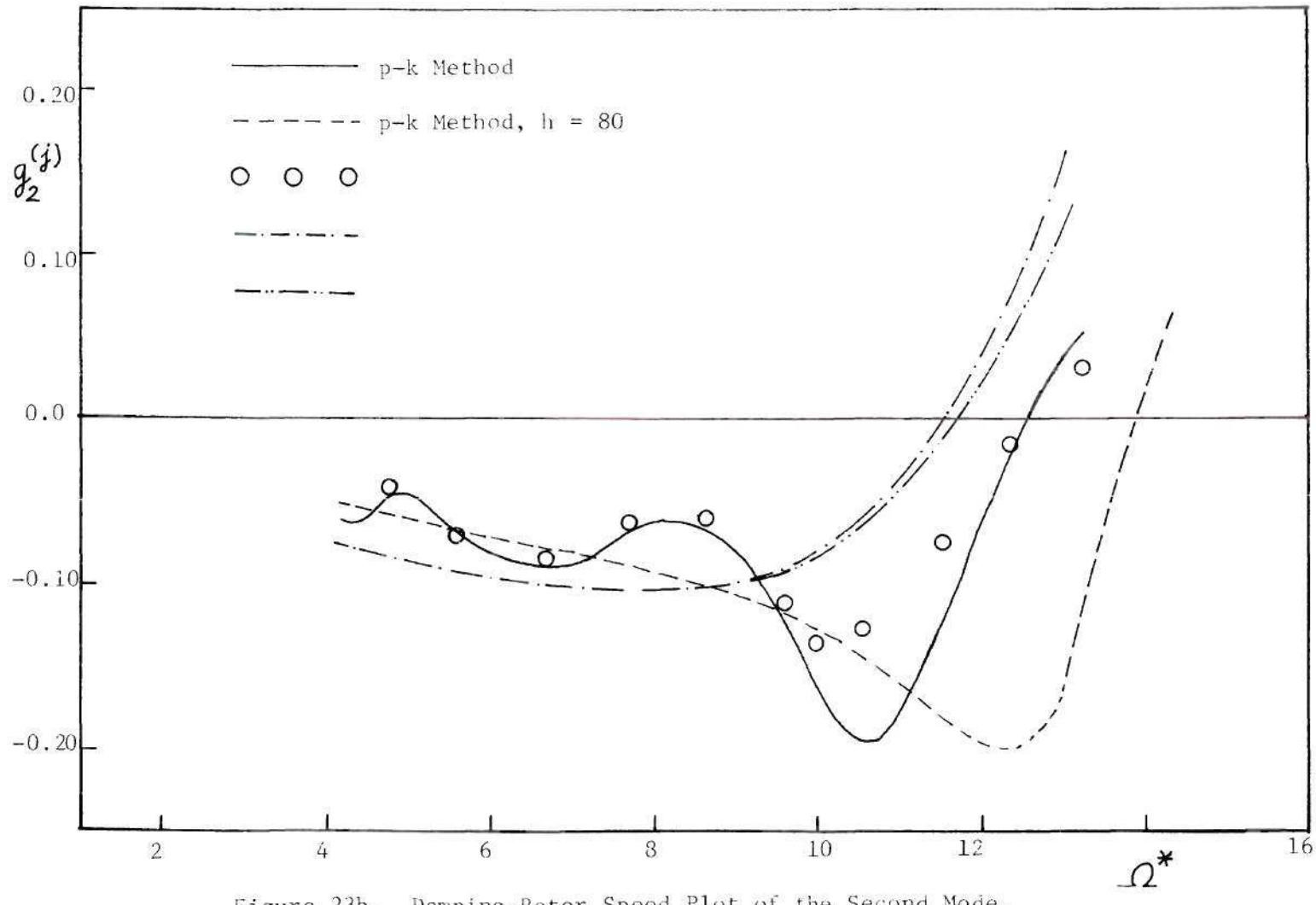

Figure 23b. Damping-Rotor Speed Plot of the Second Mode.

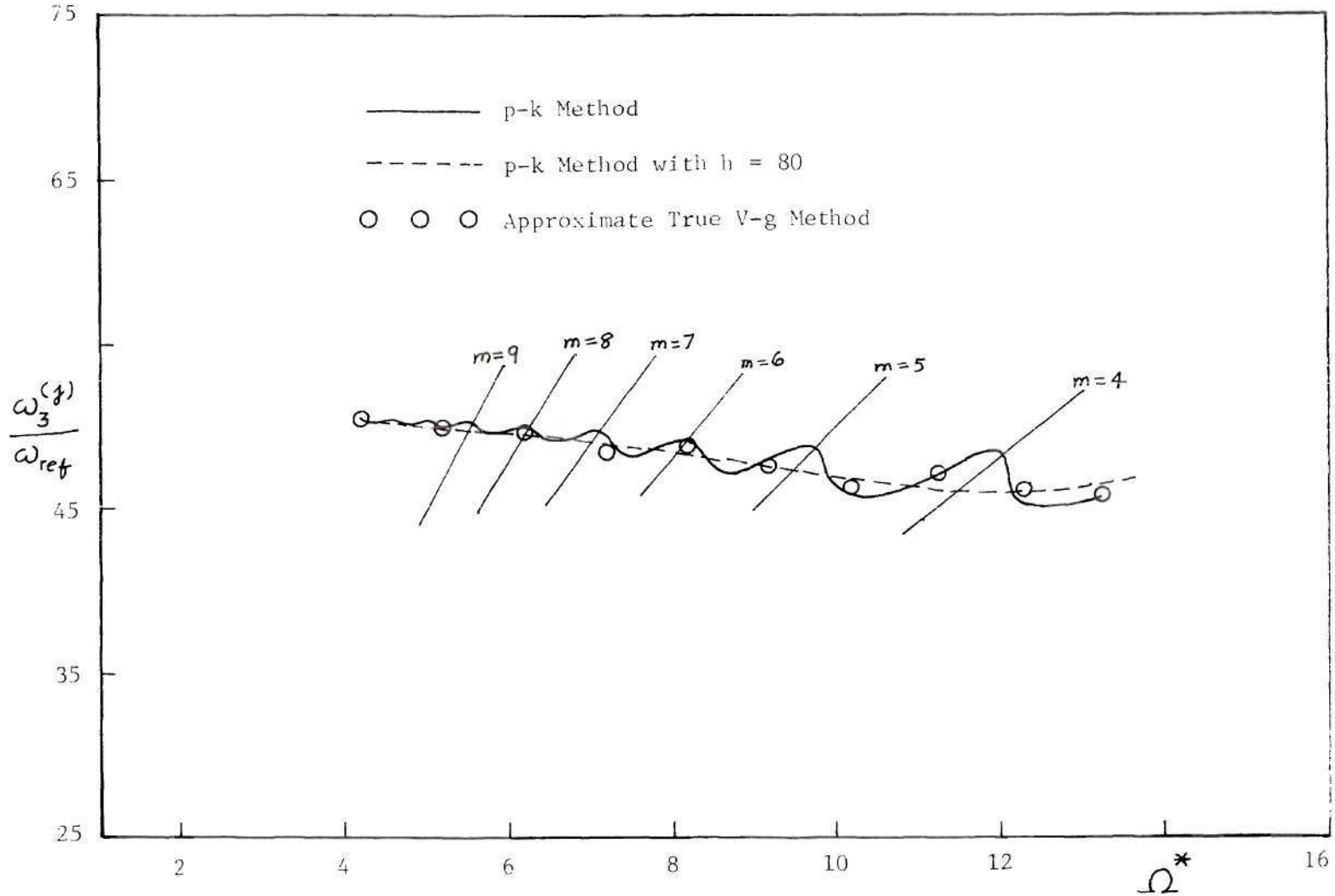

Figure 24a. Frequency-Rotor Speed Plot of the Third Mode.

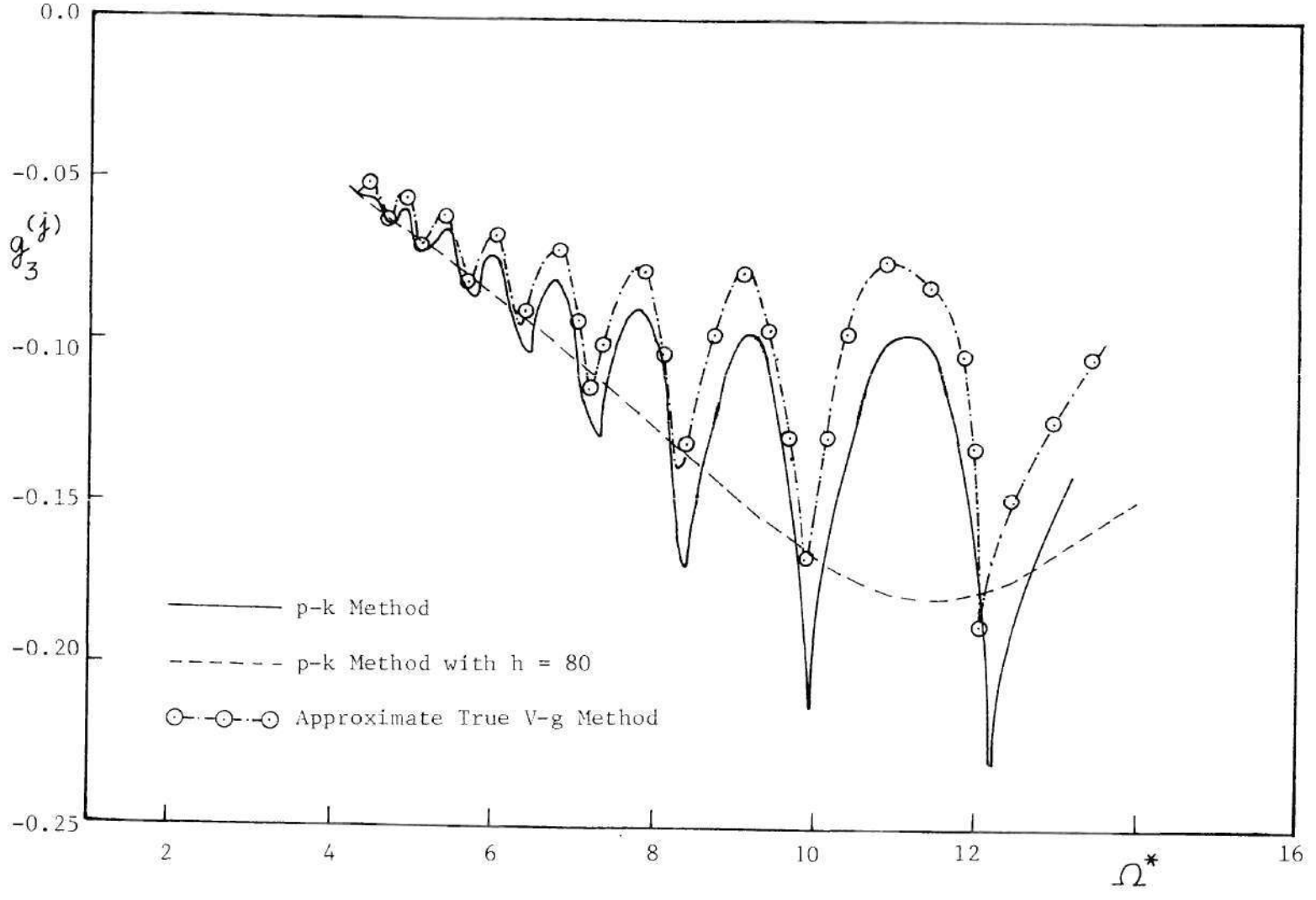

Figure 24b. Damping-Rotor Speed Plot of the Third Mode.

At Ω^* approximately equal to 5.5, the frequency ratio, m equals 9.0, and as the rotor speed increases, the frequency ratio drops to about 4.0 when Ω^* equals 12.0. In Figure 24(b), it can be seen that as the frequency ratio changes by an integer value, the damping curve completes one oscillation. However, every minimum damping point does not coincide with an integer frequency ratio. This oscillatory nature of the damping is a feature of the unsteady rotary wing aerodynamic effects at low inflow conditions. This oscillatory characteristic is due to the close proximity of the lower wakes and will be discussed in the following section.

The behavior of fourth aeroelastic mode is pictured in Figures 25(a) and (b). This mode is predominantly the second flapwise elastic bending. The decay rate plot again is oscillatory with integral values of frequency ratio.

In Figures 22 through 25, the results of the approximate true V - g method are compared with the p - k method. The comparison is good. It may be recalled from the previous chapter that for this example problem, the predictions by the conventional k-method and the approximate true V - g method were not in good agreement at subcritical speeds. The error as previously discussed is in the numerical method of solution.

Effect of the Wakes

If the wake spacing is set to infinity in the Jones and Rao [11] aerodynamic model, the result corresponds to a fixed wing model since only the bound vorticity and trailing vorticity in the plane of the airfoil remain. In the computer program that analyzed the first four aeroelastic modes of Blade No. 1, by the p - k method, the nondimensional wake

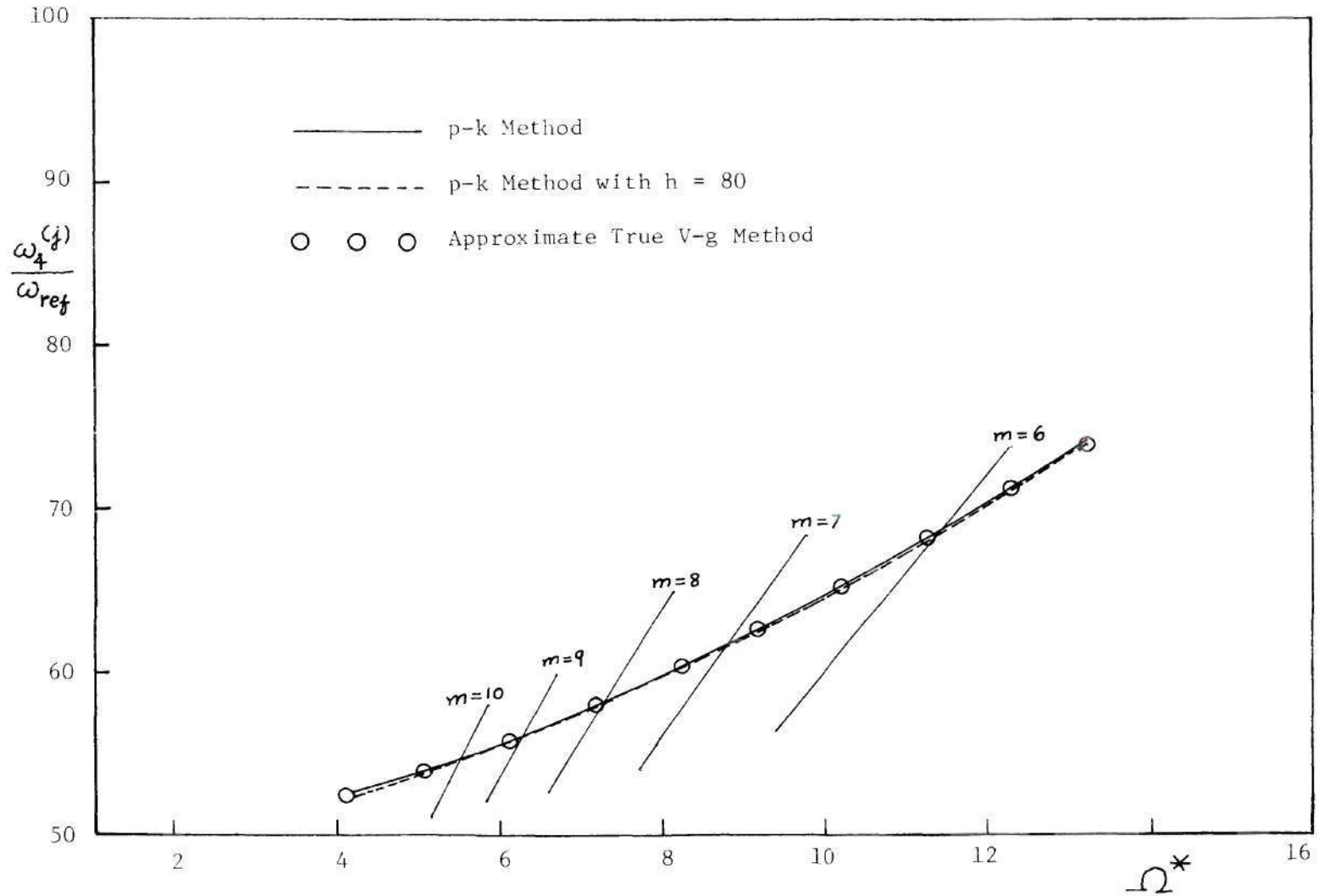

Figure 25a. Frequency-Rotor Speed Plot of the Fourth Mode.

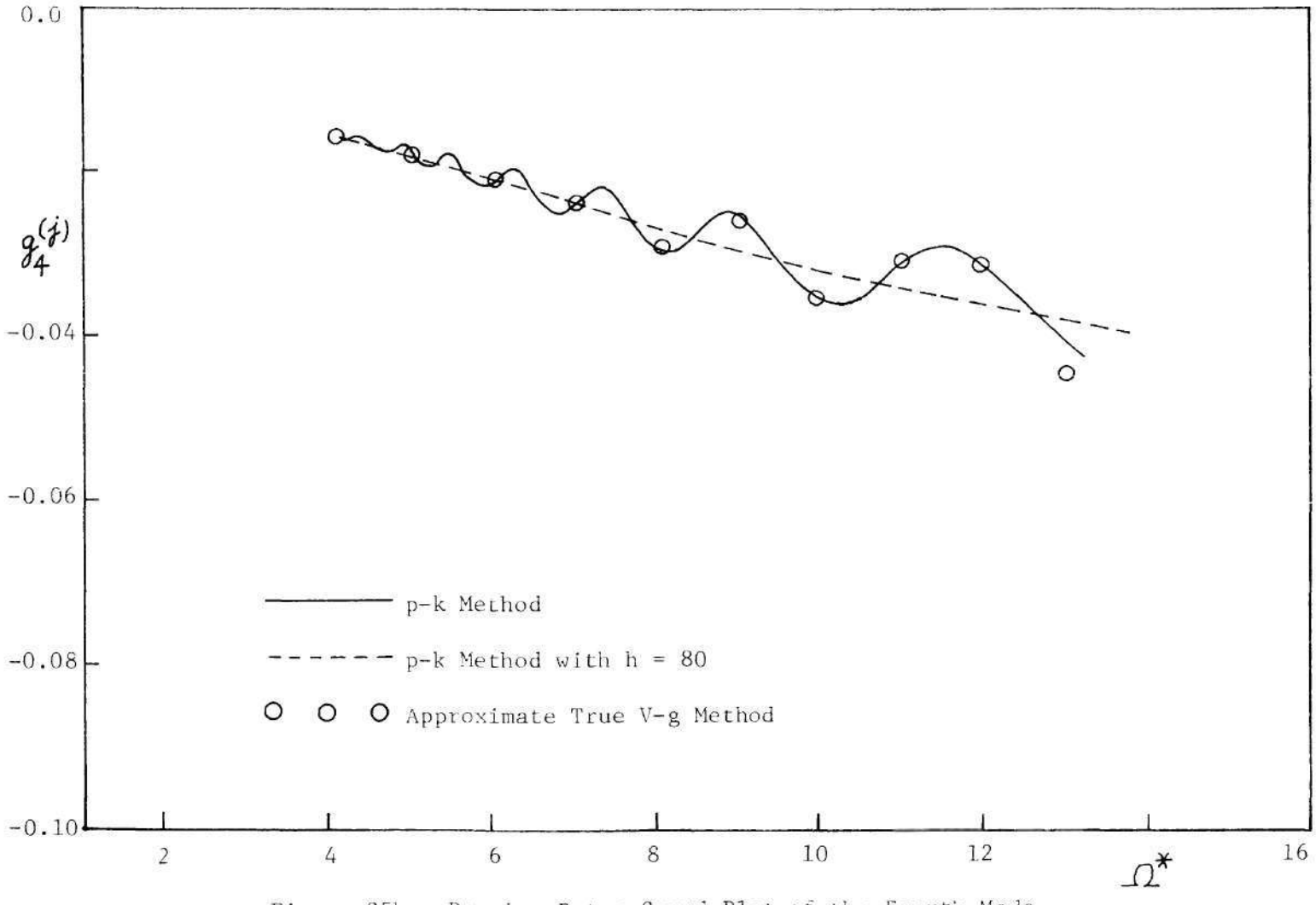

Figure 25b. Damping-Rotor Speed Plot of the Fourth Mode.

spacing, h, was set to 80.0 at all radial stations. This virtually removes the effect of the wakes lying below the rotor.

The damped natural frequency of the first mode which is predominantly the rigid body flapping mode is plotted in Figure 22(a). Figure 22(b) shows that the effect of the lower wakes is to reduce the damping in this mode.

The frequency of the second aeroelastic mode is well predicted even after neglecting the lower wakes, as seen in Figure 23(a). However, Figure 23(b) shows that the damping in this mode does not exhibit the oscillatory feature. The lower wakes induce aerodynamic pressure forces on the airfoil and therefore cause the oscillatory damping behavior that are sensitive to the frequency ratio. The flutter speed is predicted to be considerably higher in the case where the lower wakes are ignored, which implies that neglecting them is unconservative. For predicting low inflow flutter characteristics, the wakes below the rotor plane are obviously very important.

Figures 24 and 25 show that the frequencies of the third and fourth aeroelastic modes are estimated well when the lower wakes are ignored. The amount of damping in these modes do not exhibit an oscillatory nature as is seen in the case with lower wakes. Interestingly, the damping predicted is close to the average damping for the case with the lower wakes.

Two other approximate aerodynamic theories have been employed in the example problem. The first is the steady state aerodynamic theory. The plunging velocity of the airfoil and the unsteady pitch inclination are considered to constitute the instantaneous effective angle of attack. The lift is computed according to steady potential flow theory corresponding

to this angle of attack. The expressions for the aerodynamic coefficients are

$$\begin{aligned} L_h &= -2\ i/k \\ L_\alpha &= -2/k^2 \\ M_h &= 0 \\ M_\alpha &= 0 \end{aligned} \tag{82}$$

The other simplified aerodynamic theory employed is the quasi steady-state theory, which neglects the influences of the wake vortex in the plane of the airfoil. This is equivalent to replacing the Theodorsen function with the value of 1.0, approached as the reduced frequency goes to zero, in the expressions for the unsteady lift and moment of the airfoil about the quarter chord. The aerodynamic coefficients are given by

$$\begin{aligned} L_h &= 1 - 2\ i/k \\ L_\alpha &= \frac{1}{2} - \frac{3i}{k} - \frac{2}{k^2} \\ M_h &= 1/2 \\ M_\alpha &= 3/8 - i/k \end{aligned} \tag{83}$$

The flutter analyses have been performed by the p - k method employing these two approximate aerodynamic theories. The decay rates predicted for the second aeroelastic mode by the two theories are approximately equal and are shown in Figure 23(b). The flutter is predicted to occur at a rotor speed of 84.0 radians/second compared to 90.1 radians/second indicated by the sophisticated rotor unsteady aerodynamic theory [11]. Though the prediction by the simplified theories is conservative,

it does not reveal the oscillatory nature of the damping. Considering the fact that the flutter speed prediction by the unsteady fixed-wing aerodynamic theory is unconservative, it is not possible to relate definitely as to whether the simplified aerodynamic theories are in general conservative or not. For accurate analysis, the sophisticated aerodynamic theories should be resorted to.

A Brief Summary of the Various Methods

Various methods have so far been discussed for the prediction of flutter and damping characteristics. They are summarized here briefly.

1. The p-method: This is an exact method. The motion is recognized to be an exponentially decaying simple harmonic motion (p-type). The aerodynamic theory and structural dynamic theory appropriately reflect the motion.

2. The p-k method: The motion is an exponentially decaying simple harmonic motion (p-type). The aerodynamic theory suitable for simple harmonic motion (k-type) is employed after necessary modification to reflect the p-type motion. The aerodynamic theory may be considered an approximation, but the method is conceptually sound. The damping values plotted on the V - g curve are estimates for the actual damping at subcritical conditions.

3. The true V - g method: A fictitious structure is considered which possesses a structural damping of $(g_r + g)$ in the r-th vacuum normal mode. At rotor speed Ω, this structure can undergo simple harmonic motion with a frequency ω. k-type aerodynamic theory is employed. Since g varies from one rotor speed to another, and from one aeroelastic mode to

another, the fictitious structure is not a constant entity. We obtain a matched flutter boundary point for the given structure.

4. Approximate true V - g method: At chosen rotor speeds (at discrete points) the solution matches with that of the true V - g method. At other rotor speeds, the solution is an approximation to the true V - g solution.

5. The k method or the conventional V - g method: k-type aerodynamic theory is employed. The solution is exact at the matched flutter boundary point only. The solution obtained at rotor speeds below the matched flutter speed may not provide any valid information.

CHAPTER VI

UNSTEADY AERODYNAMICS OF THE p-TYPE

The Mathematical Model

In a previous chapter, the various aspects of Loewy's aerodynamic model were discussed. The model chosen for the p-type aerodynamics is basically the same except for two differences. The helical vortex contained in the wedge shaped element is not extended to infinity on either side. Instead, the arc length of the finite wake is simply projected onto the two dimensional plane of the airfoil without altering the arc length. The second difference lies in the fact that the wake vorticity strength is considered to attenuate continuously as the fluid moves in the downwash of the rotor. These two modifications to the Loewy model [10] are necessary to analyze the p-type motion of the airfoil. This can be seen mathematically in the subsequent development.

The concept of an equivalent single bladed rotor has been discussed previously. In this chapter, an attempt is made to evaluate the differences between the p-type and p-k type aerodynamic theories for the lift and moment coefficients of an aerofoil undergoing p-type motion. For this reason, only a single bladed rotor is considered. Figure 26 shows the mathematical model with finite lower lying wakes.

Governing Equations

The induced velocity on the airfoil can be obtained by application of the Biot-Savart law.

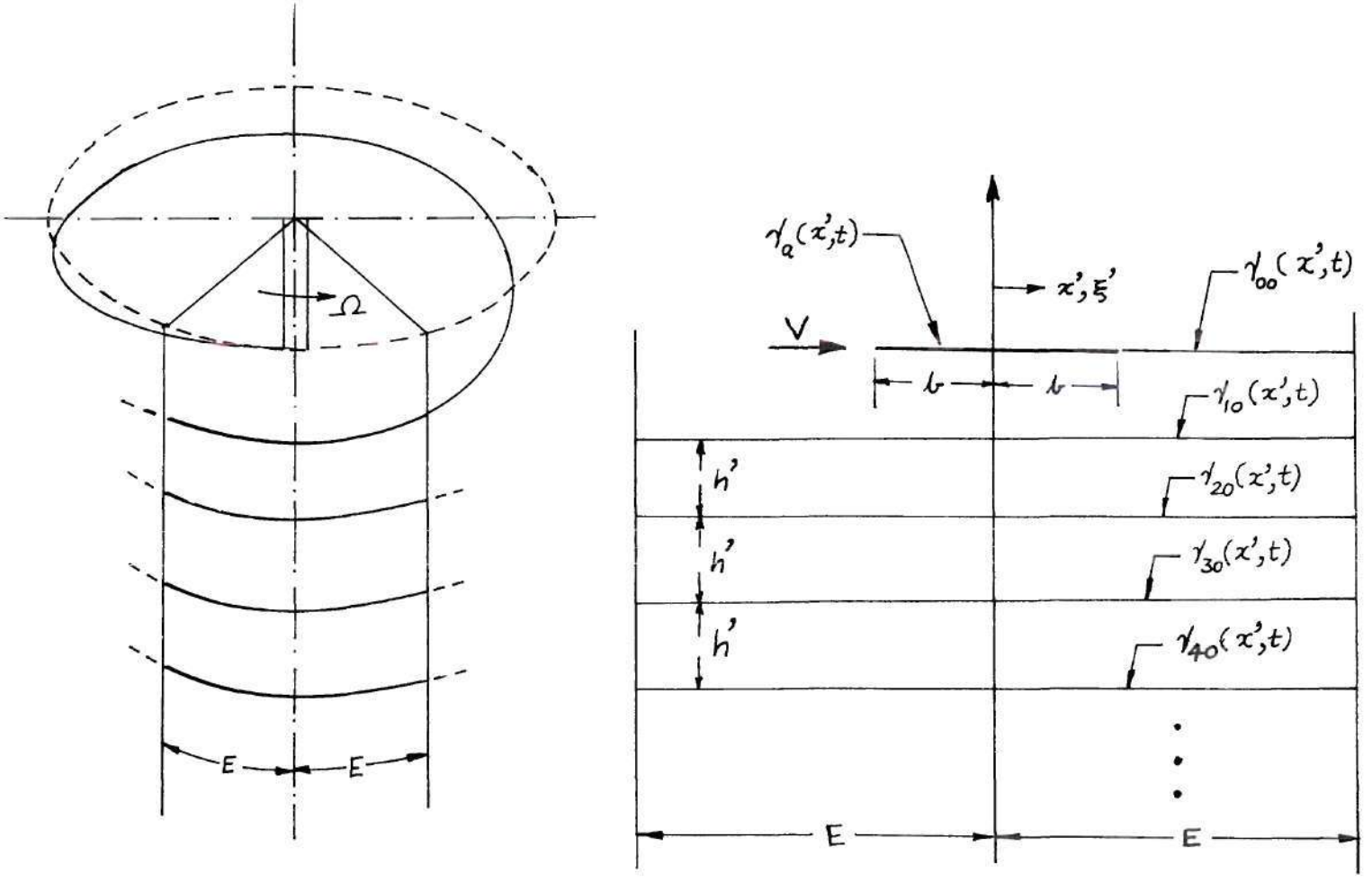

Figure 26. p-type Aerodynamic Mathematical Model for a Single Bladed Rotor.

$$v_a(x',t) = -\frac{1}{2\pi}\left[\oint_{-b}^{b} \frac{\gamma_a(\xi',t)d\xi'}{(x' - \xi')} + \int_{b}^{E} \frac{\gamma_{oo}(\xi',t)d\xi'}{(x' - \xi')} + \right.$$

$$\left. + \sum_{n=1}^{n_1} \int_{-E}^{E} \frac{\gamma_{no}(\xi',t)(x' - \xi')d\xi'}{(x' - \xi')^2 + n^2h'^2} \right] \qquad (84)$$

In the above equation, b, E, n_1 and h' are known (n_1 is the finite number of lower wakes). The total circulation on the airfoil is given by

$$\Gamma_a'(t) = \int_{-b}^{b} \gamma_a(x',t)dx' \qquad (85)$$

Kutta's wake condition requires that the pressure difference across the wake (including the trailing edge) vanish, and this mathematically leads to

$$\gamma_{oo}(b,t) = -\frac{1}{V}\frac{d}{dt}\left(\Gamma_a'(t)\right) \qquad (86)$$

The vortex strength at any point in the wake is related to the vorticity at the trailing edge by

$$\gamma_{no}(\xi',t) = \gamma_{oo}(b,t - \Delta t)\exp(-\mu\Delta t), \quad n = 0,1,2,... \qquad (87)$$

where $\mu \geq 0$ is a prescribed vortex viscous dissipation factor, and

$$\Delta t = (\xi' - b)/V + 2\pi n/\Omega \qquad (88)$$

$$V = \Omega r' \tag{89}$$

The kinematic boundary condition must be satisfied on the airfoil since the fluid velocity relative to the surface of the airfoil can only be tangential. The vertical induced velocity and the airfoil motion are related by

$$-v_a(x',t) = \frac{dw}{dt} + (x' + \frac{b}{2})\frac{d\alpha}{dt} + V\alpha(t) \tag{90}$$

where w is the instantaneous downward displacement of the airfoil at the quarter chord and $\alpha(t)$ is the instantaneous nose up angle of attack of the flat plate airfoil.

The unsteady Bernoulli equation gives the pressure distribution on the airfoil as

$$\Delta p(x',t) = \rho[V\gamma_a(x',t) + \int_{-b}^{x'} \frac{\partial}{\partial t}\gamma_a(\xi',t)d\xi'] \tag{91}$$

Solution for the Pressure Distribution

Let the airfoil motion be given by

$$w(t) = \bar{w} \exp(pt) \tag{92}$$

$$\alpha(t) = \bar{\alpha} \exp(pt)$$

Hence

$$v_a(x',t) = \overline{v_a}(x') \exp(pt) \tag{93}$$

where p is a prescribed complex constant.

When steady state conditions are reached

$$\gamma_a(x',t) = \bar{\gamma}_a(x') \exp(pt)$$

$$\gamma_{no}(x',t) = \bar{\gamma}_{no}(x') \exp(pt), \quad n = 0,1,2,\ldots,n_1 \tag{94}$$

$$\Delta p(x',t) = \overline{\Delta p}(x') \exp(pt)$$

The following nondimensional quantities are used.

$$\begin{aligned} x &= x'/b \\ \xi &= \xi'/b \\ \tilde{E} &= E/b \\ h &= h'/b \\ \omega &= \mathrm{Im}(p) \\ m &= \omega/\Omega \\ k &= \omega b/V \\ \tilde{\mu} &= (p + \mu)/\omega \\ \tilde{p} &= p/\omega \end{aligned} \tag{95}$$

The Biot-Savart law is simplified to read

$$-2\pi \frac{\bar{v}_a(x)}{V} - \oint_{-1}^{1} \frac{\bar{\gamma}_a(\xi)}{V} \frac{d\xi}{(x-\xi)} = \frac{\bar{\gamma}_{oo}(1)}{V} G(x) \tag{96}$$

where the wake function $G(x)$ is given by

$$G(x) = G(x;k,h,m;\tilde{E},\tilde{\mu},n_1) \tag{97}$$

$$= \int_1^{\tilde{E}} \frac{\exp[(1-\xi)\tilde{\mu}k]d\xi}{(x-\xi)} +$$

$$+ \sum_{n=1}^{n_1} \exp(-2\pi nm\tilde{\mu}) \cdot$$

$$\cdot \int_{-\tilde{E}}^{\tilde{E}} \frac{\exp[(1-\xi)\tilde{\mu}k](x-\xi)d\xi}{(x-\xi)^2 + n^2h^2}$$

From Kutta's condition

$$\frac{\bar{\gamma}_{oo}(1)}{V} = -\tilde{p}k \int_{-1}^{1} \frac{\bar{\gamma}_a(\xi)}{V} \, d\xi \tag{98}$$

The kinematic boundary condition is written as

$$-\frac{\bar{v}_a(x)}{V} = \bar{\alpha}[1 + \tilde{p}k(x + \frac{1}{2})] + \tilde{p}k \frac{\bar{w}}{b} \tag{99}$$

For a known airfoil motion, the procedure for solving the pressure distribution on the airfoil consists of two parts. First, the integral equation (96) has to be solved for $\bar{\gamma}_a(x)/V$. Then the amplitude of the pressure distribution is given by the unsteady Bernoulli equation as

$$\frac{\bar{\Delta p}(x)}{\rho V^2} = \frac{\bar{\gamma}_a(x)}{V} + \tilde{p}k \int_{-1}^{x} \frac{\bar{\gamma}_a(\xi)}{V} \, d\xi \tag{100}$$

The integral equation (96) can be solved by the application of the Söhngen inversion formula [22]. But in order to gain a physical insight

into the problem the following approach is taken.

The Pressure Mode Approach

Assume that $\bar{\gamma}_a(x)/V$ can be written as a combination of various pressure modes:

$$\frac{\bar{\gamma}_a(x)}{V} = A_o \cot\frac{\phi}{2} + \sum_{\ell=1}^{6} A_\ell \sin \ell\phi + \sum_{\ell=0}^{3} B_\ell \cos \ell\phi \qquad (101)$$

where A_o, A_ℓ, B_ℓ are undetermined coefficients, and ϕ is an airfoil chordwise coordinate defined by

$$x = -\cos \phi \qquad (102)$$

The cot $(\phi/2)$ term represents the appropriate singular behavior of the bound vorticity at the leading edge of a flat plate airfoil in a steady potential flow. The cosine terms would not be present in steady flow. This is because γ_a and Δp are proportional in steady flow and as Δp vanishes at the trailing edge, γ_a also does. The unsteady flow relationship between γ_a and Δp as given by Equation (100) indicates that γ_a does not necessarily vanish at the trailing edge. In fact, it is proportional to the time rate of change of bound circulation as indicated by Equation (98).

After substituting Equations (98) and (101) into Equation (96) the Biot-Savart law becomes

$$[1 - \tilde{p}kG(x)]A_o + [-\cos\phi - \frac{1}{2}\tilde{p}kG(x)]A_1 +$$
$$+ [-\cos 2\phi]A_2 + [-\cos 3\phi]A_3 + [-\cos 4\phi]A_4 +$$
$$+ [-\cos 5\phi]A_5 - [\cos 6\phi]A_6 + [-\sigma_1 - \frac{2}{\pi}\tilde{p}kG(x)]B_o +$$
$$+ [\sigma_2]B_1 + [-2x\sigma_2 + \sigma_1 + \frac{2}{3\pi}\tilde{p}kG(x)]B_2 +$$
$$+ [(4x^2 - 3)\sigma_2 + \frac{8}{3\pi}]B_3 = -2\frac{\bar{v}_a(x)}{V} \qquad (103)$$

where

$$\sigma_1 = \sigma/\pi,\ \sigma_2 = (2 + x\sigma)/\pi \quad \text{and}$$
$$\sigma = \ln[(1 - x)/(1 + x)] \qquad (104)$$

Since the vorticity must be continuous at the trailing edge, $\bar{\gamma}_{oo}(b)/V$ as calculated from Equations (98) and (101) must equal $\bar{\gamma}_a(b)/V$ as calculated from Equation (101). This yields

$$[-\pi\tilde{p}k]A_o + [-\frac{\pi}{2}\tilde{p}k]A_1 + [-1 - 2\tilde{p}k]B_o +$$
$$+ B_1 + [\frac{2}{3}\tilde{p}k - 1]B_2 + B_3 = 0 \qquad (105)$$

The eleven undetermined coefficients $A_o, A_1, \ldots, A_6, B_o, \ldots, B_3$ can be uniquely determined by a collocation method. Ten control points are chosen on the airfoil where Equation (103) is evaluated. It is desirable to choose the control points so that they are nearly equidistant from each other and also not too close to the leading and trailing edges. This evaluation of Equation (103) can be written in matrix form as

$$\begin{Bmatrix} \bar{v}_a \\ \hline \bar{V} \end{Bmatrix} = \underset{10 \times 11}{[C]} \begin{Bmatrix} A \\ B \end{Bmatrix} \tag{106}$$

Equation (105) can be written in a similar fashion as

$$0 = \lfloor D \rfloor \begin{Bmatrix} A \\ B \end{Bmatrix} \tag{107}$$

Combining these two matrix equations yields

$$\begin{Bmatrix} \bar{v}_a \\ \hline \bar{V} \\ \hline 0 \end{Bmatrix} = \begin{bmatrix} [C] \\ \hline \lfloor D \rfloor \end{bmatrix} \begin{Bmatrix} A \\ B \end{Bmatrix} = [E] \begin{Bmatrix} A \\ B \end{Bmatrix} \tag{108}$$

The unknown pressure mode coefficients can now be obtained from

$$\begin{Bmatrix} A \\ B \end{Bmatrix} = [E]^{-1} \begin{Bmatrix} \bar{v}_a/V \\ \hline 0 \end{Bmatrix} \tag{109}$$

and the resulting pressure distribution can be computed directly from Equation (100).

The Lift and Moment Coefficients

If the lift and the moment about the quarter chord of the airfoil per unit span are represented by $\bar{L}$ exp (pt) and $\bar{M}$ exp(pt), then

$$\bar{L} = b \int_{-1}^{1} \overline{\Delta p}(x)\,dx \tag{110}$$

$$\bar{M} = -b^2 \int_{-1}^{1} \overline{\Delta p}(x)\left(x + \frac{1}{2}\right)dx \tag{111}$$

Define a set of non-dimensional coefficients by

$$\bar{L} = -\pi\rho\omega^2 b^3 [L_{hp}(\bar{w}/b) + L_{\alpha p}\,\bar{\alpha}]$$

$$\bar{M} = \pi\rho\omega^2 b^4 \,[M_{hp}(\bar{w}/b) + M_{\alpha p}\,\bar{\alpha}] \qquad (112)$$

Since this is a linear theory, the pressure distributions due to pitching and plunging oscillations can be separated to advantage. First the motion is considered to be plunging and the undetermined coefficients are evaluated which yield L_{hp} and M_{hp}. Then the motion is considered to be pitching, and $L_{\alpha p}$ and $M_{\alpha p}$ are evaluated. The coefficients will be different in each case reflecting the different types of pressure distributions induced by the two types of airfoil motion. These lift and moment coefficients are given by

$$L_{hp} \text{ (or } L_{\alpha p}) = -\frac{1}{k^2}\,[(A_o + A_1/2) +$$

$$+ \tilde{p}k(3A_o/2 + A_1/2 + A_2/4)] +$$

$$-\frac{2}{\pi k^2}\,[(B_o - B_2/3) +$$

$$+ \tilde{p}k(B_o + B_1/3 - B_2/3 - B_3/5)] \qquad (113)$$

and

$$M_{hp} \text{ (or } M_{\alpha p}) = (-1/4k^2)[(A_1 - A_2) + \tilde{p}k(4A_o +$$

$$+ 7A_1/4 + A_2/2 - A_3/4)] +$$

$$+ (1/\pi k^2)[(-B_o + 2B_1/3 + B_2/3 +$$

$$- 2B_3/5) + \tilde{p}k(-5B_o/3 +$$

$$- B_1/3 + 11B_2/15 + B_3/5)] \qquad (114)$$

Discussion of Results

A FORTRAN Computer program has been prepared to evaluate L_{hp}, $L_{\alpha p}$, M_{hp} and $M_{\alpha p}$ as functions of (k, h, m; $\tilde{p}$, $\tilde{\mu}$; $\tilde{E}$, n_1). By setting $h = \infty$, $\tilde{p} = i$, $\tilde{\mu} = i$, $\tilde{E} = \infty$, $n_1 = 0$, in this program, the model becomes a fixed wing two dimensional airfoil undergoing simple harmonic oscillatory motion in an incompressible flow. The lift and moment coefficients are functions of the Theodorsen function. The computer program was executed for this condition over a range of reduced frequency between 0.1 and 0.7, and the well known results were reproduced. When h is finite, $\tilde{p} = i$, $\tilde{\mu} = i$, $\tilde{E} = \infty$, $n_1 = \infty$, the lift and moment coefficients correspond to Loewy's results [10]. This computer program successfully reproduced these results also, and hence it is considered that the program has been satisfactorily checked out.

Three example flow conditions have been chosen as described in the table below.

Case	k	h	m	μ/ω	$\tilde{E}$	n_1
1	0.1	3.0	2.3	0.1398	23.0	8
2	0.3	4.5	3.5	0.1262	11.67	8
3	0.5	1.5	6.0	0.1153	12.0	8

It is recalled that $\tilde{\mu} = \tilde{p} + \mu/\omega$ and $\tilde{p} = p/\omega$. The airfoil motion is of the form $\exp(\tilde{p}\omega t)$, and the imaginary part of $\tilde{p}$ is always 1.0. The negative of the real part of $\tilde{p}$ is defined as the airfoil motion decay factor and is equal to the logarithmic decrement of the motion divided by 2π.

For each of the three flow conditions mentioned above, once a value for the airfoil motion decay factor is chosen, all the parameters are specified and the aerodynamic coefficients L_{hp}, $L_{\alpha p}$, M_{hp}, $M_{\alpha p}$ can be evaluated. These coefficients are complex functions because the unsteady lift and moment are not exactly in phase with the plunging or the pitching motion of the airfoil. The absolute values of these coefficients are plotted against the airfoil motion decay factor in Figures 27 through 30. These coefficients are plotted for each case after being normalized with respect to the value of that coefficient for simple harmonic motion of the airfoil, which is the value corresponding to the airfoil motion decay factor of zero.

For simple harmonic motion, it may be noted that this p-type aerodynamic model differs from that of Loewy [10] in two ways. Firstly, the lengths of the sheets of wake vorticity as well as the number of the lower sheets of vorticity are finite in the p-type model. Secondly, the

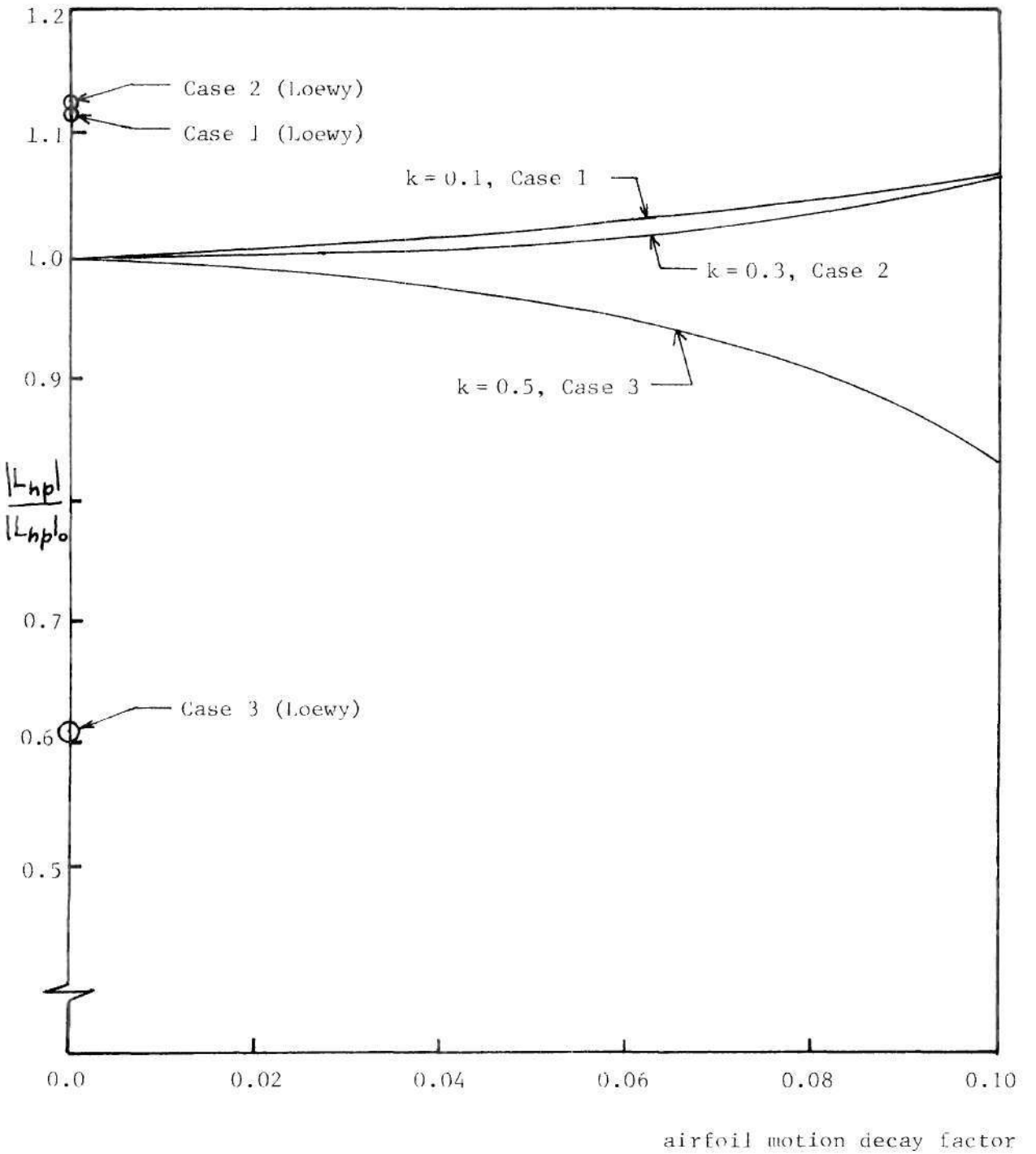

Figure 27. Variation of L_{hp} with Airfoil Motion Decay Factor

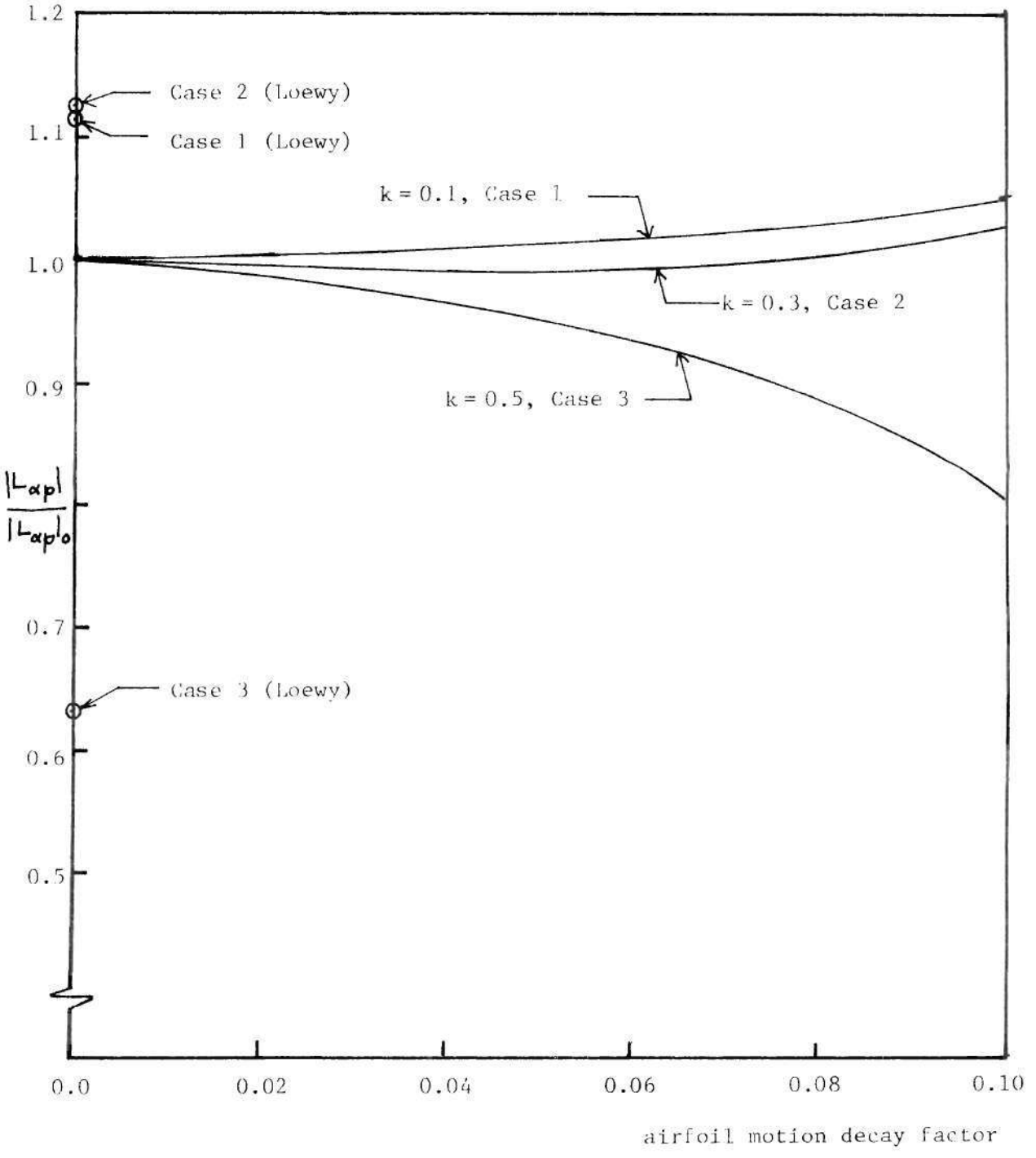

Figure 28. Variation of $L_{\alpha p}$ with Airfoil Motion Decay Factor.

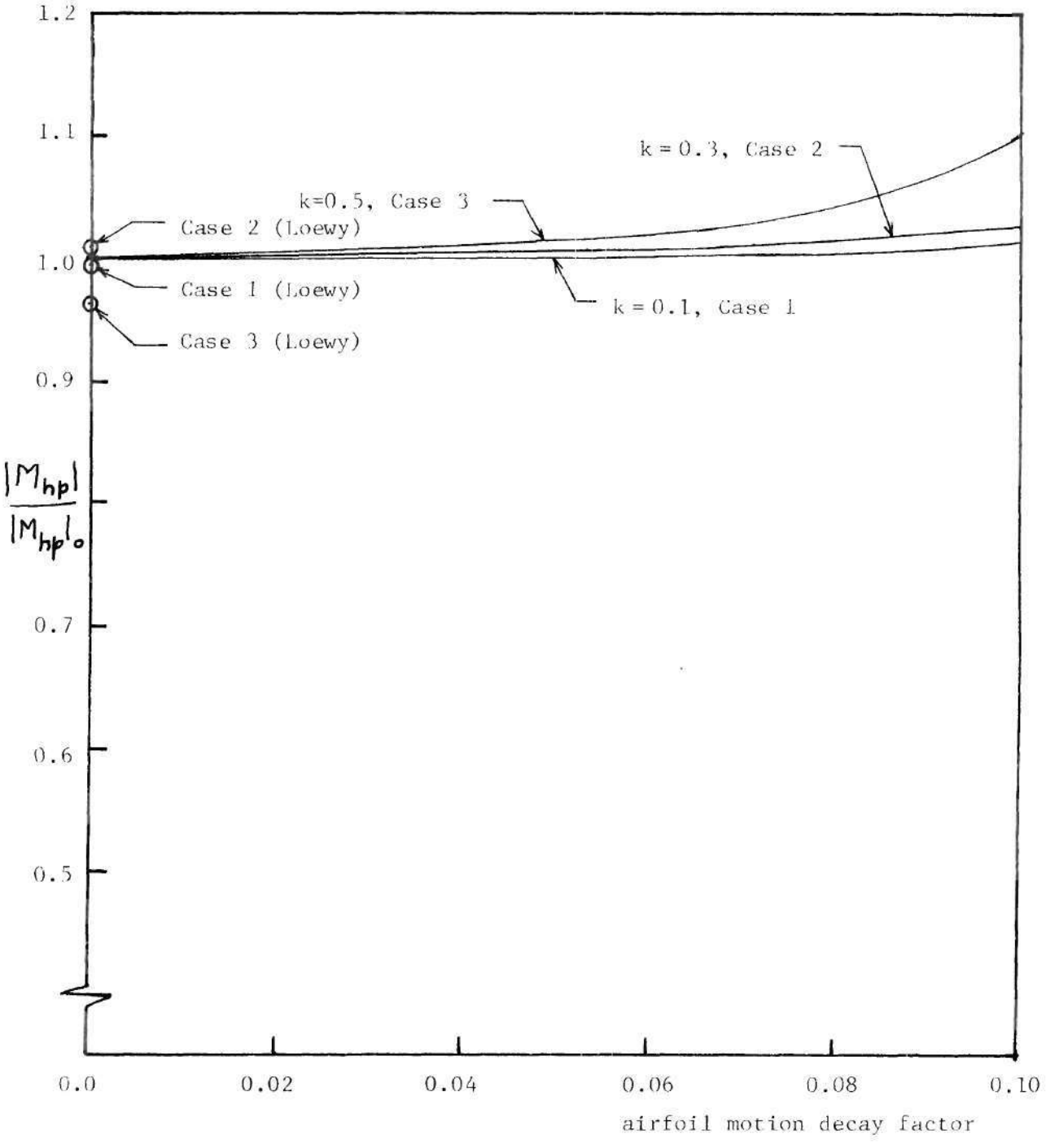

Figure 29. Variation of M_{hp} with Airfoil Motion Decay Factor.

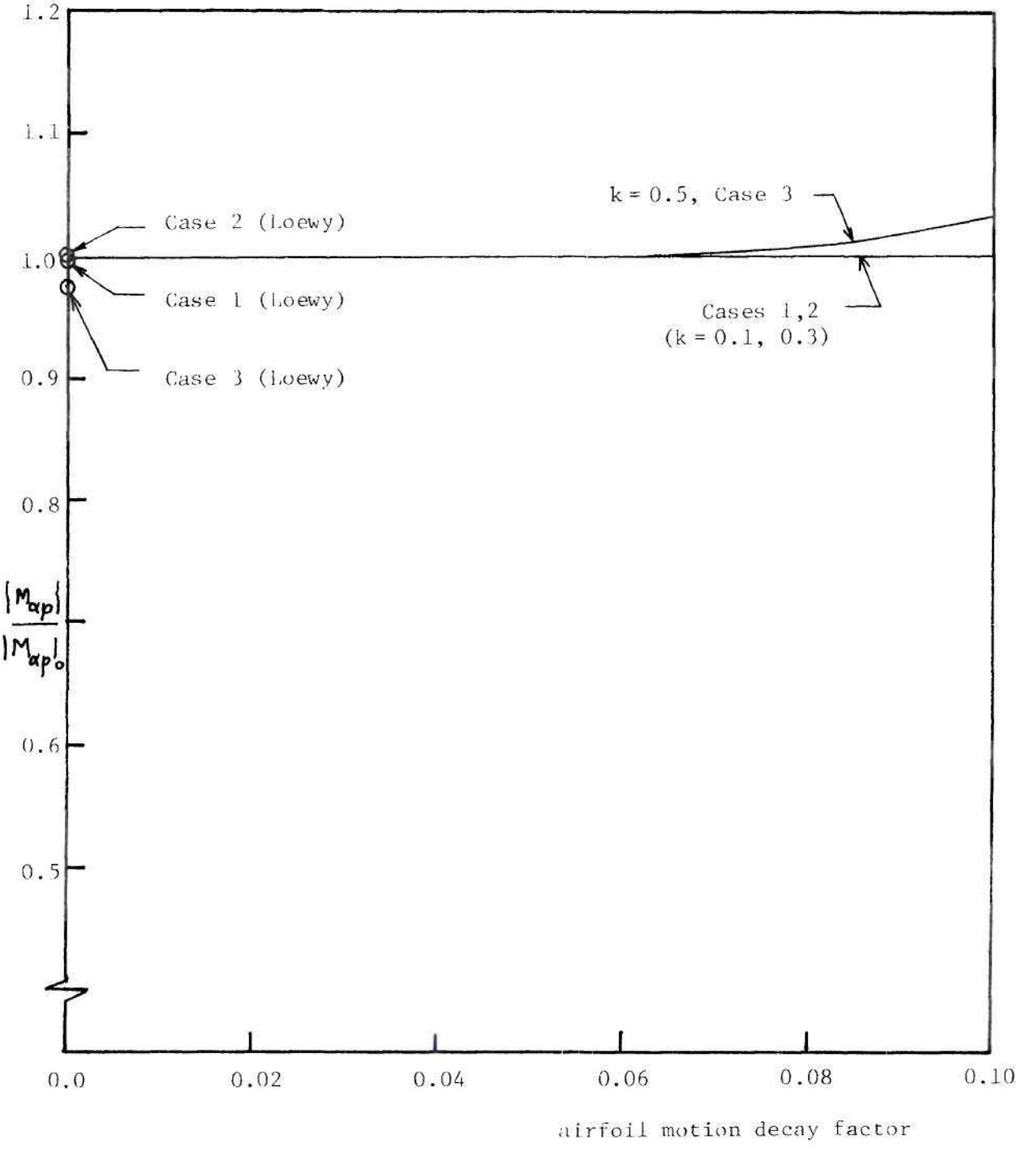

Figure 30. Variation of $M_{\alpha p}$ with Airfoil Motion Decay Factor

vortex strength in the wake is allowed to attenuate continuously with increasing distance downstream. Because of these two differences, for simple harmonic motion (k type aerodynamics), the values of the coefficients are different in the two methods. The values from Loewy's theory are also shown in the figures.

It is observed from the plots that for values of airfoil motion decay factor up to approximately 0.05, the variation in the coefficients from their value for simple harmonic motion is less than 5% in all cases. This substantiates the implied assumption of the p-k method. The differences between the predictions of the p and the p-k method will depend on the aeroelastic system being investigated. Figures 27 through 30 compare only magnitudes of the coefficients, but not their phase. The full implications of any possible differences in phase can be seen only by a decay rate analysis.

For an aeroelastic system to be investigated, it would be worthwhile to first evaluate the system characteristics by both the p-k and p methods, for a typical case. The differences in the results can be considered to reflect on the accuracy of the p-k method. If for this case the p-k method is found to be satisfactory, then the remaining cases of the problem can be analyzed by the p-k method alone.

CHAPTER VII

CONCLUSIONS AND RECOMMENDATIONS

Two relatively new methods of carrying out vibrational analyses of a nonuniform rotating beam in combined bending and torsion have been reviewed. The structual dynamic characteristics of an example blade have been evaluated using the transmission matrix method. The flutter determinant method, the k method, the approximate true V - g method, and the p - k method have been employed in an attempt to predict the flutter speed of an example blade. The principle of the p-k method is explained from the fundamental concept of decay rates, and an alternative numerical scheme is proposed for the decay rate solution by this method. An unsteady rotor aerodynamic theory of the $\wp$ type has been derived to evaluate the implied assumption of the p-k method.

Conclusions

The following conclusions have been drawn from this research program:

1. An automated procedure to obtain the matched flutter point of a rotor blade in an axial flight condition has been developed. A similar procedure is applicable for determining the matched flutter point of a fixed wing.

2. The flutter determinant method is not a practicable method for rotary wing flutter analysis.

3. A method called approximate true V - g method has been developed. It is illustrated that the errors in the damping prediction at subcritical rotor speeds by the k method are largely due to the method of numerical solution rather than the formulation of the problem.

4. The p - k method is shown to be a viable method for predicting the damping in several aeroelastic modes at subcritical speeds. An alternative numerical method of solution to the determinant iteration procedure of Hassig [2] is provided.

5. Inference of the damping present in the aeroelastic modes from a frequency response plot for external simple harmonic excitation is not a reliable procedure.

6. In rotary wing flutter analyses, the vorticity lying in the downwash of the rotor should not be neglected in the unsteady aerodynamic theory, because the ignoring of this vorticity results in an unconservative flutter speed estimation.

7. An unsteady rotor aerodynamic theory of the p type has been developed. The variation of the unsteady lift and moment coefficients with respect to the airfoil motion decay factor indicates that the implied assumption of the p - k method is sound.

8. The p - k method shows considerable promise and may become a standard method of the future.

Recommendations

The following suggestions are made regarding future research in the area of rotor aeroelasticity.

1. Since the p - k method has considerable potential, more research may be carried out regarding application of this method to the various areas of rotor aeroelasticity including the case of a helicopter rotor in forward flight.

2. Further work may be done to improve the eigenvalue method of solution to the p - k method.

3. More p type unsteady aerodynamic formulations may be developed so that the validity of the p - k method can be established for a variety of aeroelastic systems.

4. Since comprehensive experimental results are invaluable in substantiating any analytical model, more experiments may be planned to verify the predictions of the p - k method.

APPENDIX A

THE EIGENVALUE ROUTINE OF DESMARAIS AND BENNETT

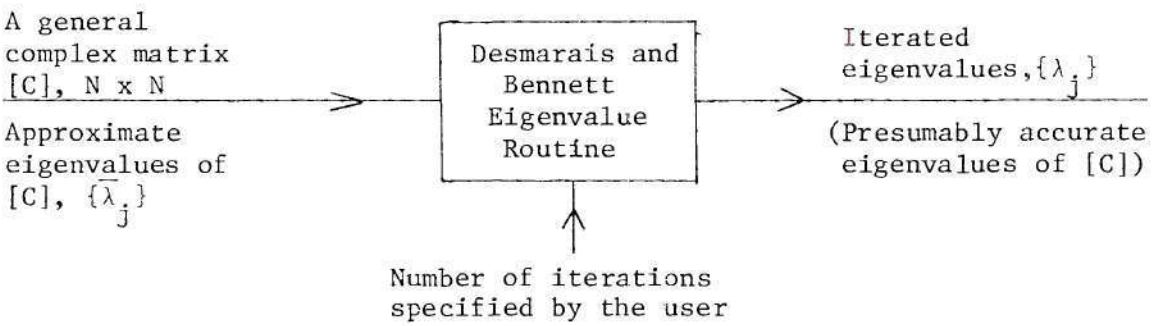

a) The matrix [C] is transformed to upper Hessenberg form [H] by Gaussian elimination.

b) The trial eigenvalues are improved by Laguerre iteration as follows: The first approximate eigenvalue is iterated the specified number of times. Then the second approximate eigenvalue is iterated and so on until the N-th eigenvalue is iterated the specified number of times. With this the program ends.

The iteration on the j-th eigenvalue consists of the following steps:

1. The trial eigenvalue = $\bar{\lambda}_j$
2. The quantity

$$f(\tau) = |[H] - \tau[I]| \qquad \text{(A-1)}$$

and its first two derivatives $f'(\tau)$ and $f''(\tau)$ are computed at $\tau = \bar{\lambda}_j$

from Hyman's recurrence relations [23].

3. The improved eigenvalue $\tilde{\lambda}_j$ is given by

$$\tilde{\lambda}_j = \bar{\lambda}_j - n_\ell / \{S_1 [1 + \sqrt{(n_\ell - 1)(-1 + n_\ell S_2 / S_1^2)}\,]\} \tag{A-2}$$

where

$$\ell = j - 1 \tag{A-3}$$

$$n_\ell = N - \ell \tag{A-4}$$

$$S_1 = \frac{f'(\bar{\lambda}_j)}{f(\bar{\lambda}_j)} - \sum_{i=1}^{\ell} \frac{1}{(\bar{\lambda}_j - \lambda_i)} \tag{A-5}$$

$$S_2 = \left[\frac{f'(\bar{\lambda}_j)}{f(\bar{\lambda}_j)}\right]^2 - \frac{f''(\bar{\lambda}_j)}{f(\bar{\lambda}_j)} - \sum_{i=1}^{\ell} \frac{1}{(\bar{\lambda}_j - \lambda_i)^2} \tag{A-6}$$

Note that λ_i is the i-th eigenvalue of [C], and $i < j$. The terms with Σ sign must be ignored if $j = 1$.

4. Set $\bar{\lambda}_j = \tilde{\lambda}_j$. Repeat steps 2 and 3 above until the number of iterations has been completed.

5. After the specified number of iterations have been carried out, set $\lambda_j = \tilde{\lambda}_j$, the iterated value at the end of the last iteration. Thus the j-th eigenvalue is obtained.

REFERENCES

1. Pierce, G. A. and White, W. F., "Unsteady Rotor Aerodynamics at Low Inflow and Its Effect on Flutter," AIAA Paper No. 72-959, presented at 2nd AIAA Atmospheric Flight Mechanics Conference, Palo Alto, California (September 11-13, 1972).

2. Hassig, H. J., "An Approximate True Damping Solution of the Flutter Equation by Determinant Iteration," J. of Aircraft, Vol. 8, No. 11, November 1971, pp. 885-889.

3. Gessow, A., and Myers, Jr., G. C., Aerodynamics of the Helicopter, Frederick Ungar Publishing Co., New York, N. Y., 1967.

4. Houbolt, J. C. and Brooks, G. W., "Differential Equations of Motion for Combined Flapwise Bending, Chordwise Bending, and Torsion of Twisted Nonuniform Rotor Blades," NACA Technical Report 1346, 1958.

5. Nagaraja, K. S. S., "Analytical and Experimental Aeroelastic Studies of a Helicopter Rotor in Vertical Flight," Ph.D. Thesis, Georgia Institute of Technology, 1975.

6. Murthy, V. R., "Determination of the Structural Dynamic Characteristics of Rotor Blades and the Effect of Phase Angle on Multibladed Rotor Flutter," Ph.D. Thesis, Georgia Institute of Technology, 1975.

7. Rubin, S., "Review of Mechanical Immittance and Transmission Matrix Concepts," J. of Acoustical Society of America, Vol. 41, No. 5, May 1967, pp. 1171-1179.

8. Hunter, W. F., "Integrating Matrix Method for Determining the Natural Vibration Characteristics of Propeller Blades," NASA Technical Note D-6064, 1970.

9. Brooks, G. N. and Baker, J. E., "An Experimental Investigation of the Effect of Various Parameters Including the Tip Mach Number on the Flutter of Some Helicopter Rotor Models," NACA Technical Note 4005, 1958.

10. Loewy, R. G., "A Two Dimensional Approximation to the Unsteady Aerodynamics of Rotary Wings," Journal of the Aerospace Sciences, Vol. 24, No. 2, pp. 81-92, 144, February 1957.

11. Jones, W. P. and Rao, B. M., "Compressibility Effects on Oscillating Rotor Blades in Hovering Flight," AIAA Journal, Vol. 8, No. 2, pp. 321-329, February 1970.

12. Jones, W. P., "The Oscillating Airfoil in Subsonic Flow," British Aeronautical Research Council, R & M 2921, 1956.

13. Hammond, C. E. and Pierce, G. A., "A Compressible Unsteady Aerodynamic Theory for Helicopter Rotors," presented at the AGARD Specialists' Meeting on "The Aerodynamics of Rotary Wings," Marseille, France, September 13-15, 1972.

14. White, W. F., Jr., "Effect of Compressibility on Three Dimensional Helicopter Rotor Blade Flutter," Ph.D. Thesis, Georgia Institute of Technology, School of Aerospace Engineering, August 1972.

15. Ham, N. D., Moser, H. H. and Zvara, J., "Investigation of Rotor Response to Vibrating Aerodynamic Inputs, Part I. Experimental Results and Correlation with Theory," U. S. Air Force, Air Research and Development Command, WADC TR 58-87, AD 203389, October 1958.

16. Daughaday, H., Du Walt, F. and Gates, C., "Investigation of Helicopter Blade Flutter and Load Amplification Problems," Journal of the American Helicopter Society, Vol. 2, No. 3, pp. 27-45, July 1957.

17. Theodorsen, T. and Regier, A. A., "Effect of the Lift Coefficient on Propeller Flutter," NACA ACR L5F30, July 1954.

18. Desmarais, R. N., and Bennett, R. M., "An Automated Procedure for Computing Flutter Eigenvalues," Journal of Aircraft, Volume 11, No. 2, Feb. 1974, pp. 75-80.

19. Francis, J. G. F., "The QR Transformation," Parts I and II, Computer Journal, Vol. 4, Oct. 1961, Jan. 1962, pp. 265-271 and 232-245.

20. Irwin, C. A. K. and Guyett, P. R., "The Subcritical Response and Flutter of a Swept Wing Model," Tech. Rept. 65186, Aug. 1965, Royal Aircraft Establishment, Farnborough, U. K., also, Aeronautical Research Council R & M 3497, London, England.

21. Mazelsky, B. and O'Connell, R. F., "Transient Aerodynamic Properties of Wings: Review and Suggested Electrical Representation for Analog Computers," LR 11577, July 1956, Lockheed Aircraft Corp., California Div., Burbank, Calif.

22. Söhngen, H., Die Lösungen der Integralgleichung und deren Anwendung in der Tragflügeltheorie, Math. Z., Band 45, pp. 245-264, 1939.

23. Wilkinson, J. H., The Algebraic Eigenvalue Problem, Clarendon Press, Oxford, 1967, pp. 426-427.

VITA

Sathy Padmanaban Viswanathan was born to Janaki Jambunathan and Sathy Gopalan Padmanaban on April 5, 1949 in Coimbatore, Tamil Nadu, India. After attending the T.A.R. Chettiar High School and Suburban High School, he joined A. M. Jain College in Madras. He studied Bachelor of Technology course in Aeronautical Engineering in the Indian Institute of Technology at Madras from 1965 to 1970, and obtained first rank in the University. He received M.S. Degree in Aerospace Engineering from Georgia Institute of Technology, Atlanta, Ga. in 1972. Presently he is employed by Bell Helicopter Textron in Fort Worth, Texas as a Senior Dynamics Engineer in Rotor Dynamics Group.